Observations des atmosphères d'exoplanètes par les missions spatiales

Jean-Philippe Beaulieu

About composition and density

- Densities and distances of objects in solar system supports this condensation theory:

  - Rocky planets : 3-6 *g cm*$^{-3}$
    => *mostly rocks and metals*.

  - Gazeous planets: 1-2 *g cm*$^{-3}$
    => Rocky-core, ices and gazes

  - Inner belt asteroids: contains metals and rocks

  - Outer main belt, KBOs: less metals, more ices

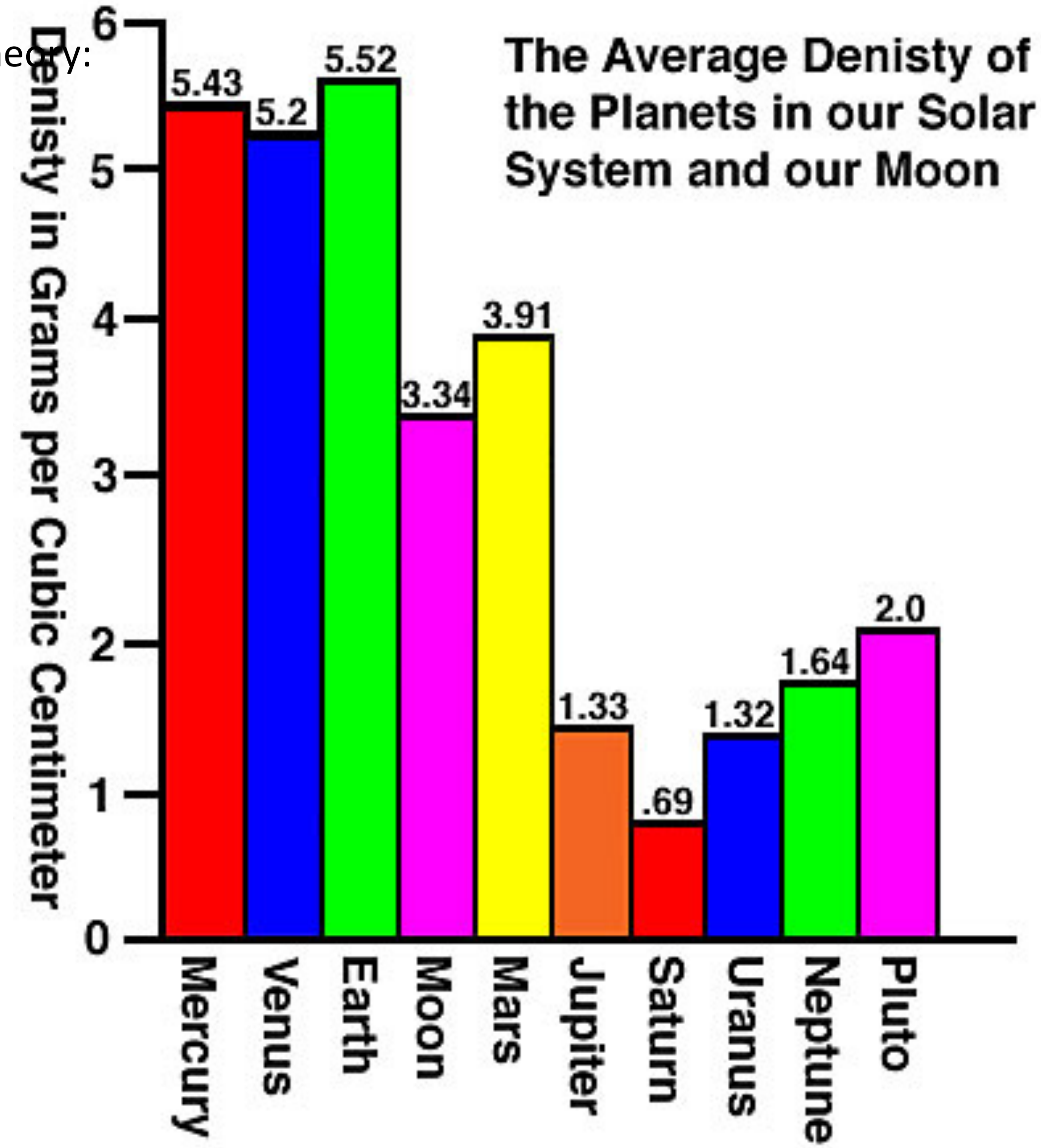

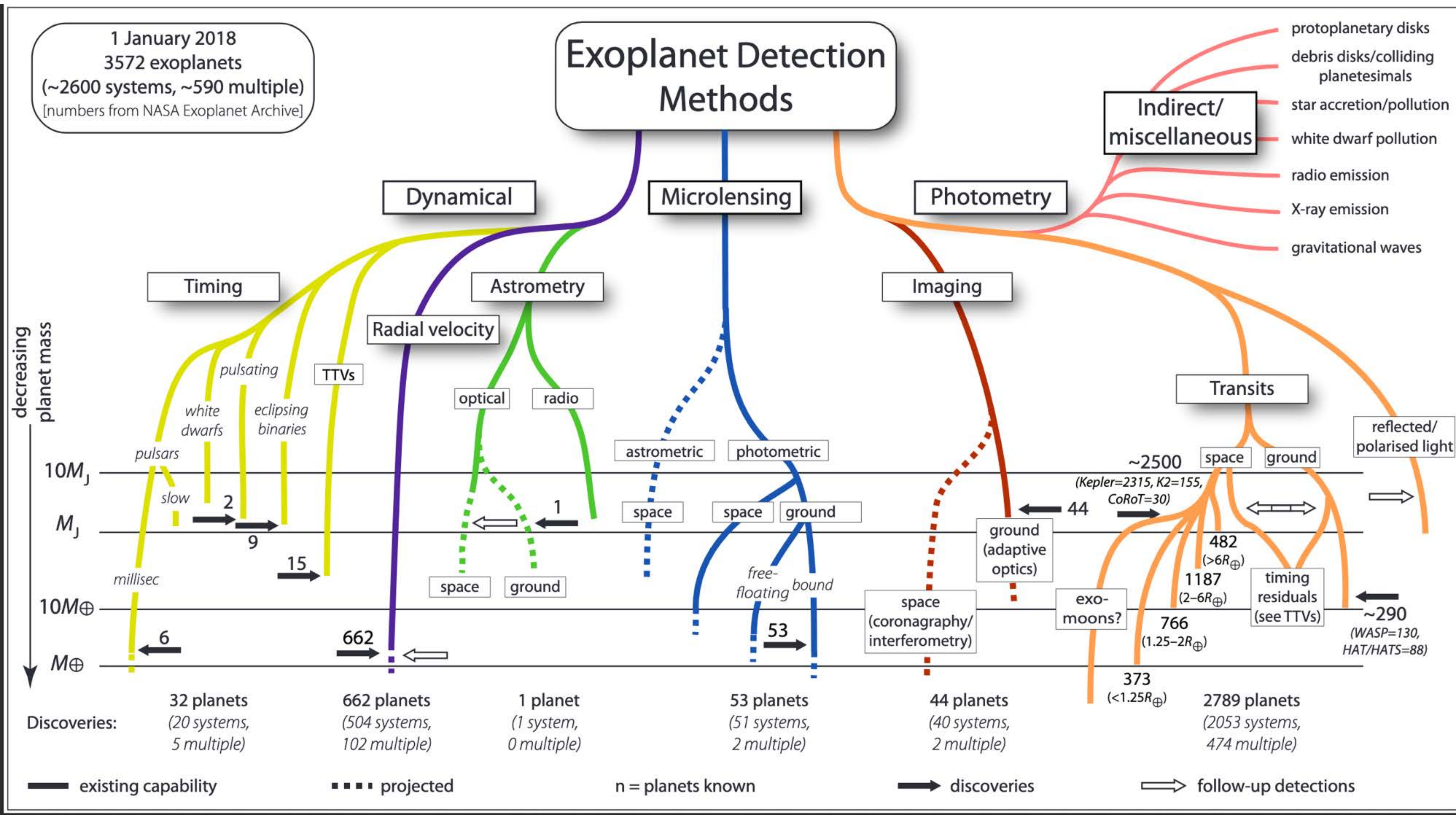

1 January 2018
3572 exoplanets
(~2600 systems, ~590 multiple)
[numbers from NASA Exoplanet Archive]
Exoplanet Detection Methods
Dynamical
Microlensing
Photometry
Indirect/ miscellaneous
protoplanetary disks
debris disks/colliding planetesimals
star accretion/pollution
white dwarf pollution
radio emission
X-ray emission
gravitational waves
Timing
Astrometry
Radial velocity
Imaging
Transits
decreasing planet mass
pulsars
white dwarfs
pulsating
eclipsing binaries
TTVs
optical
radio
astrometric
photometric
space
ground
reflected/ polarised light
10MJ
MJ
10M⊕
M⊕
slow
millisec
2
9
15
6
662
1
space
ground
space
space
ground
free-floating
bound
53
44
ground (adaptive optics)
space (coronagraphy/ interferometry)
~2500
(Kepler=2315, K2=155, CoRoT=30)
482 (>6R⊕)
1187 (2–6R⊕)
766 (1.25–2R⊕)
373 (<1.25R⊕)
exo-moons?
timing residuals (see TTVs)
~290
(WASP=130, HAT/HATS=88)
Discoveries:
32 planets (20 systems, 5 multiple)
662 planets (504 systems, 102 multiple)
1 planet (1 system, 0 multiple)
53 planets (51 systems, 2 multiple)
44 planets (40 systems, 2 multiple)
2789 planets (2053 systems, 474 multiple)
existing capability
projected
n = planets known
discoveries
follow-up detections

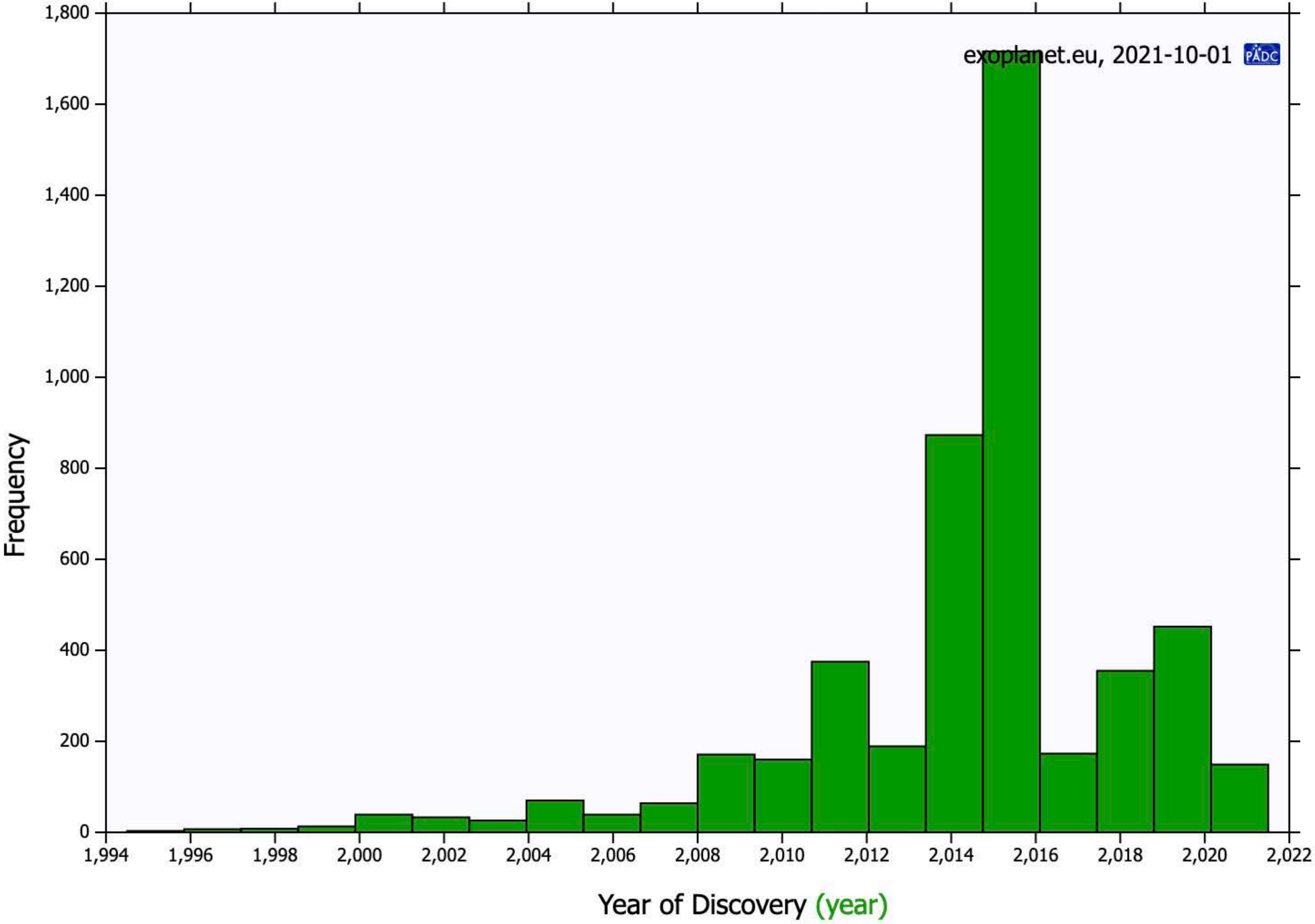
exoplanet.eu, 2021-10-01
PADC
Frequency
1,800
1,600
1,400
1,200
1,000
800
600
400
200
0
1,994
1,996
1,998
2,000
2,002
2,004
2,006
2,008
2,010
2,012
2,014
2,016
2,018
2,020
2,022
Year of Discovery (year)

Extrasolar planet detection

Sept 10 2022, 5168 planets / 3812 planetary systems / 835 multiple planet systems

Astrometry (17 objects, 6 planets ??+53 GAIA candidates)

Radial Velocity (1005 planets in 747 systems, 177 multiple planet systems)

Transit (3618 planets in 2734 systems, 576 multiple planet systems)

Microlensing (215 planets in 195 systems, 710 multiple planet systems)

Direct detection (213 planets in 125 systems, 8 multiple planet systems)

Planets are ubiquitous

The transit technique

Only planets closed to ~ 90 deg inclinaison

Transit probability $\mathcal{P}_{\rm tr} = \frac{R_* + R_{\rm p}}{a\,(1-e^2)} \simeq R_*/a$

10 % probability for a planet at 0.05 AU around a solar like star

Transit depth $\Delta F/F \simeq R_p^2/R_*^2$

Jupiter : 1 % depth   Earth: 0.01 % depth

transit and occultations

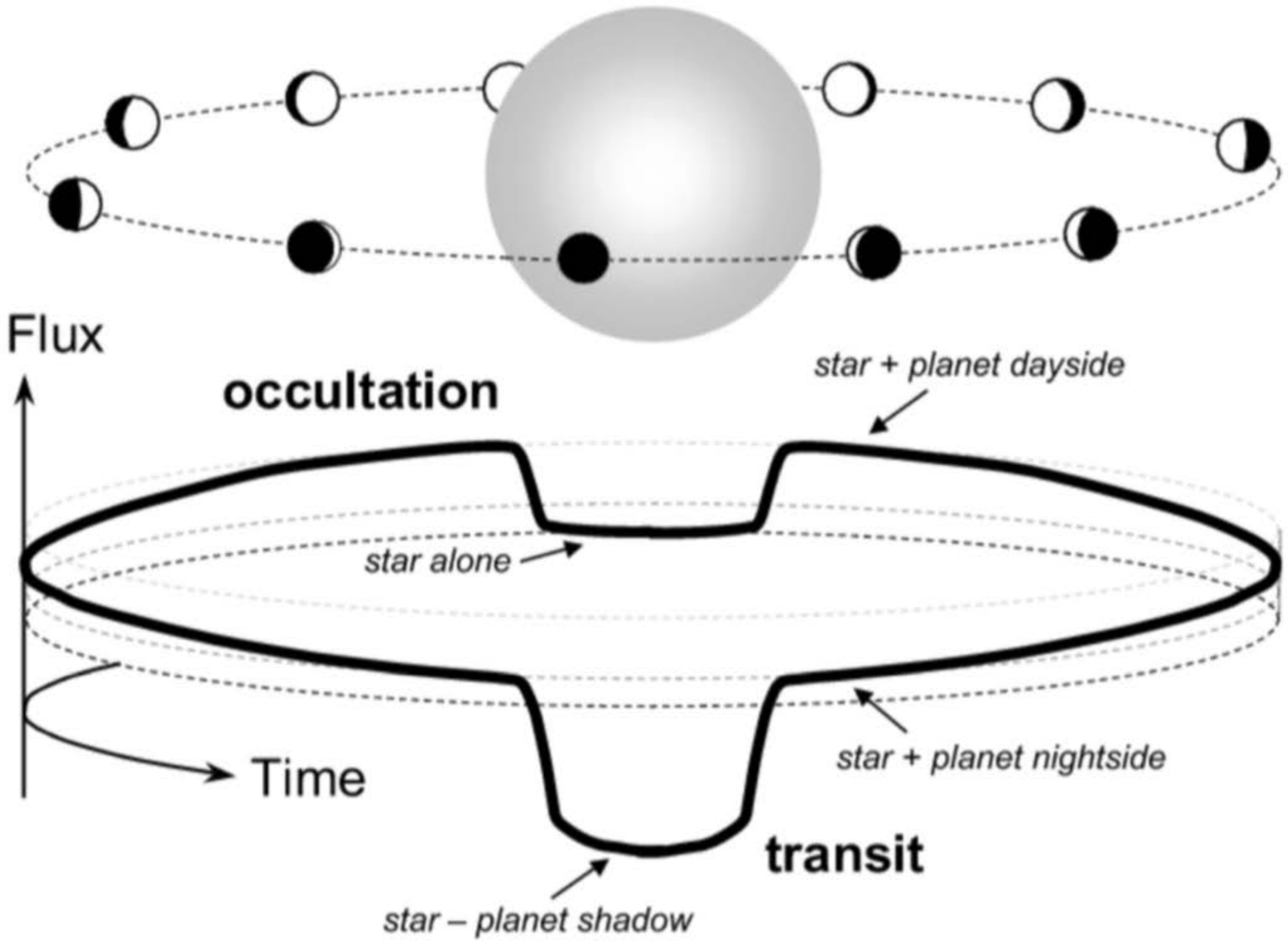

Native Apps

https://astro.unl.edu/nativeapps/

Executables (64-bit and 32-bit) for Windows and (64-bit) for Macintosh computers are available for all of our older projects (NAAP, ClassAction, & Ranking Tasks). The appropriate package for your (or your student's) computer system must be downloaded and installed locally. Note that these are actual applications that run in your native OS and their longevity depends only upon your OS. There is no similar viable solution for Chromebooks.

Note that every simulation available in the past on this site is contained in either the ClassAction or NAAP Labs native app. (In ClassAction look under the Animations tab.) The following guide to content is provided to assist you in navigating. Student guides and demonstration guides can be found on the NAAP Resources page.

Windows Executables (for 64-bit machines, what most people want)

ClassAction - v2.3.msi	97.4 MB	January 30, 2020
NAAP Labs - v1.1.msi	22.4 MB	January 30, 2020
Interactives - v1.1.msi	46.7 MB	January 30, 2020

MacOS Executables

ClassAction - v2.3.pkg	97.1 MB	January 30, 2020
NAAP Labs - v1.1.pkg	22.4 MB	January 30, 2020
Interactives - v1.1.pkg	46.2 MB	January 30, 2020

HD209458b transiting hot Jupiter in 1999

Observations du sol

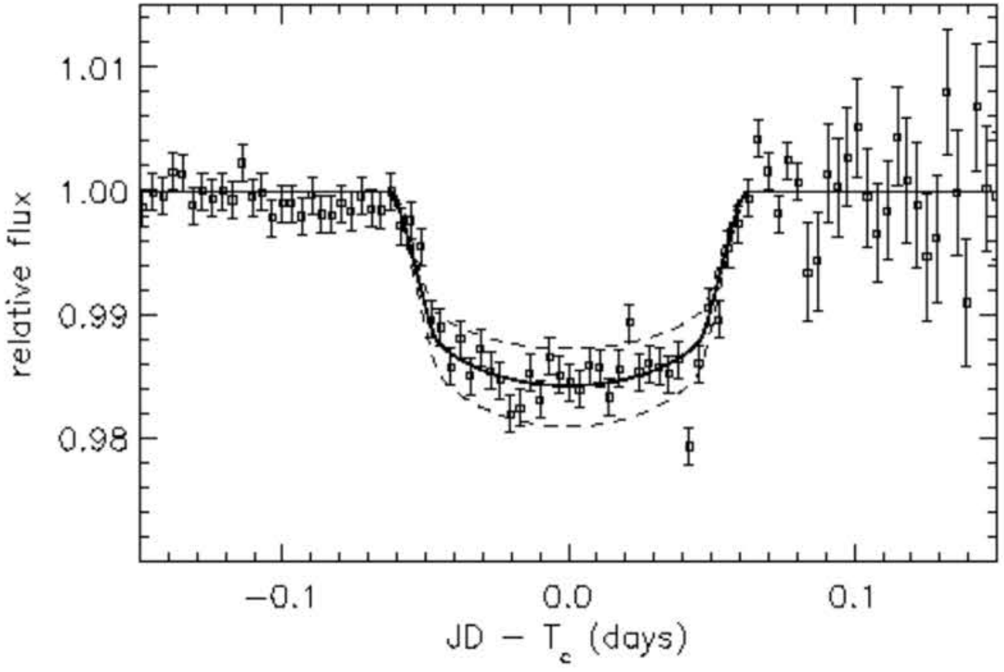

Charbonneau et al. (1999)

Observations spatiale HST

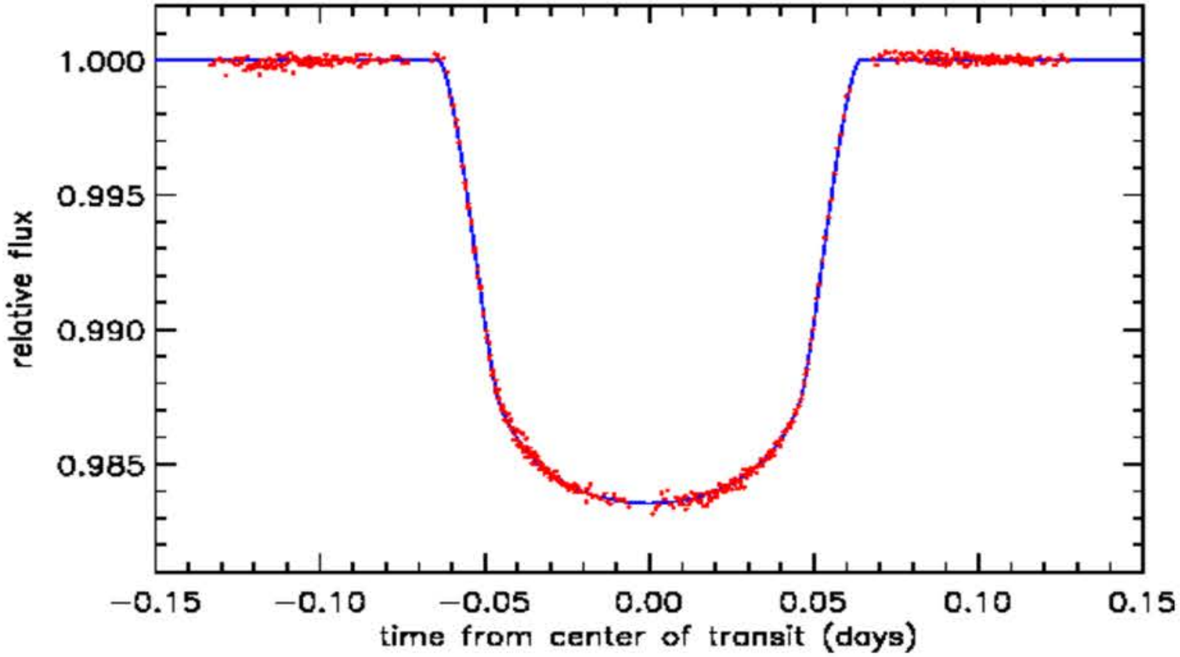

Charbonneau et al. (2000)

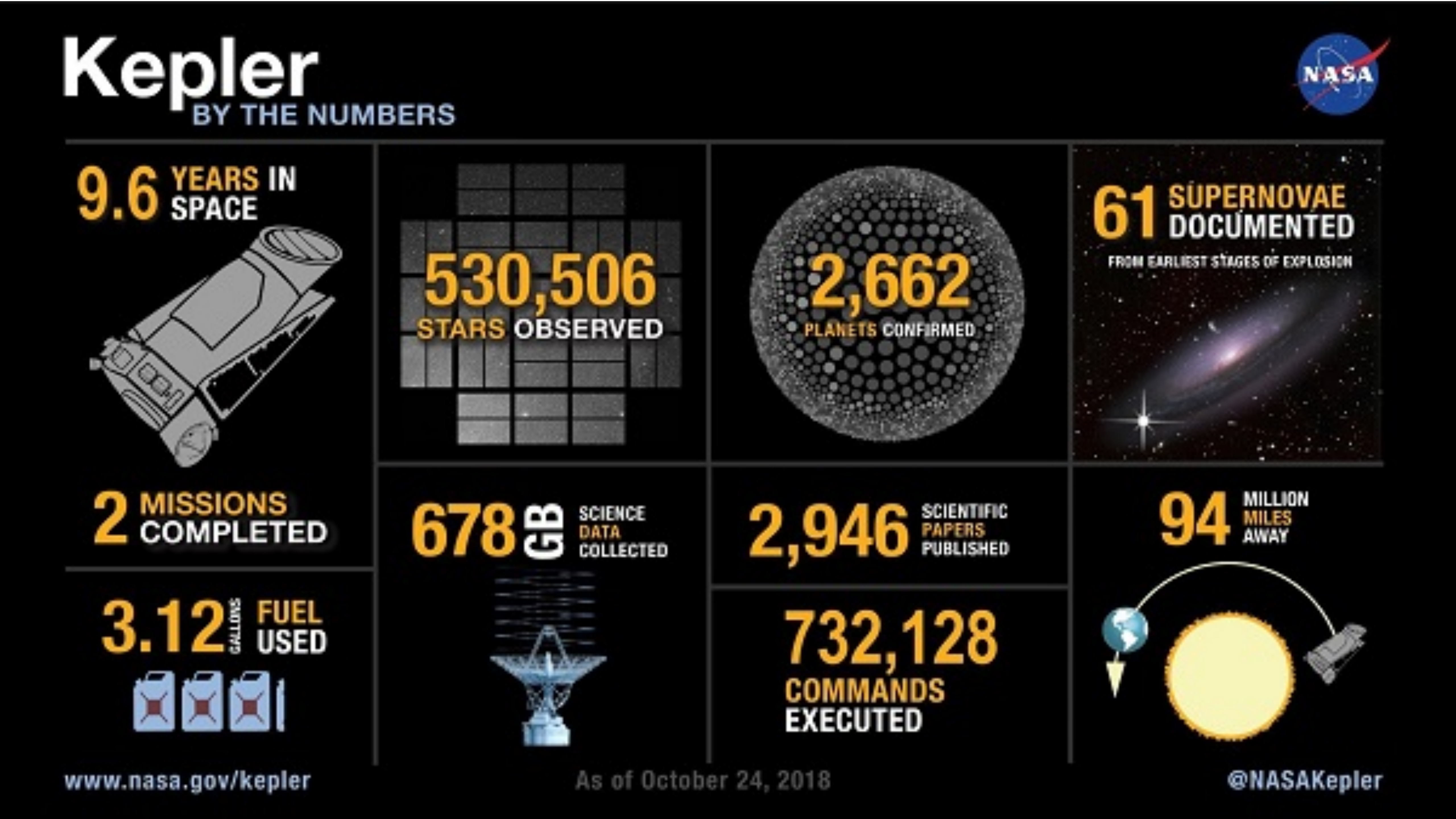
Kepler
BY THE NUMBERS
NASA
9.6 YEARS IN SPACE
530,506 STARS OBSERVED
2,662 PLANETS CONFIRMED
61 SUPERNOVAE DOCUMENTED
FROM EARLIEST STAGES OF EXPLOSION
2 MISSIONS COMPLETED
678 GB SCIENCE DATA COLLECTED
2,946 SCIENTIFIC PAPERS PUBLISHED
94 MILLION MILES AWAY
3.12 GALLONS FUEL USED
732,128 COMMANDS EXECUTED
www.nasa.gov/kepler
As of October 24, 2018
@NASAKepler

Kepler Planet Candidates

January 2014

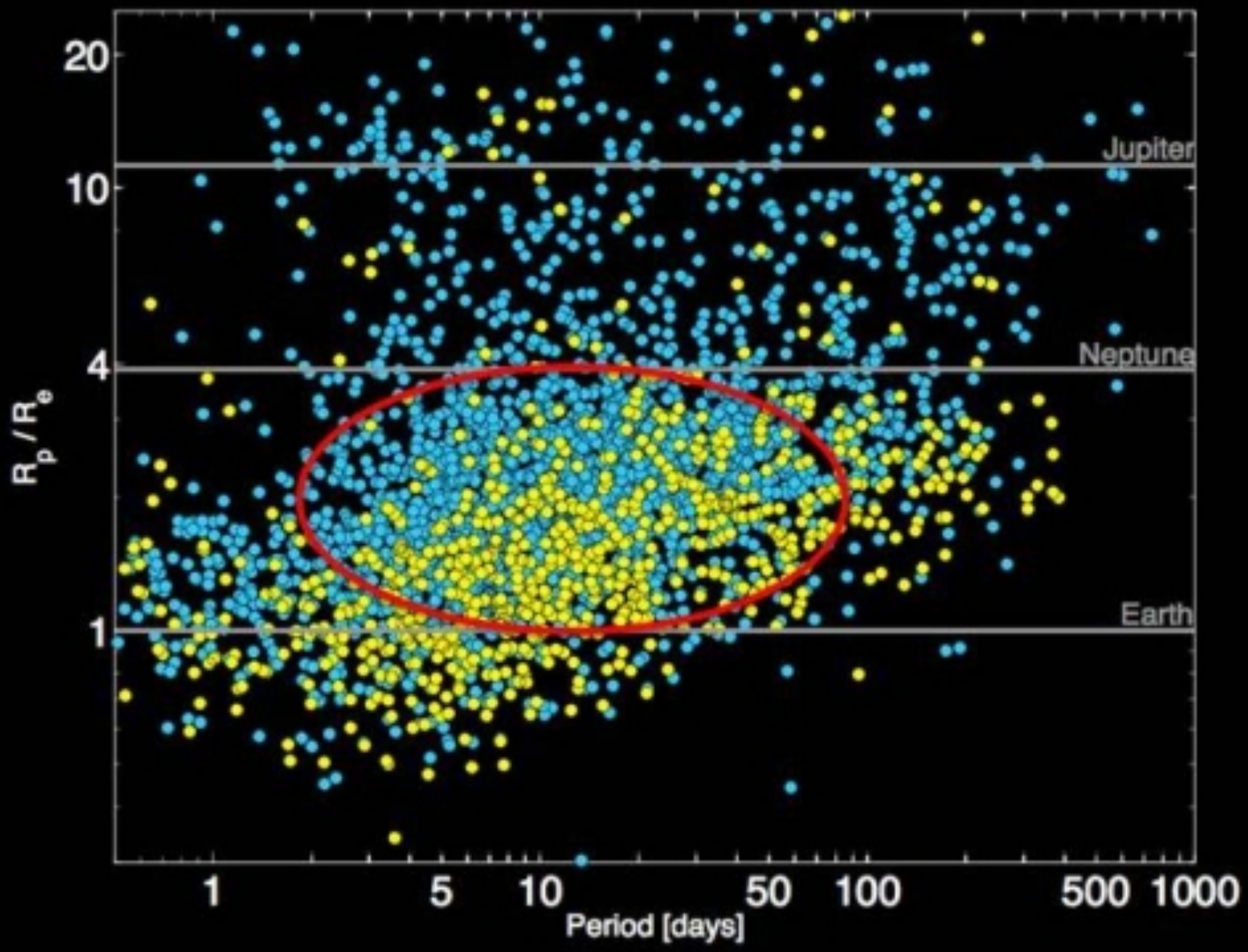

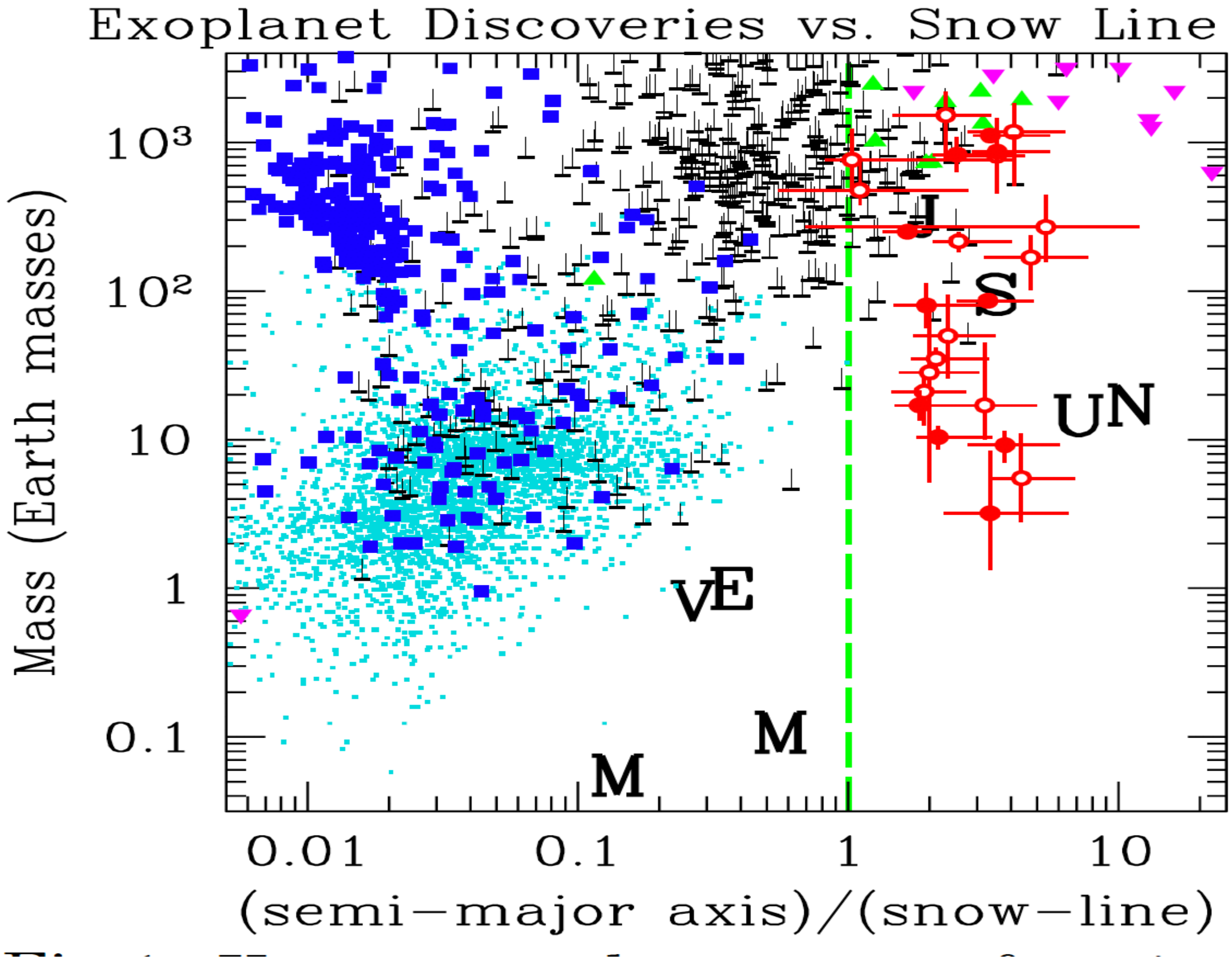

Snow line approximated as 2.7 x M / Mo (AU)

Mass radius relations and isodensity curves with firsdt small planets

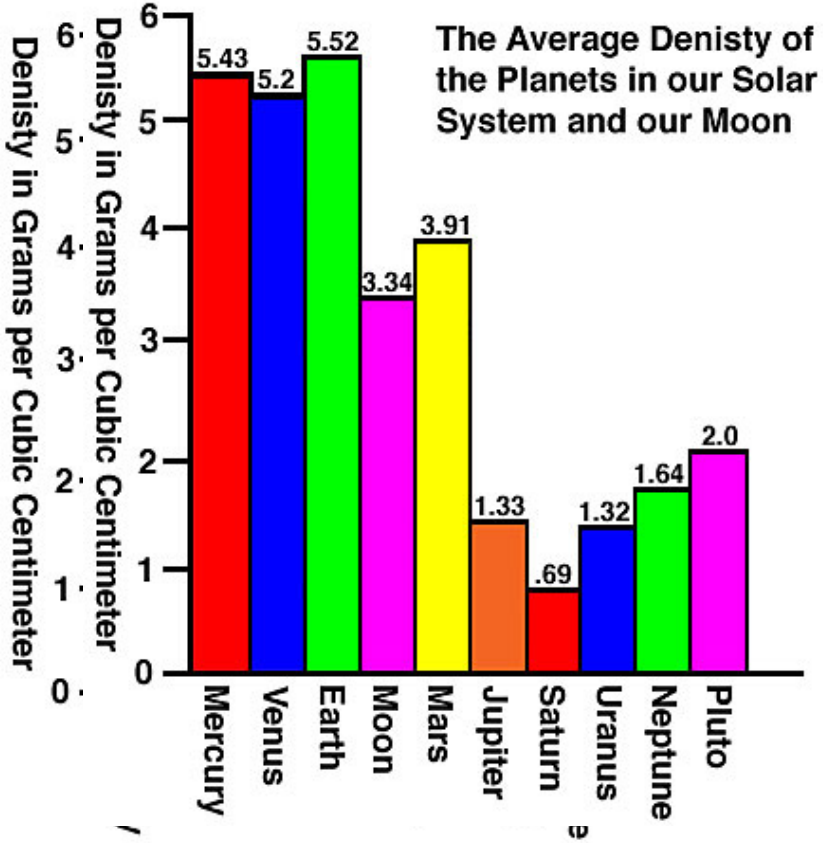

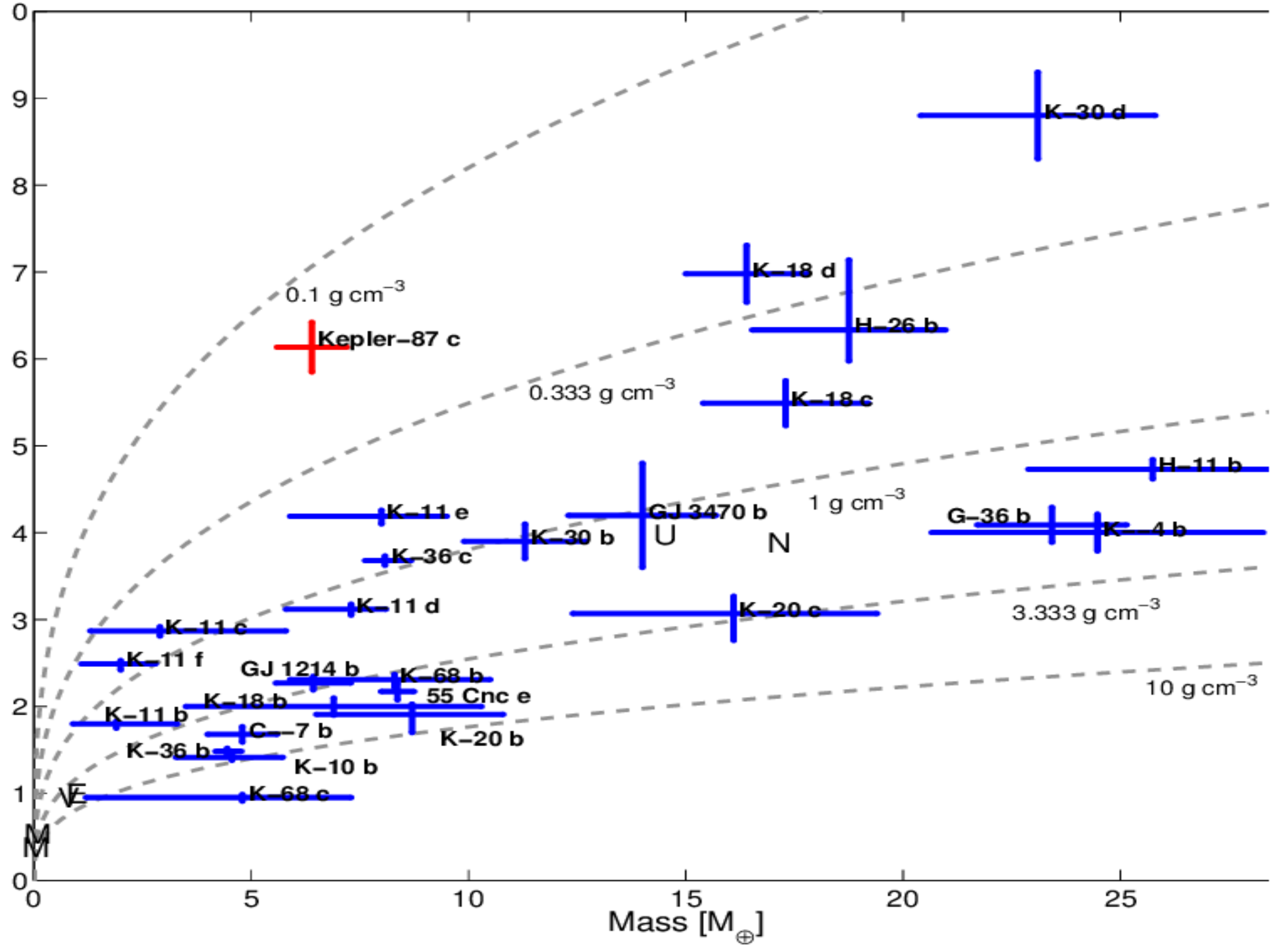

Histogram of planet radii, 2 peaks, super-Earth and Mini-Neptune

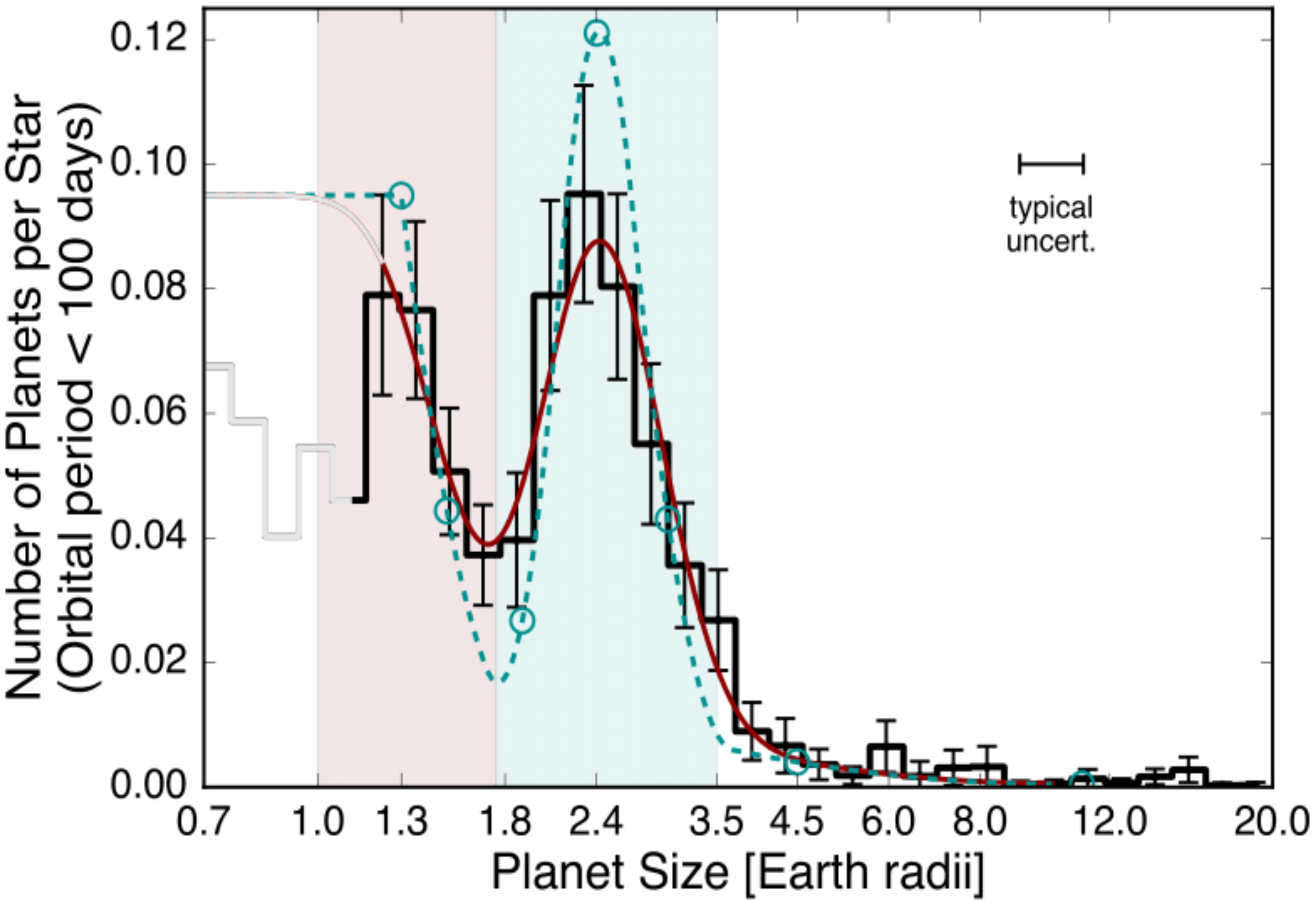

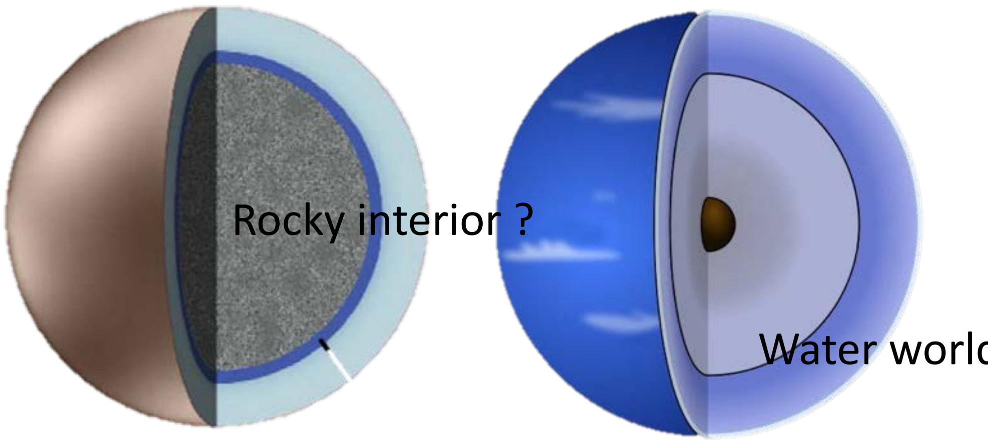

Completeness-corrected histogram of planet radii for planets with orbital periods shorter than 100 days.

Lightly shaded regions encompass our definitions of "super-Earths" (light red) and "sub-Neptunes" (light cyan). The dashed cyan line is a plausible model for the underlying occurrence distribution after removing the smearing caused by uncertainties on the planet radii measurements.

Classification according to density

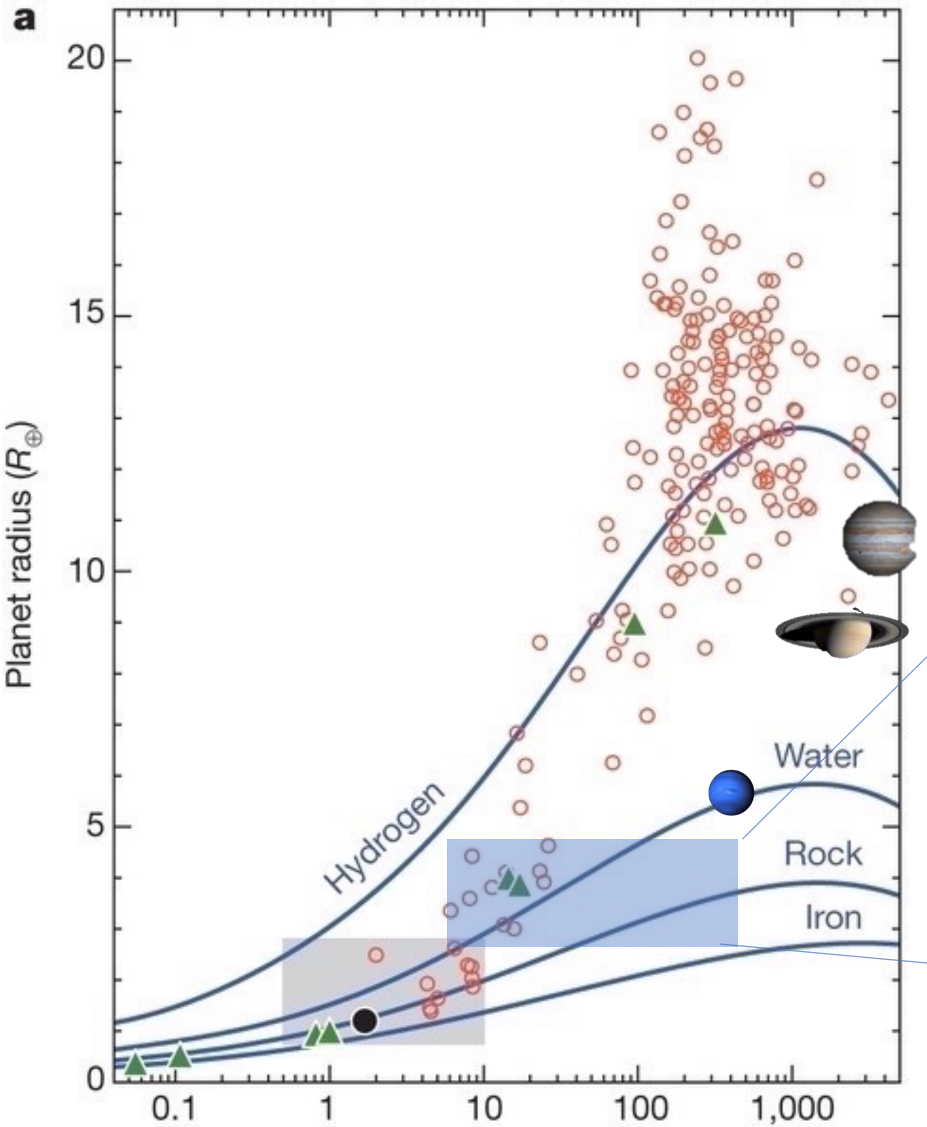

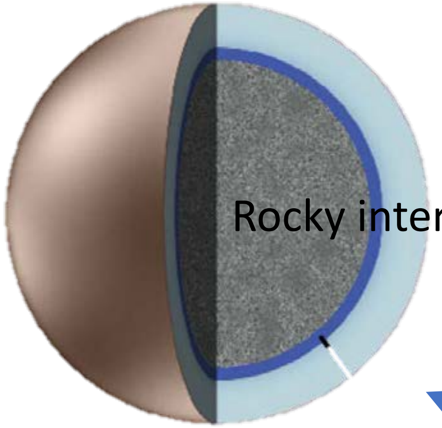

Or ?

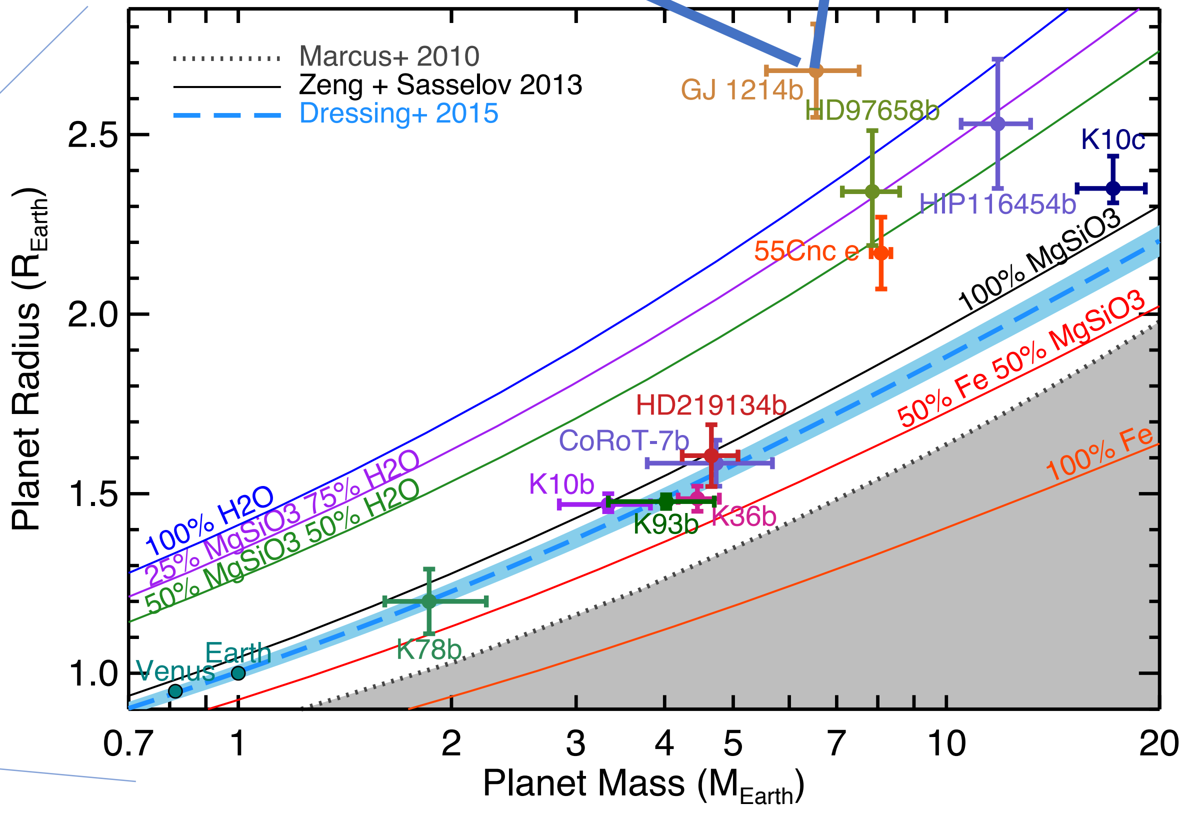

Howard et al., 2013; Motalebi et al., 2015

Ternary diagrams

- A+B+C=100 %
- How to plot the 3 variables together

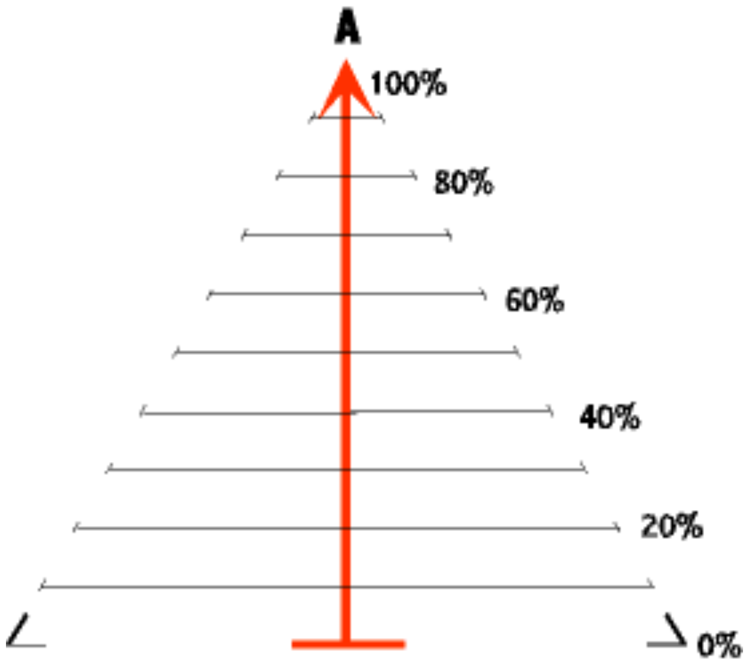

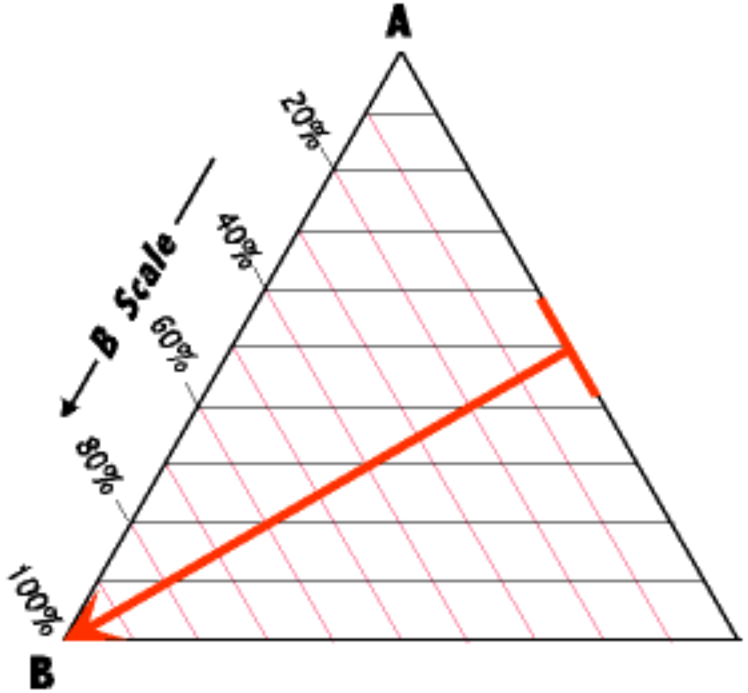

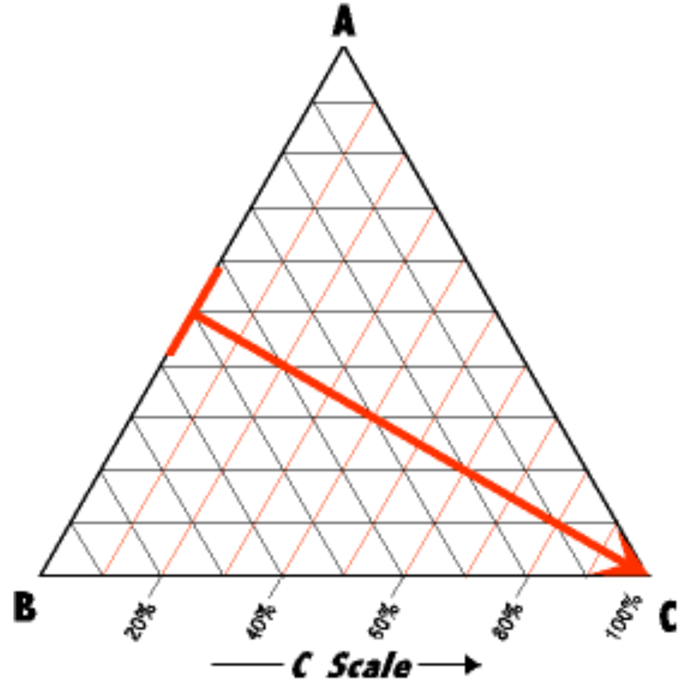

Example of reading the figure

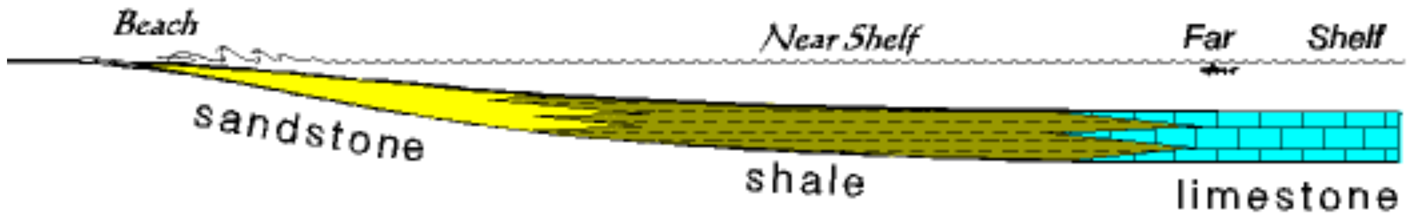

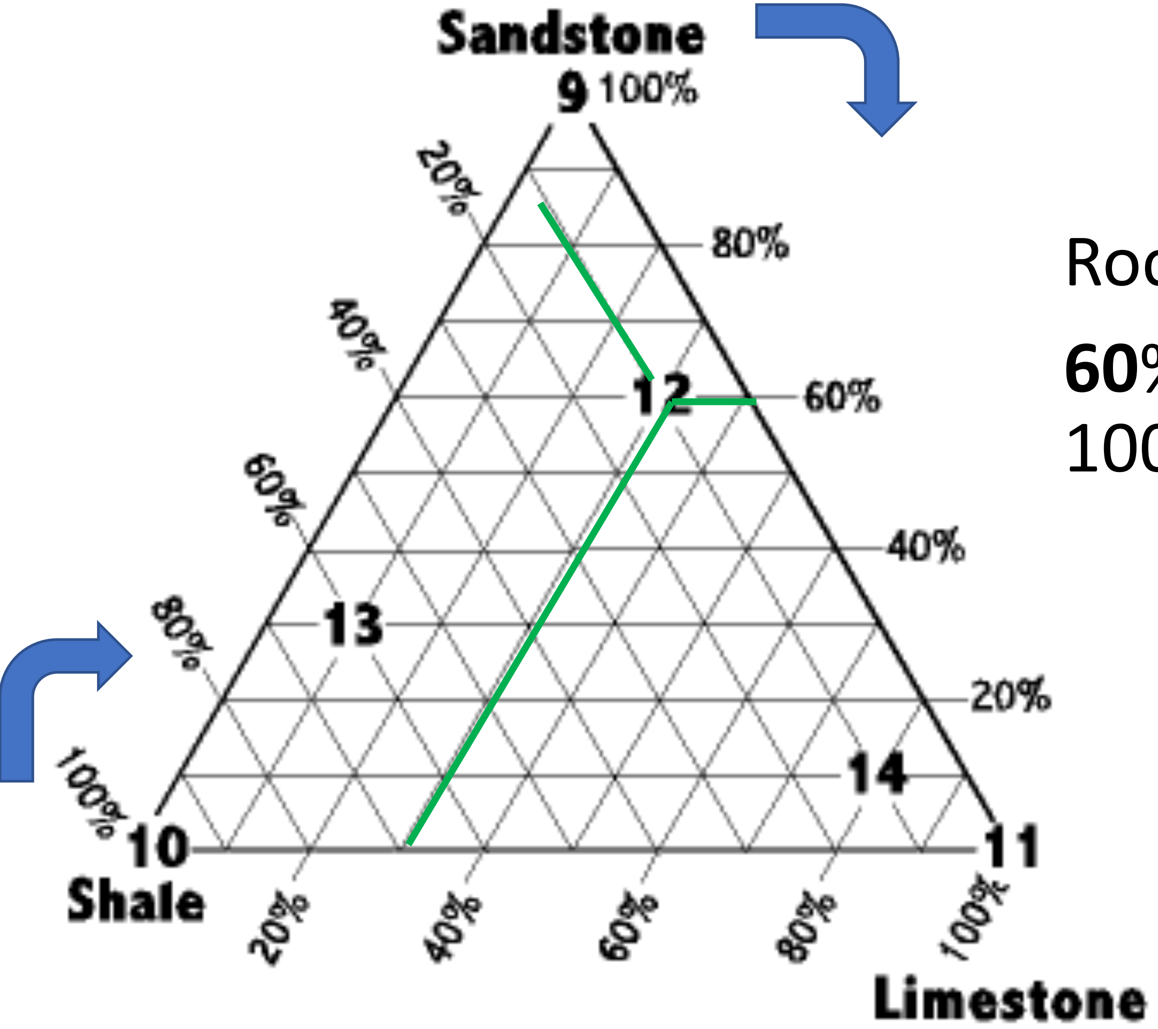

Rock 12:

60% Sandstone | **10**% Shale | **30**% Limestone = 100%

GJ1214b, 6.55 Mearth
Calculating different models H-He, H2O, Earth like nucleus fractions.
Isocurves for Radiu 2.5, 3, ..., 10, 12, 15 Rearth

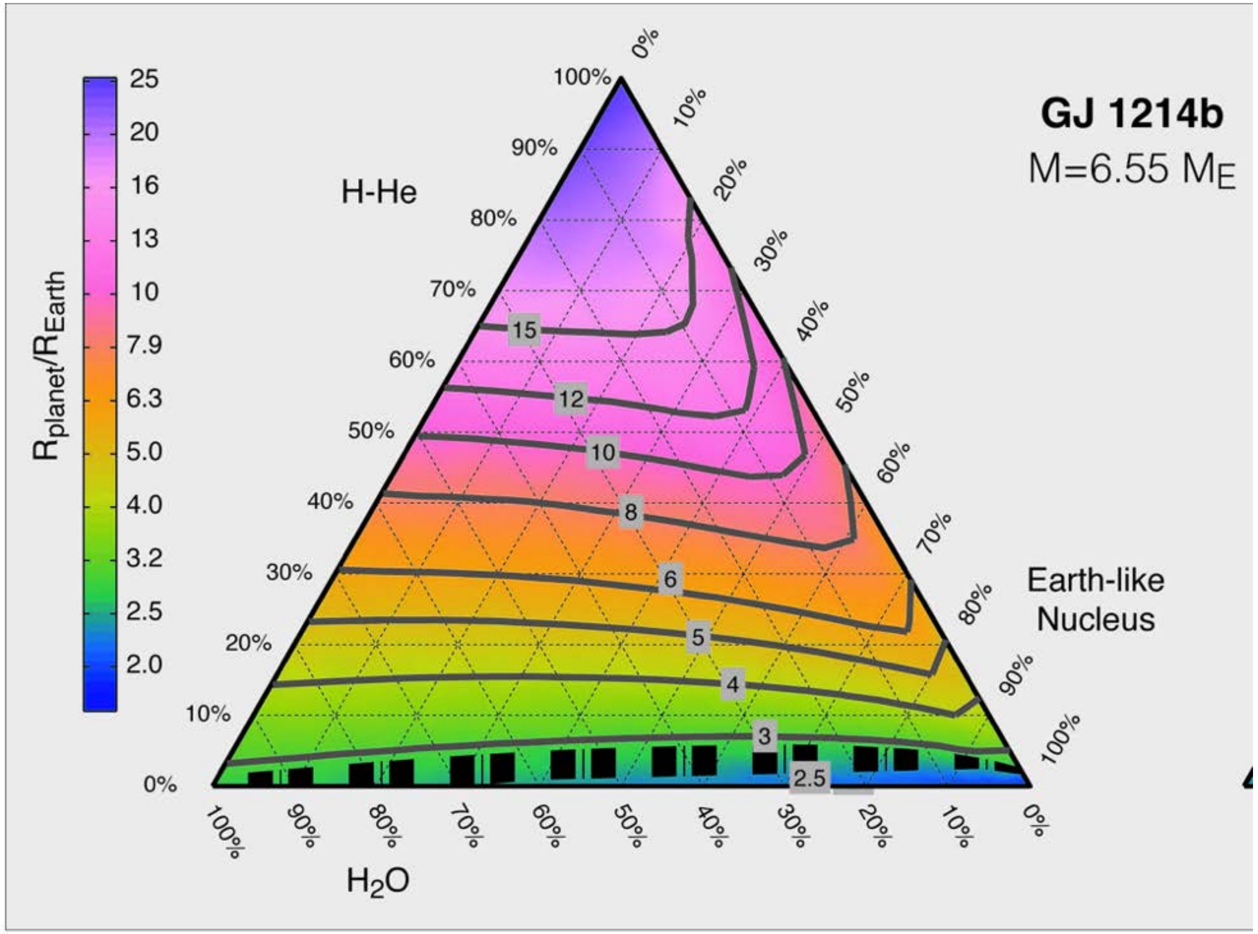

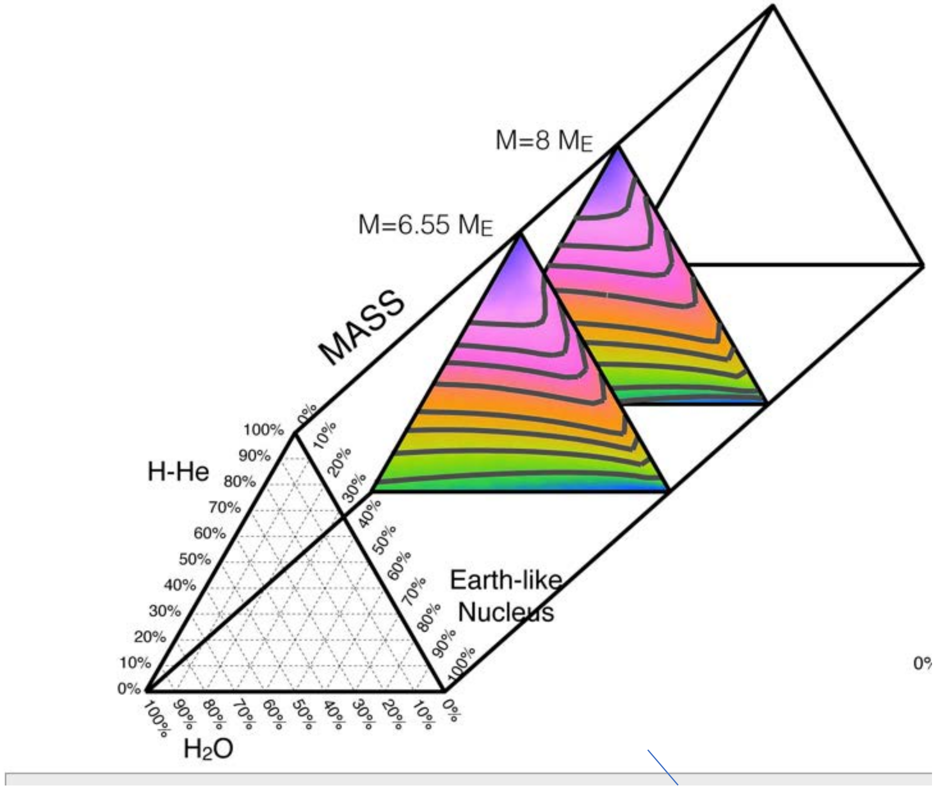

Valencia, 2013

GJ1214b, radius ~2.6 Earth radii

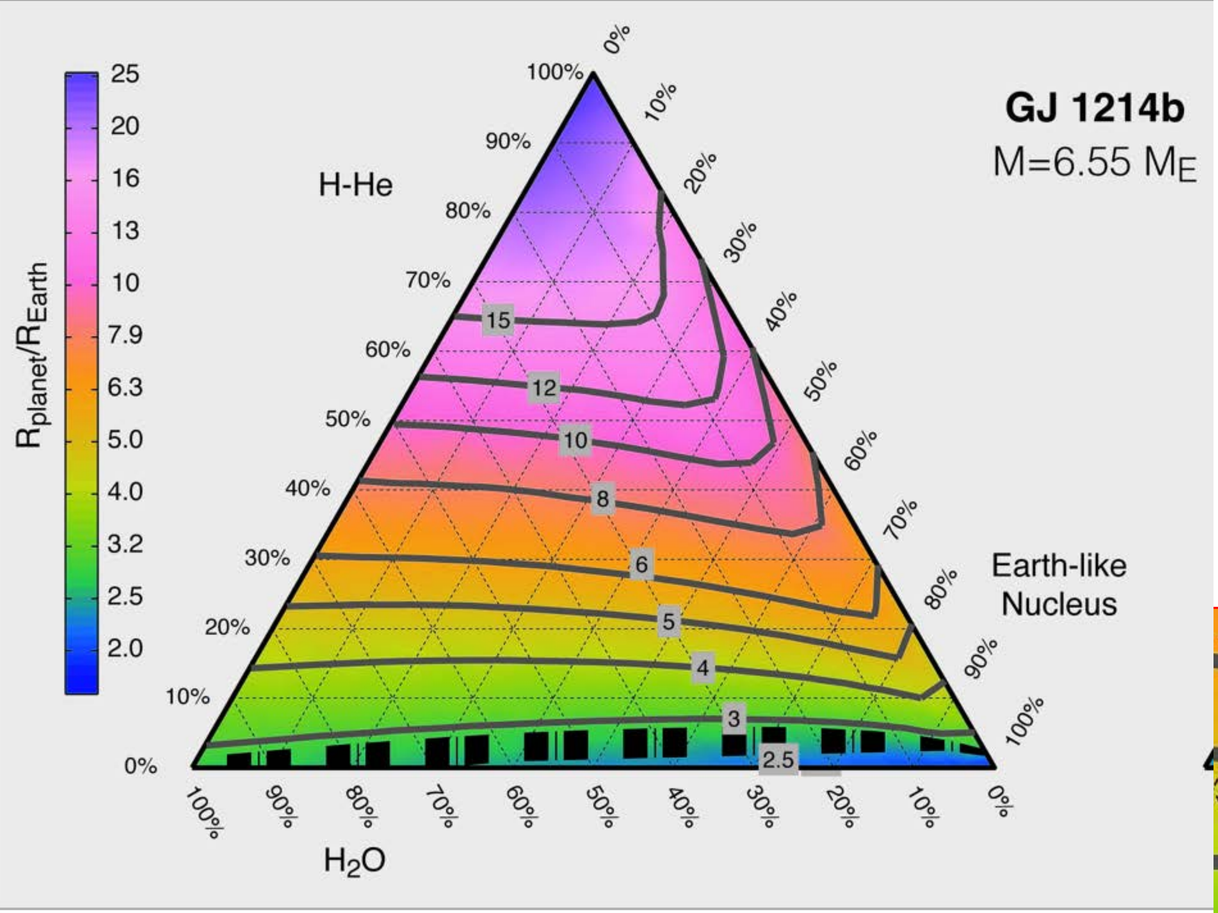

18% H2O + 5% H-He +77 % Earth like

Or 100 % water ?

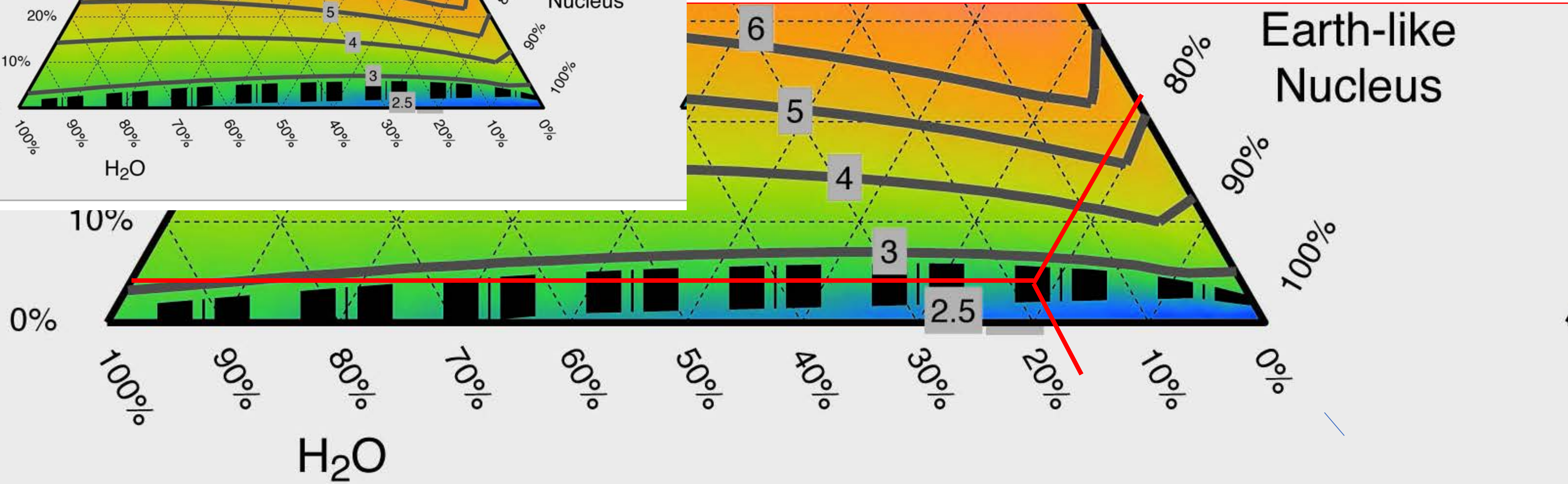

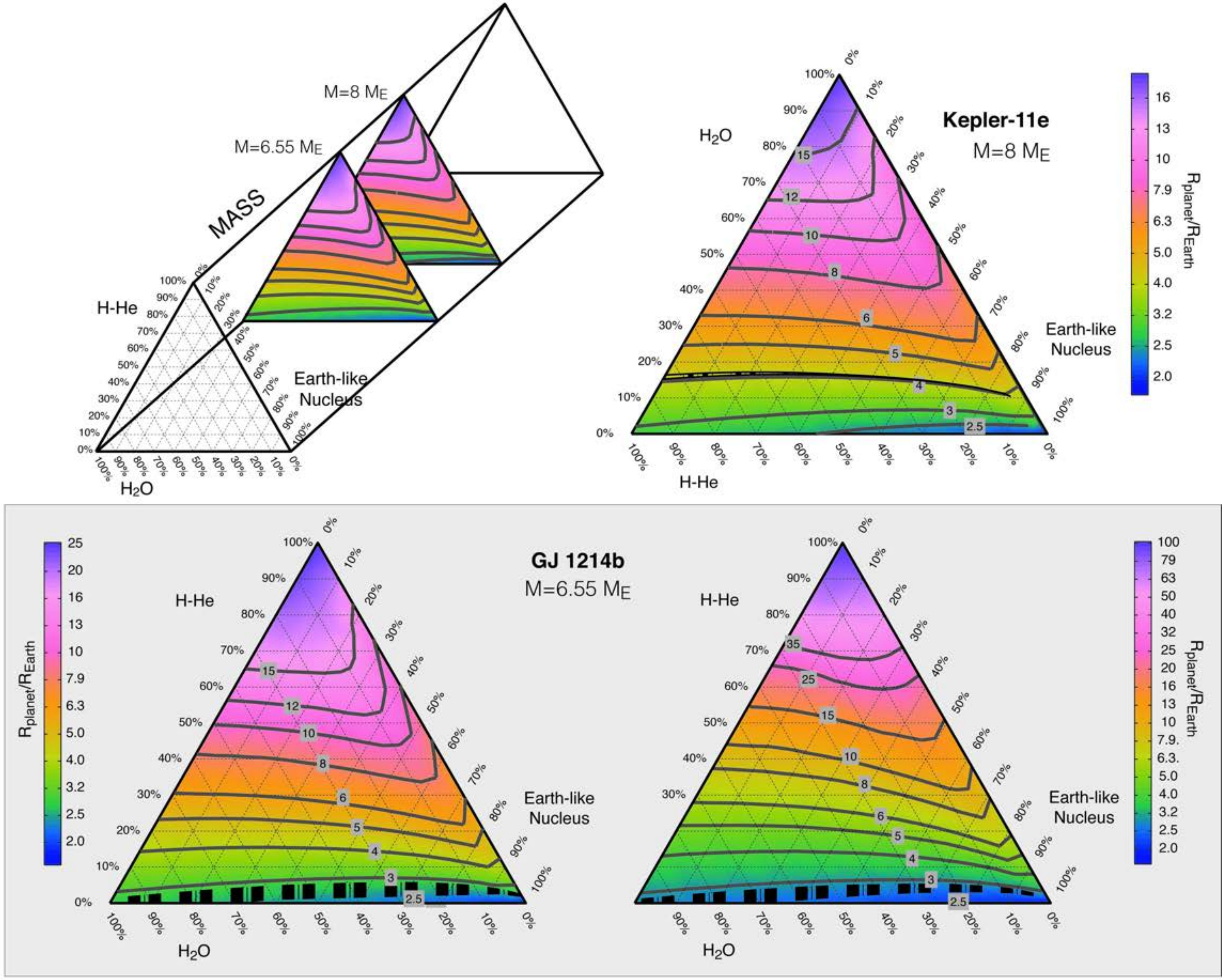

Ternary Diagrams for GJ 1214b and Kepler-11e. These triangular diagrams relate the composition in terms of earth-like nucleus fraction, water+ices fraction, and H/He fraction to total mass, to the radius for a specific planetary mass. Each vertex corresponds to 100%, and the opposite side to 0% of a particular component. The color bar shows the radius in terms of Earth-radii, and the grey lines are the isoradius curves labeled in terms of Earth-radii. The collection of ternary diagrams for a range of planetary masses forms a triangular prism. The black band shows the compositions constrained by data for GJ 1214b for a grain-free envelope (top left), and a grainy envelope (bottom right), and Kepler-11e for a grain free envelope (top right) as projected onto the planetary mass MMM from the ternary diagrams at M+ΔMM+Delta MM+ΔM and M−ΔMM-Delta MM−ΔM (where ΔM Delta MΔM are the uncertainty values taken from the observational data).

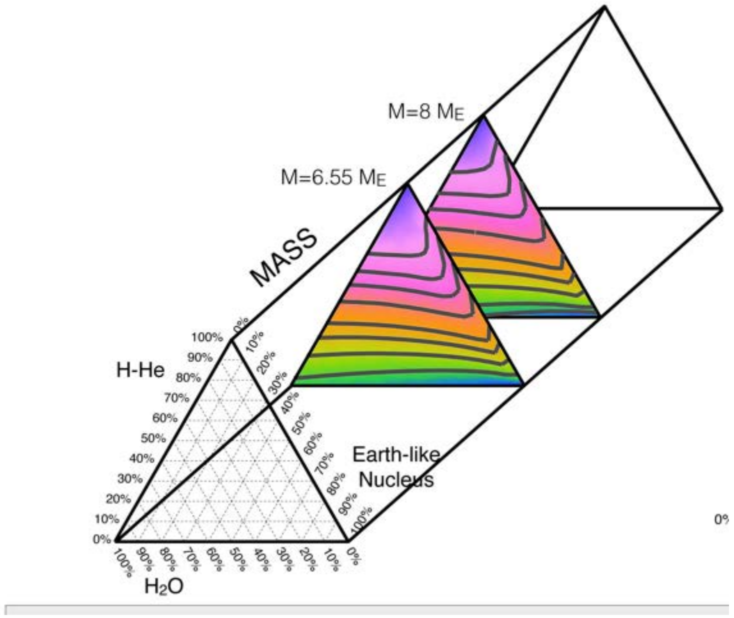

15% H2O + 30% H-He +55 % Earth like

18% H2O + 72% H-He +10 % Earth like

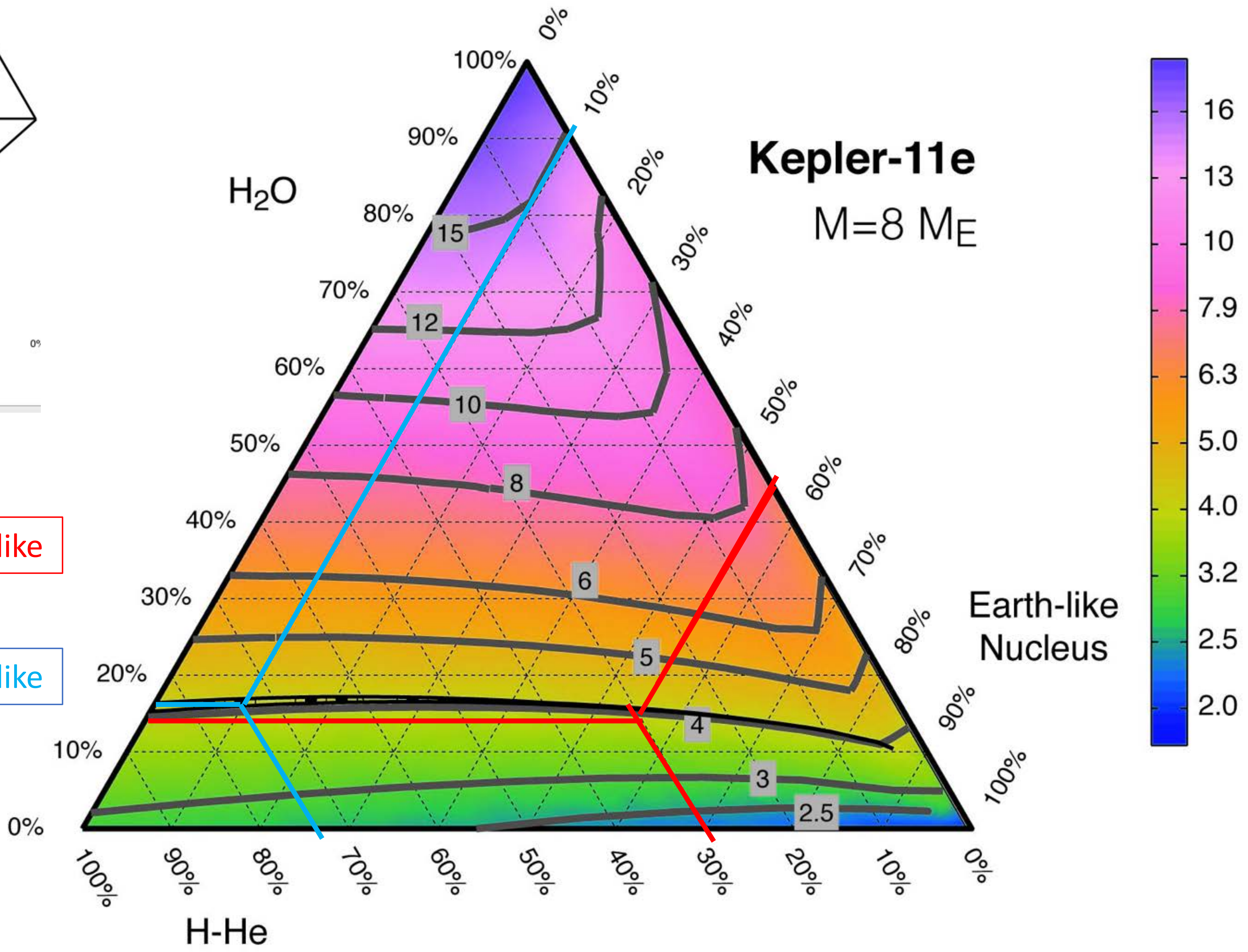

Histogram of planet radii, 2 peaks, super-Earth and Mini-Neptune

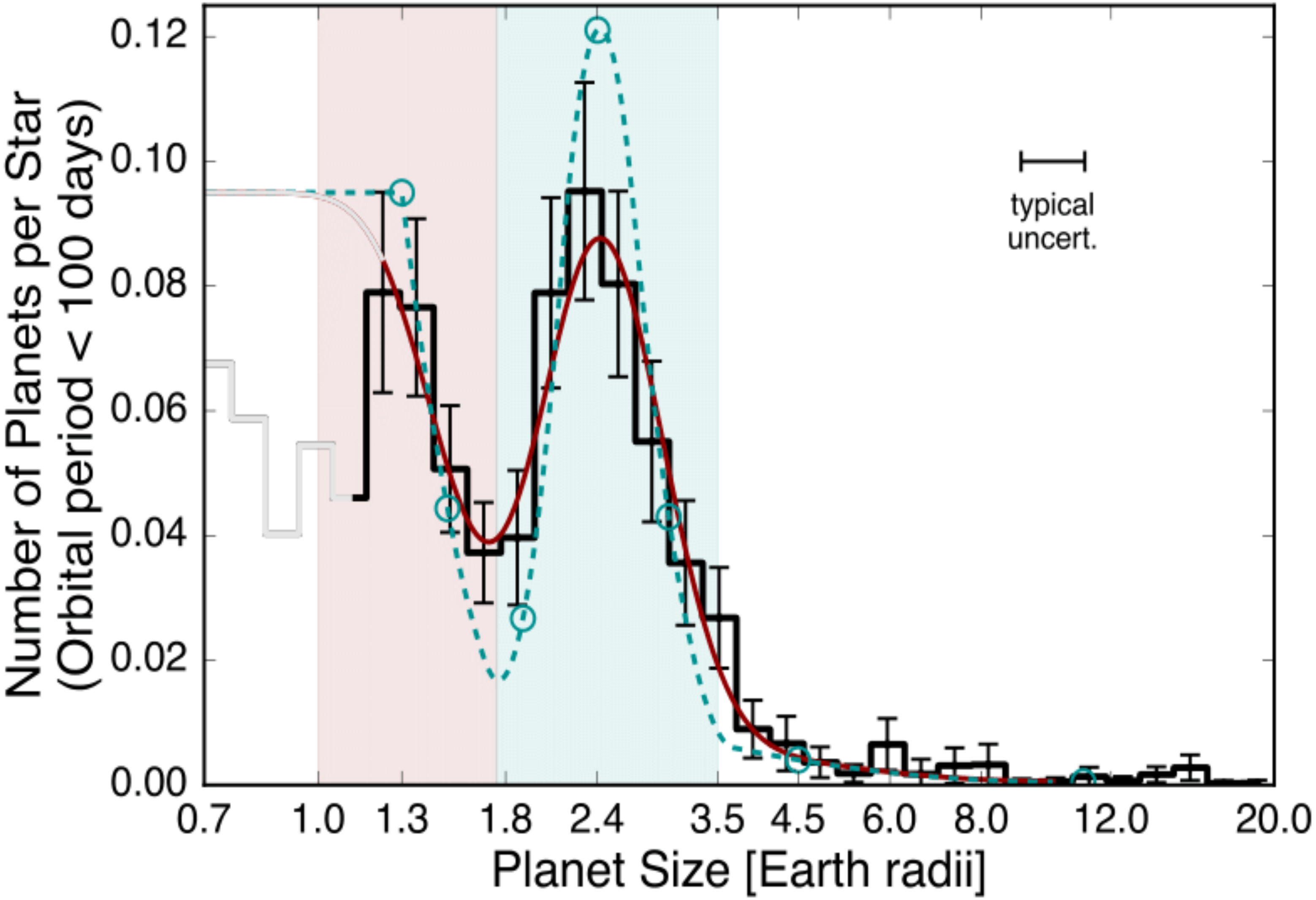

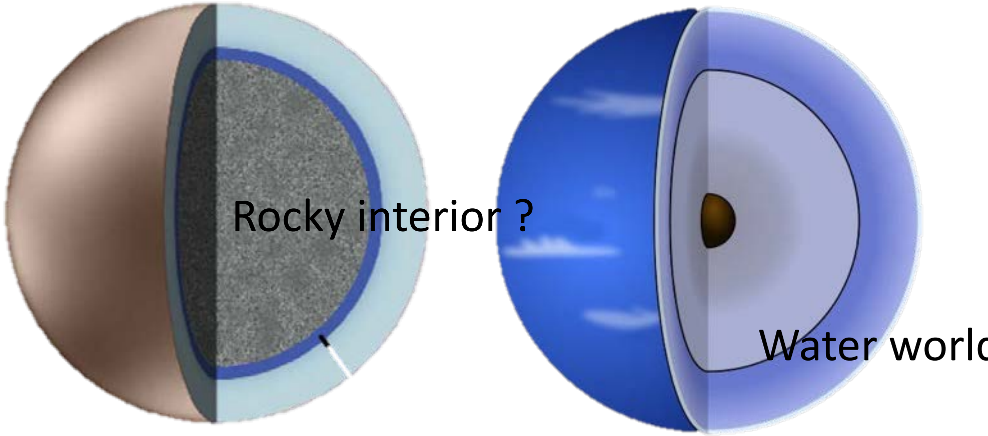

Completeness-corrected histogram of planet radii for planets with orbital periods shorter than 100 days.

Lightly shaded regions encompass our definitions of “super-Earths” (light red) and “sub-Neptunes” (light cyan). The dashed cyan line is a plausible model for the underlying occurrence distribution after removing the smearing caused by uncertainties on the planet radii measurements.

A fabulous diversity in the exoplanet zoo

Mass and Radius are not enough

5 Super Earth / Mini Neptunes in Kepler 11. Very different atmospheres !

(Lissauer et al. 2011, Valencia et al., 2013)

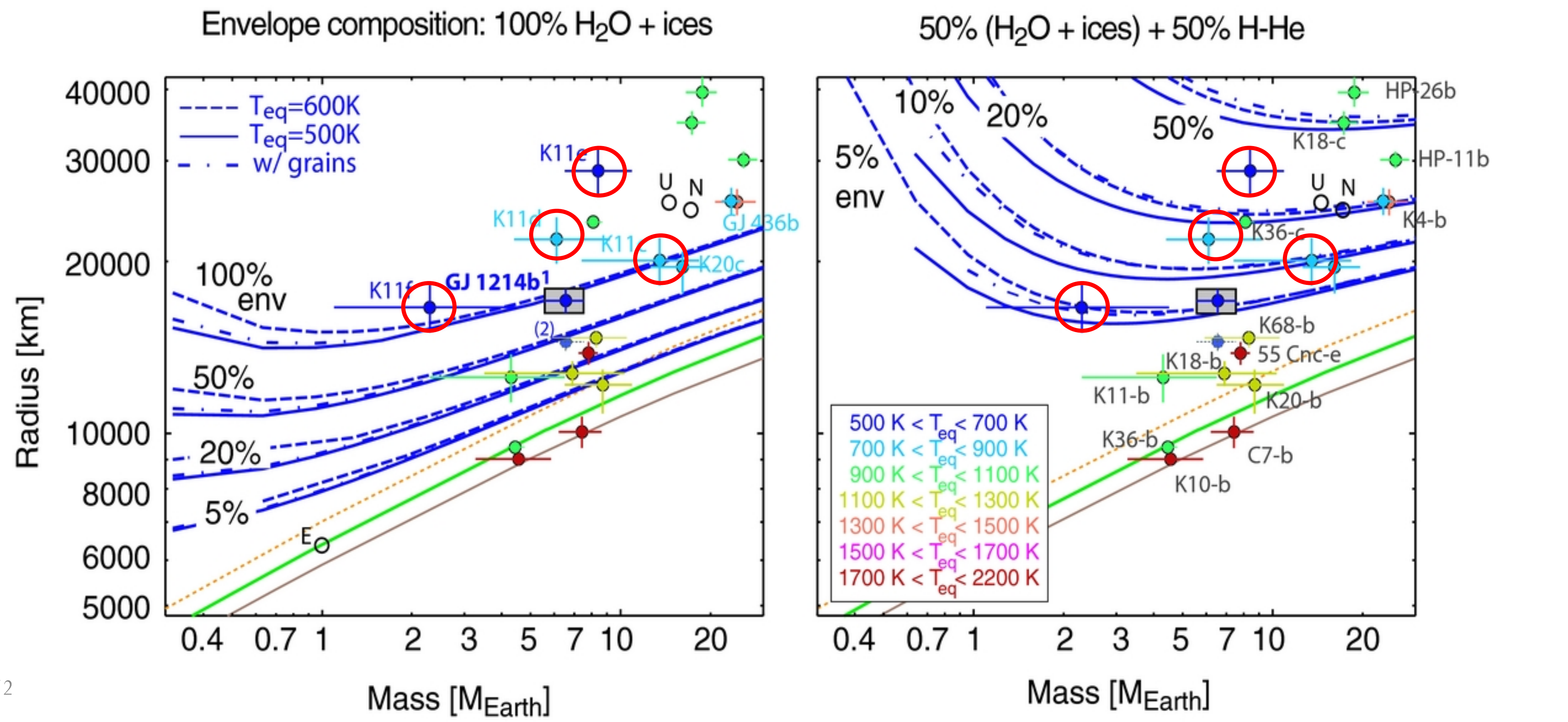

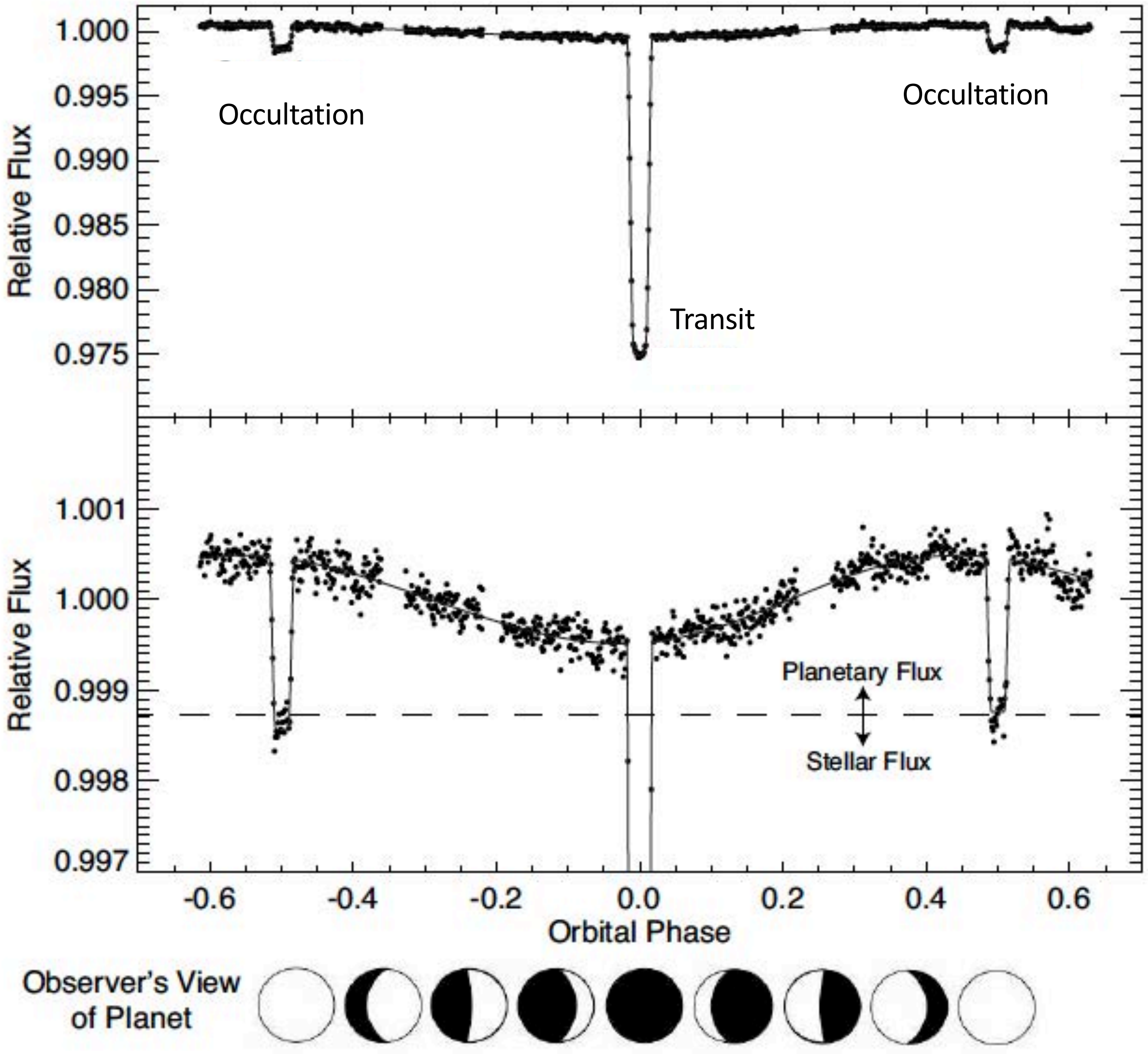

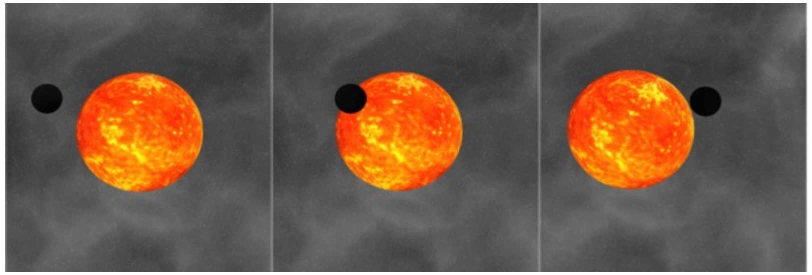

Transit depth:

$$\delta_{tra} = \left(\frac{R_p}{R_\star}\right)^2$$

Occultation depth:

$$\delta_{occ} = \frac{I_p}{I_\star}\left(\frac{R_p}{R_\star}\right)^2$$

Flux ratio day side of the planet / star

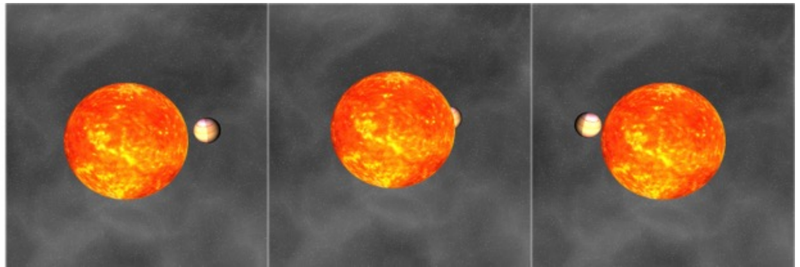

At different wavelength, because of different absorbing molecules-> different effective radius

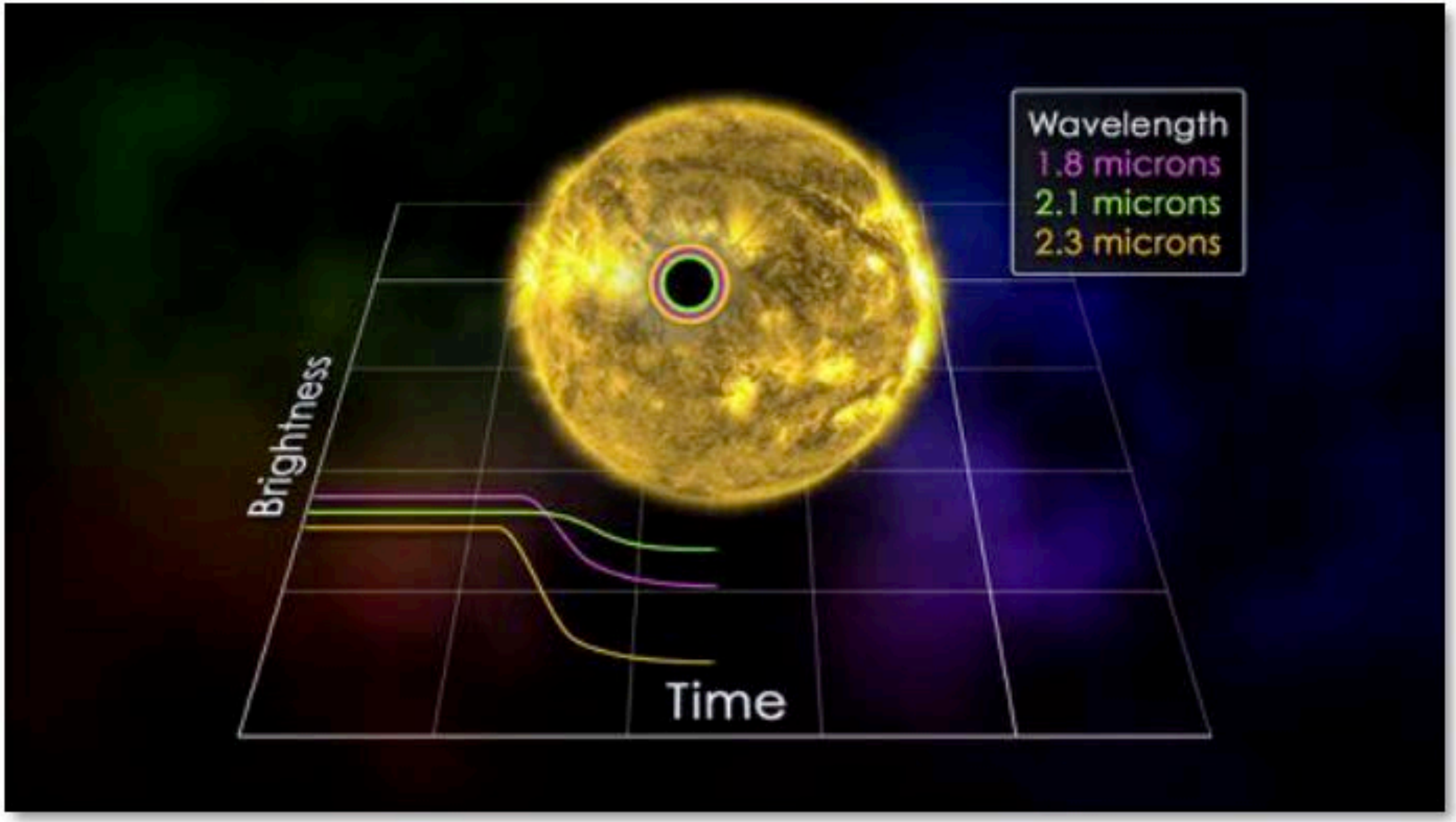

Scale height in an atmosphere

$$P(z) = P(z_{0)}\ exp\left(-\frac{Z-Z}{H}\right)$$

Pressure falls off exponentially with height in atmosphere with uniform temperature.

$H = \left(\frac{RT}{Mg}\right)$ has the dimension of distance and is called, the scale height.

M is the mean molecular mass, 2.3 g/MOL for hot Jupiter, 28 g/MOL for Earth

Atmosphere of gazeous planets more extended than Earth like !

scale height is the perpendicular distance over which a particular physical variable drops by a factor of e

I) Transit

Spectroscopy

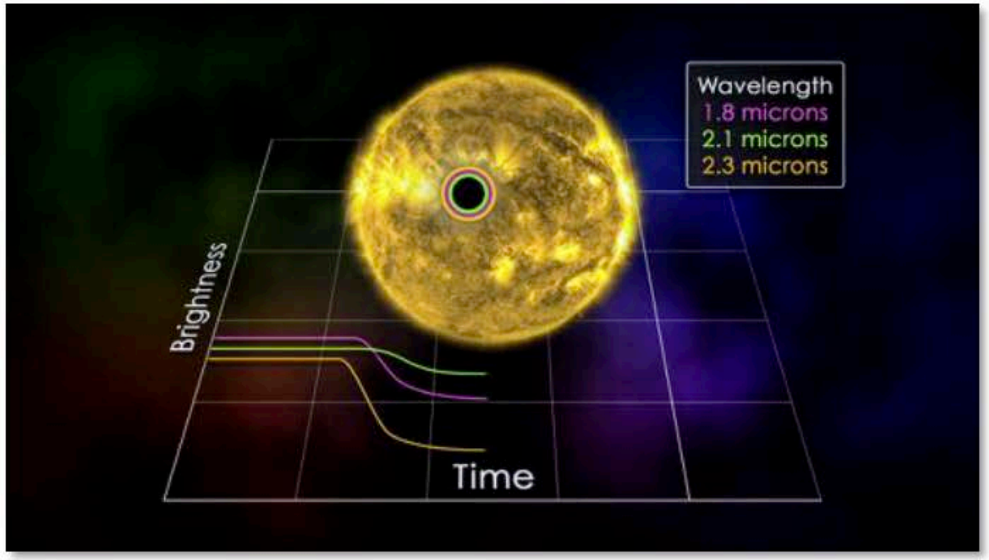

Effect of mean molecular weight

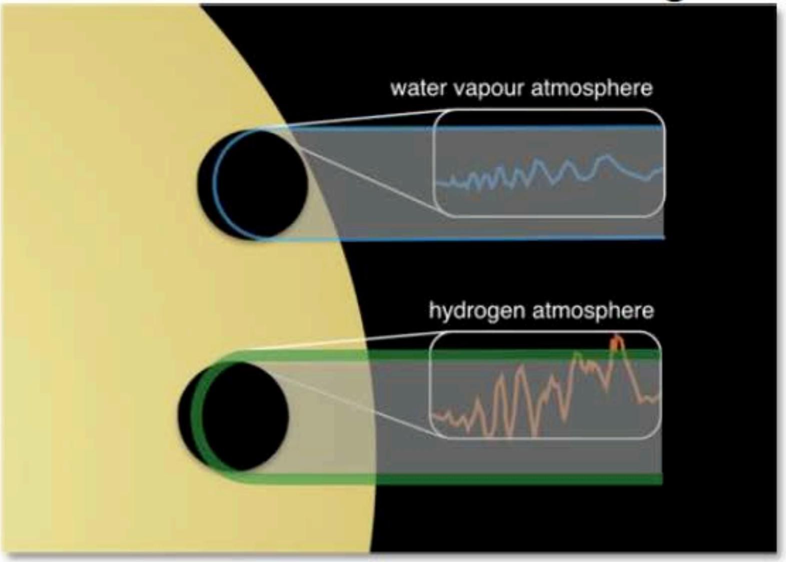

- The expected depth of the absorption features in a haze-free atmosphere is proportionalto the atmospheric scale height

Variation of transit depth:

$$\Delta\delta_{tra} = \frac{\pi (R_p + N_H H)^2}{\pi R_\star^2} - \frac{\pi R_p^2}{\pi R_\star^2} \approx 2 N_H \delta_{tra} \left(\frac{H}{R_p}\right)$$

Scale height: $H = \frac{RT}{Mg}$; Number of scale heights: $N_H \approx 7$ (for low resolution)

→ Transit spectroscopy easier for high scale height (e.g. hot giant planets)

I) Transit

Spectroscopy

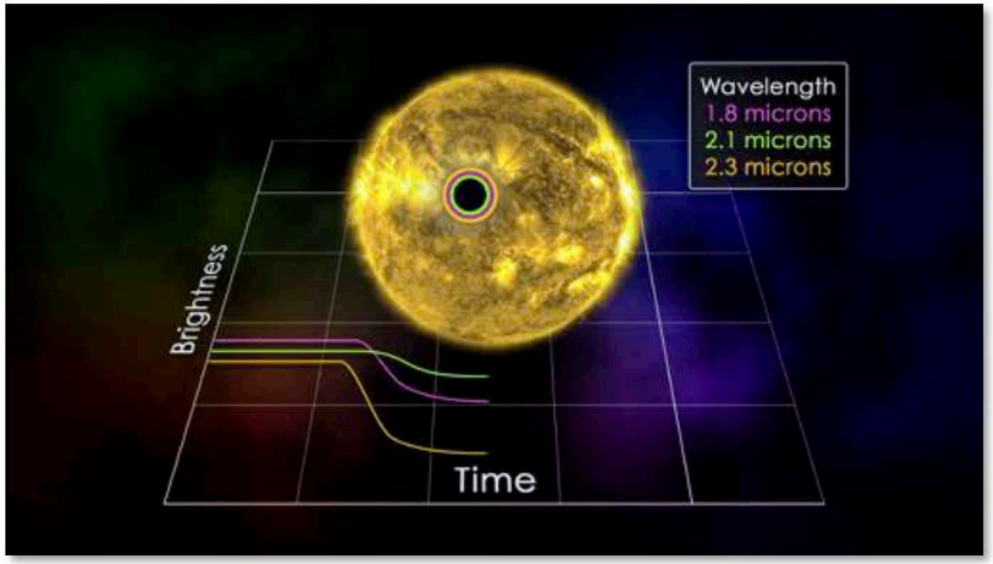

Effect of mean molecular weight

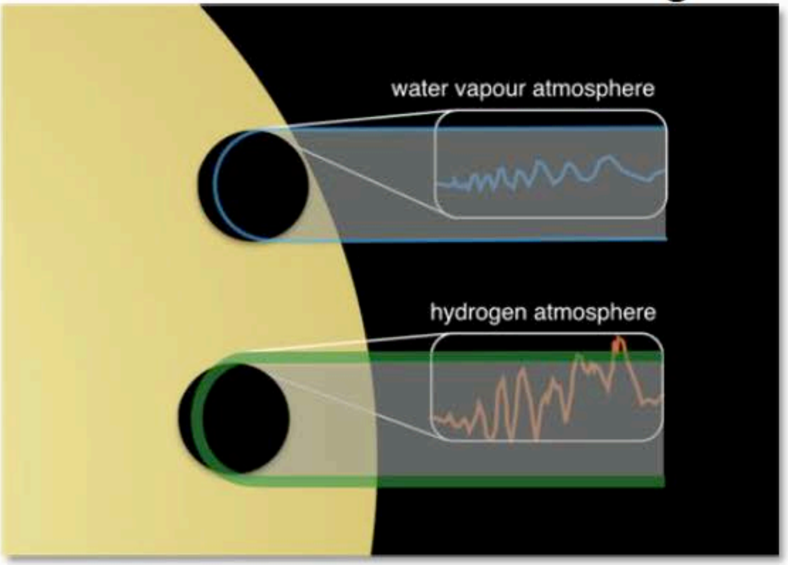

M = mean mass of one mol of atmospheric particles = 0.029 kg/mol for Earth

T = mean atmospheric temperature in kelvins = 250 K for Earth

R=Molar gas constant, units of energy per temperature increment per mole, meaning Avogadro constant multiplied by the Boltzmann constant k

Variation of transit depth:

$$\Delta\delta_{tra} = \frac{\pi(R_p+N_H H)^2}{\pi R_\star{}^2} - \frac{\pi R_p{}^2}{\pi R_\star{}^2} \approx 2N_H\delta_{tra}\left(\frac{H}{R_p}\right)$$

Scale height: $H = \frac{RT}{Mg}$; Number of scale heights: $N_H \approx 7$ (for low resolution)

For an Sun-like star:

- Hot Jupiter (T=1300 K, g=25 m s^{-2}, M=2.3 g/mol): $\delta_{tra} \approx 0.01$, $\Delta\delta_{tra} \approx 4.10^{-4}$
- Earth-like planet (T=280 K, g=10 m s^{-2}, M=28g/mol): $\delta_{tra} \approx 10^{-4}$, $\Delta\delta_{tra} \approx 2.10^{-6}$

The Sun's planets are cold

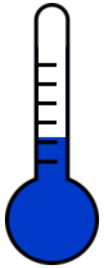

SOME KEY O, C, N, S MOLECULES ARE **NOT** IN GAS FORM

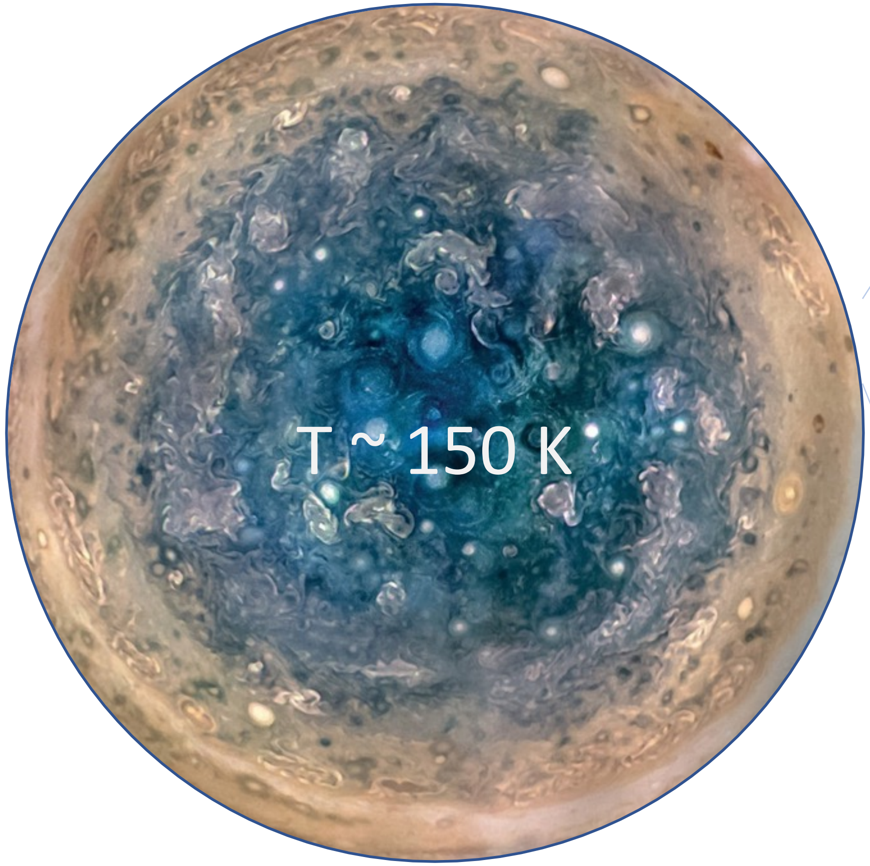

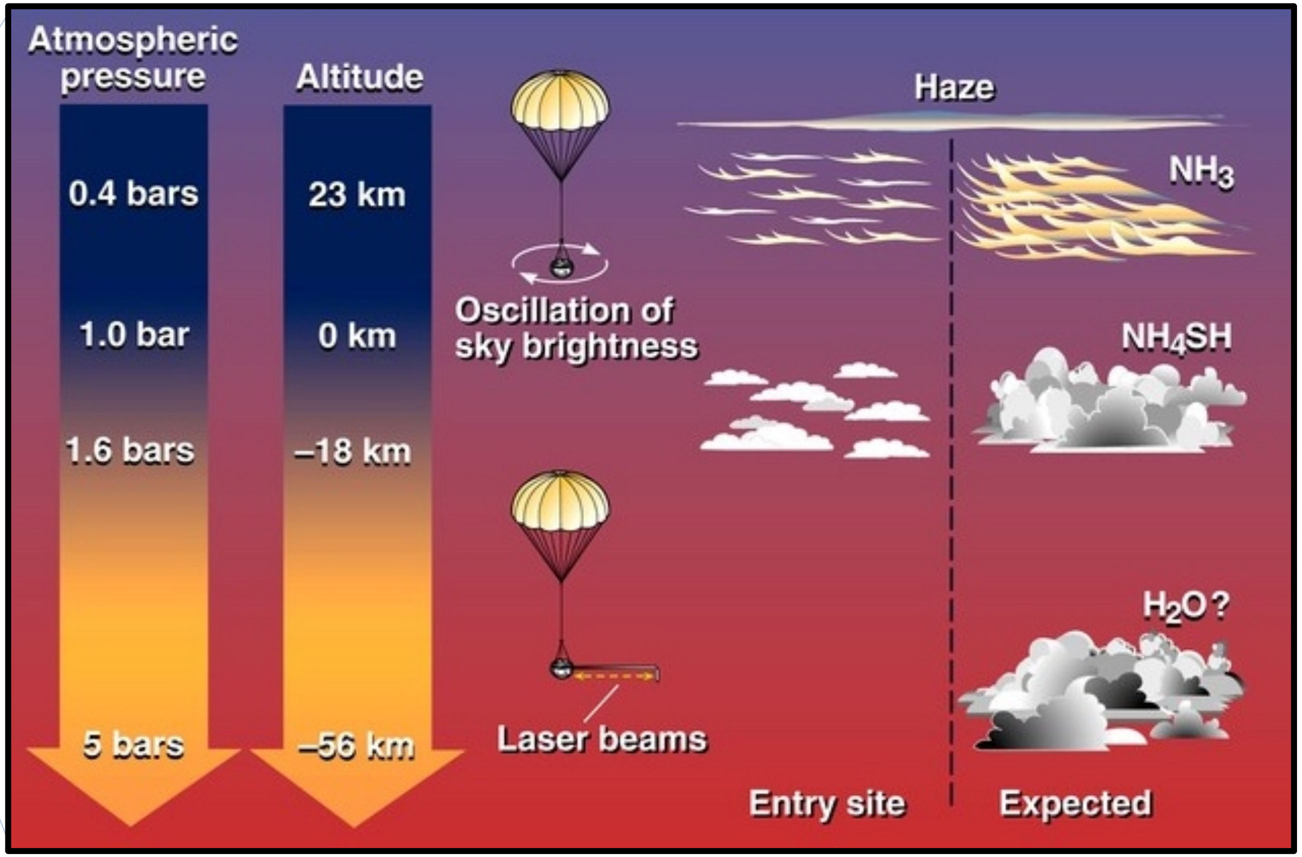

Warm/hot exoplanets

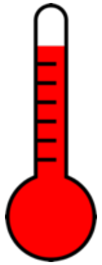

O, C, N, S (Ti, VO, Si) molecules are in gas form

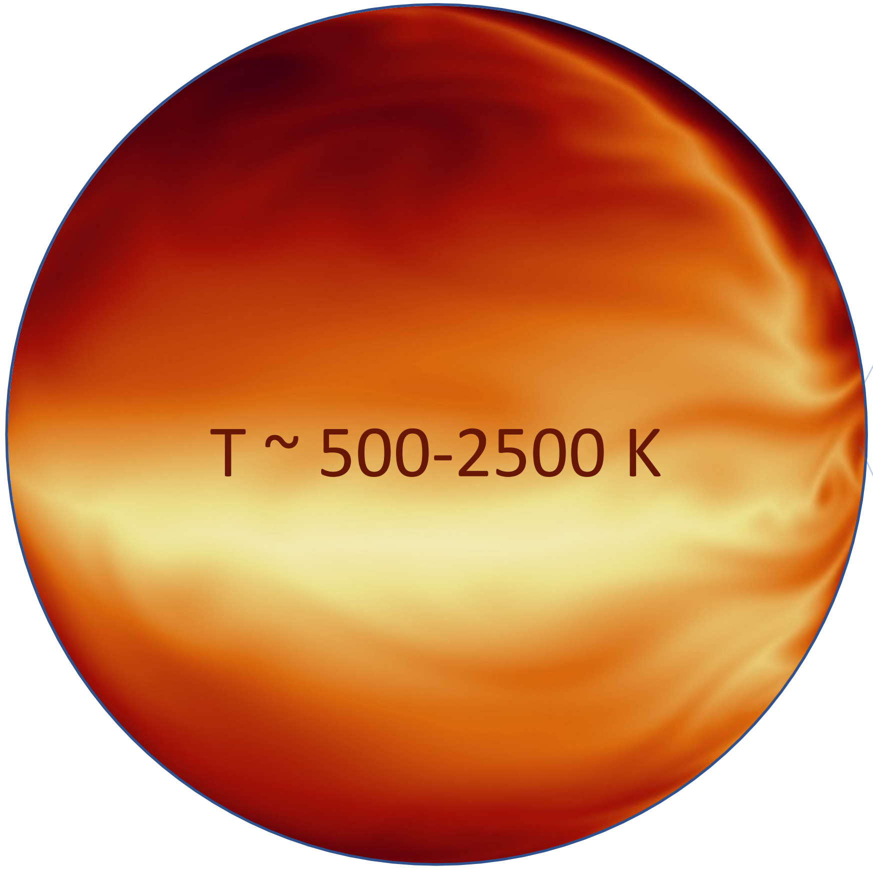

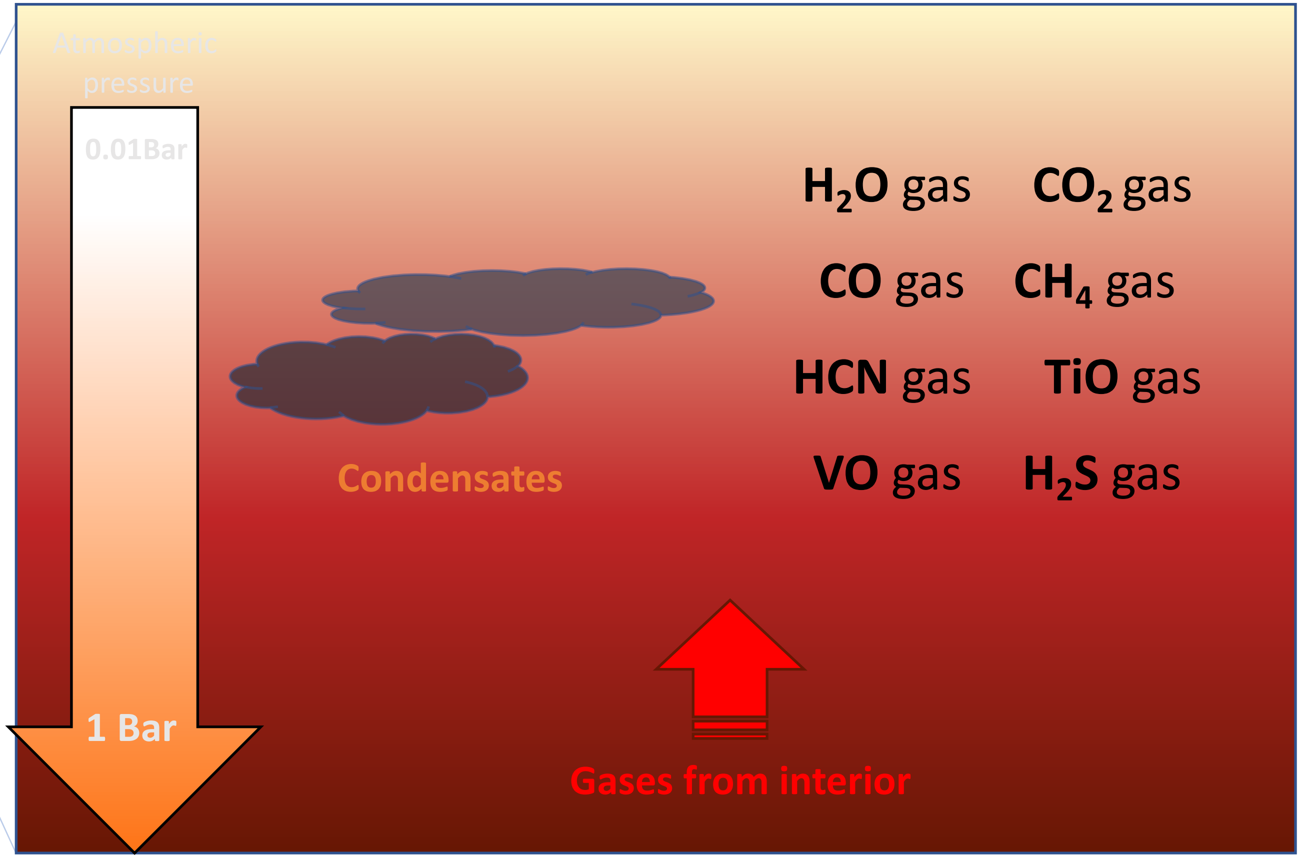

MARS ATTACKS!

LOWELL OBSERVATORY

BULLETIN No. 103

Vol. IV

FURTHER EVIDENCE OF VEGETATION ON MARS

William M. Sinton

There has long been evidence pointing to the presence of vegetation on Mars. Photographs taken by E. C. Slipher at the Lowell Observatory have for decades shown the seasonal variation of the intensity of the dark regions. Every spring and summer a wave of darkening spreads from the polar regions toward the equator (1). In addition to the seasonal variation there are non-systematic changes; areas that were never dark have become dark, and a few dark areas have become light and blended into the desert regions. A striking case of the appearance of a dark region occurred in 1954 when an area of 580,000 square miles at 240° longitude and 20° latitude was newly dark (2). The region in which it is situated has, however, been undergoing development for many years.

The author using the 61-inch telescope of the Harvard College Observatory during the 1956 opposition made a new test for the presence of organic molecules on Mars (3). Organic molecules possess strong absorption bands at 3.5 μ as a result of the resonance of their carbon-hydrogen bonds. It was found that in the plants tested, this band was double, most likely as a result of interaction between a pair of hydrogen atoms attached to the same carbon atom, as occurs in paraffin molecules.

The results of the 1956 observations indicated the presence of the band in the light reflected from Mars, but they left some doubt as to the reality of the absorption. Furthermore, the regions of Mars which produced the absorption were not ascertained in this work. At the 1958 opposition the test was made again with improved equipment and the reality and distribution of the band were established.

Detection of 3 molecular bands in 1956…

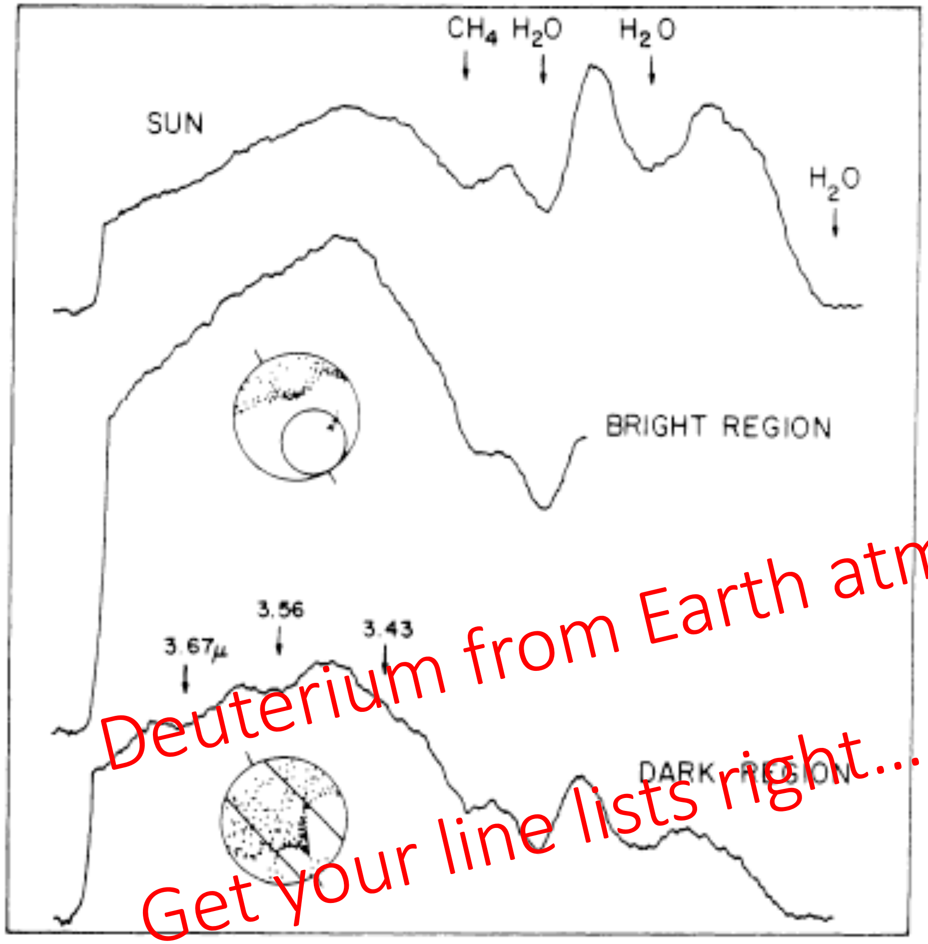

Figure 1. Infrared spectra of Mars and the sun. The upper curve shows the spectrum of the sun with absorptions produced by water and methane in the earth's atmosphere. The middle curve is the spectrum of Amazonis, the desert region within the circle in the sketch. The bottom curve shows the spectrum of a strip across Mars as shown in the sketch and includes Syrtis Major. The last spectrum shows the absorptions supposedly due to organic molecules.

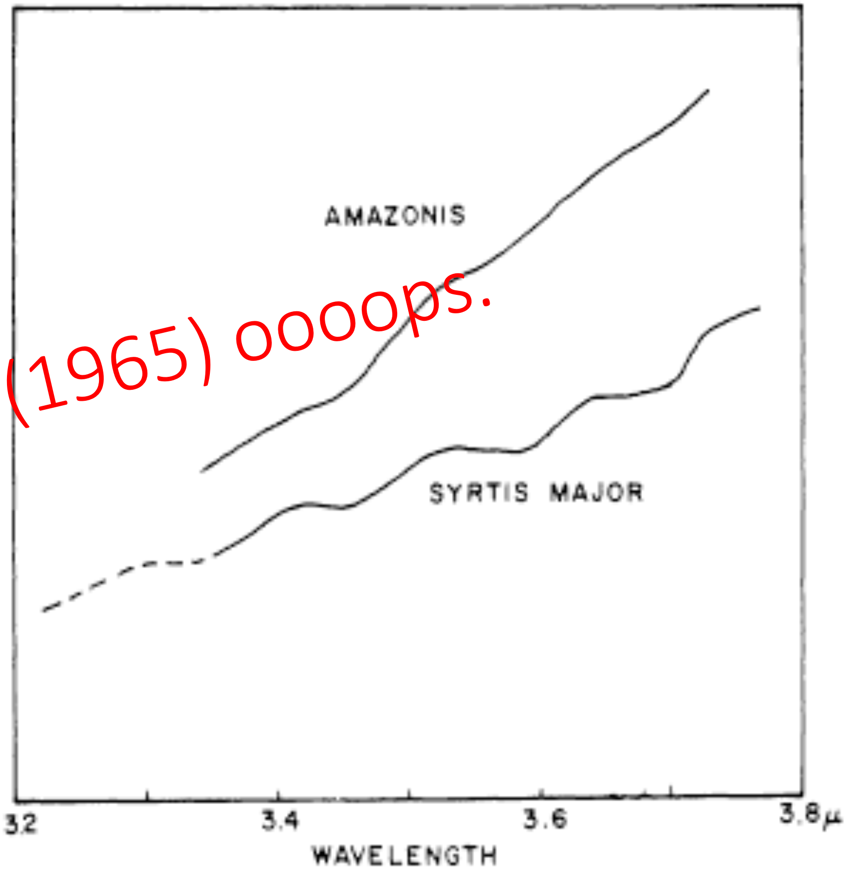

Figure 2. The spectra of Amazonis and Syrtis Major after division by the solar spectrum. The dashed portion of the curve is the region through strong methane and water-vapor absorption and the variations are not believed to be significant.

Deuterium from Earth atmosphere… (1965) oooops.

Get your line lists right…

We need good line lists…
Exomol and other groups

Water vapour absorption as a function of temperature and wavelength

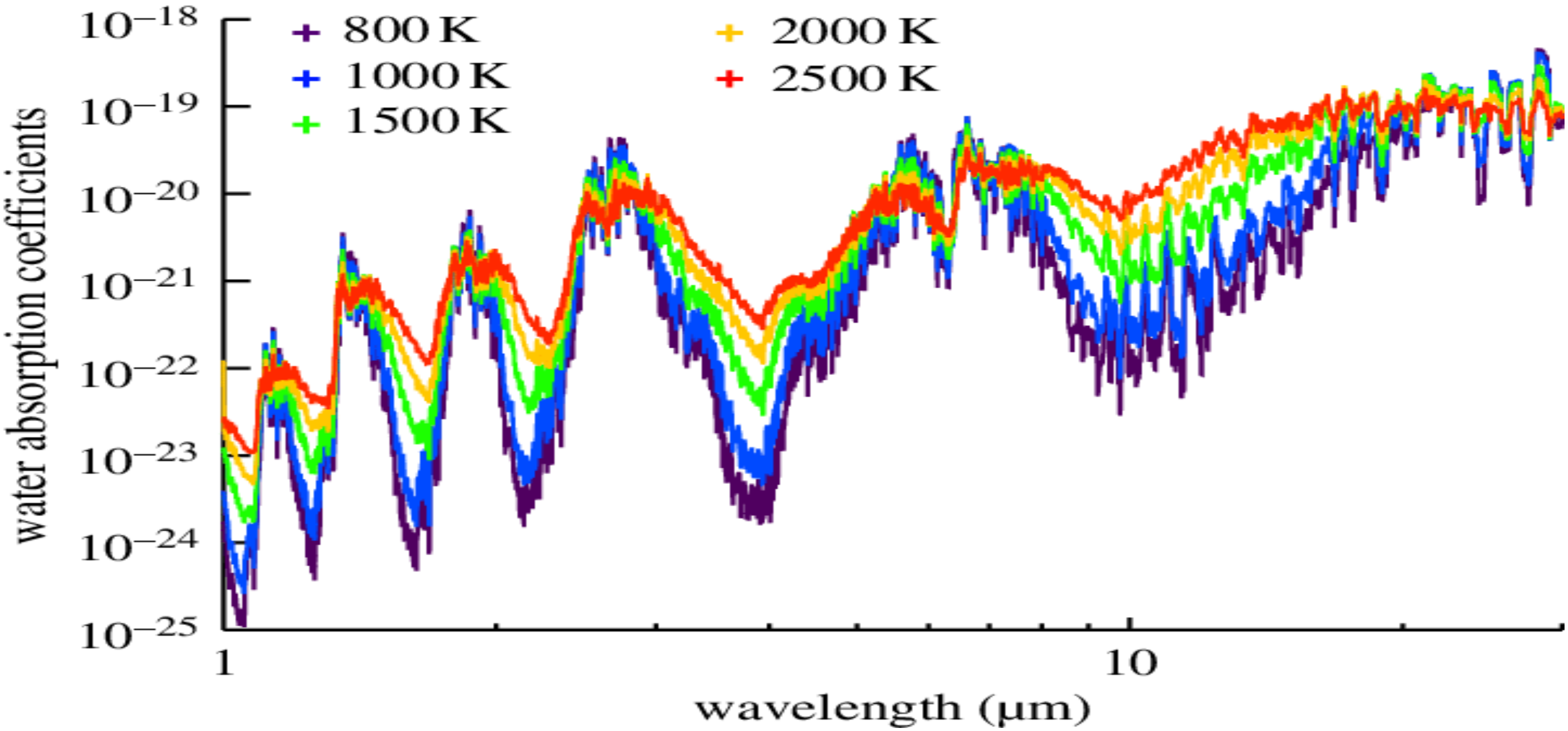

Key molecules absorbing in IR

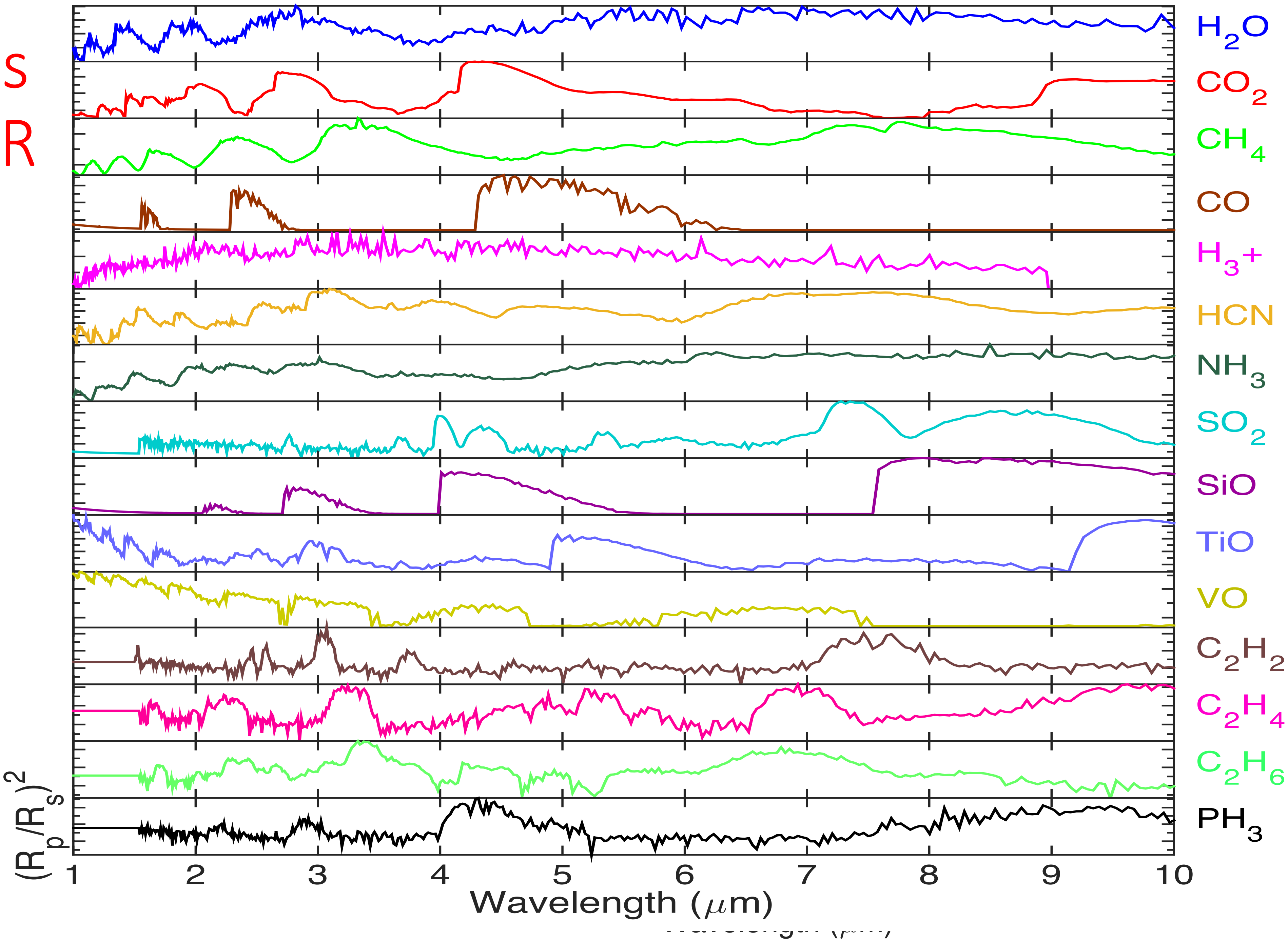

Temperature-Pressure profile in hot Jupiters

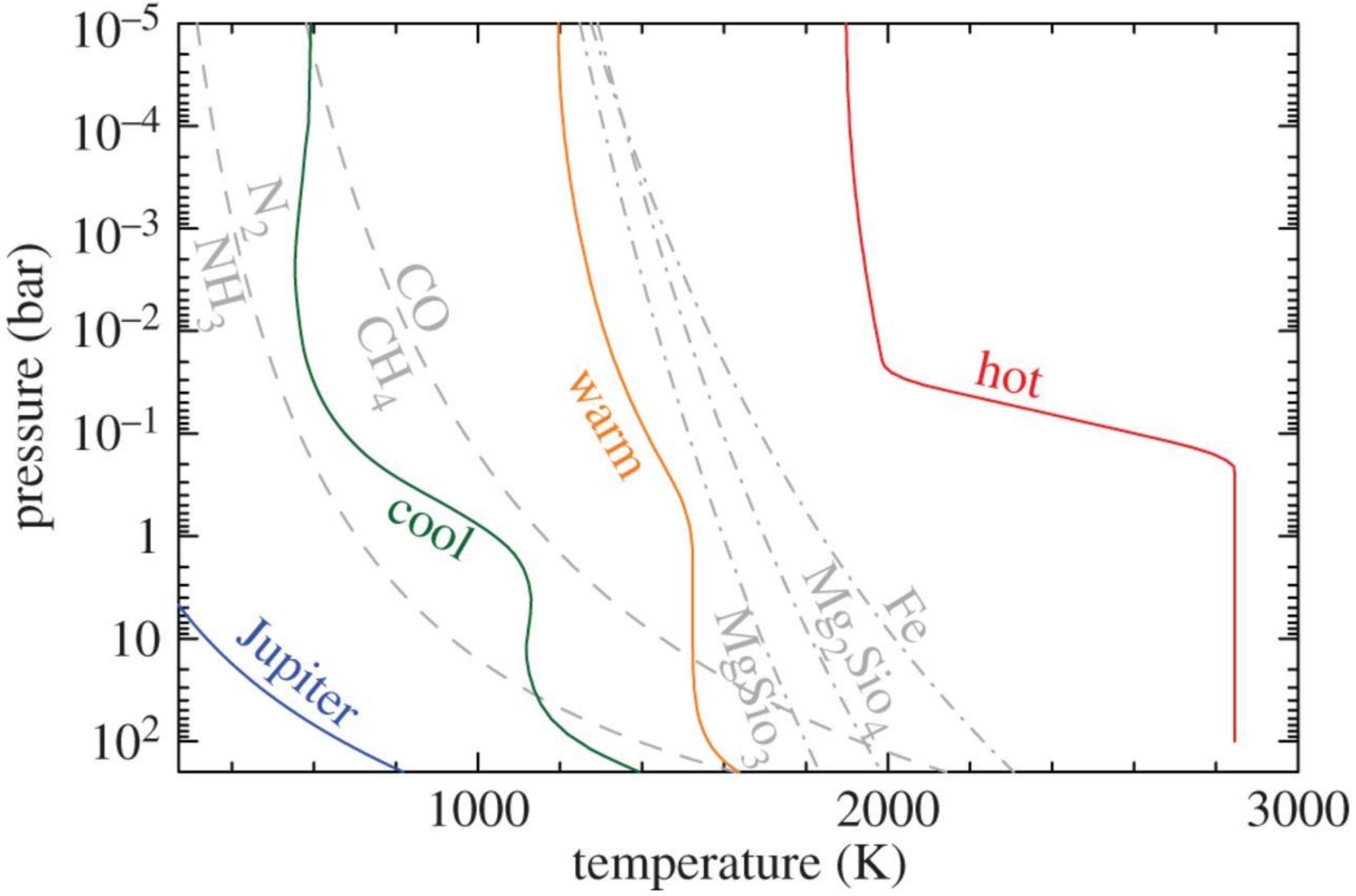

Thermal profiles for the hypothetical 'hot', 'warm' and 'cool' exoplanets (as labelled) used in the chemical models shown in figure. The grey dashed lines represent the equal-abundance curves for CH4–CO and NH3–N2. Profiles to the right of these curves are within the N2 and/or CO stability fields. The dot-dashed lines show the condensation curves for MgSiO3, Mg2SiO4 and Fe (solid, liquid). Moses 2014

Temperature matters !

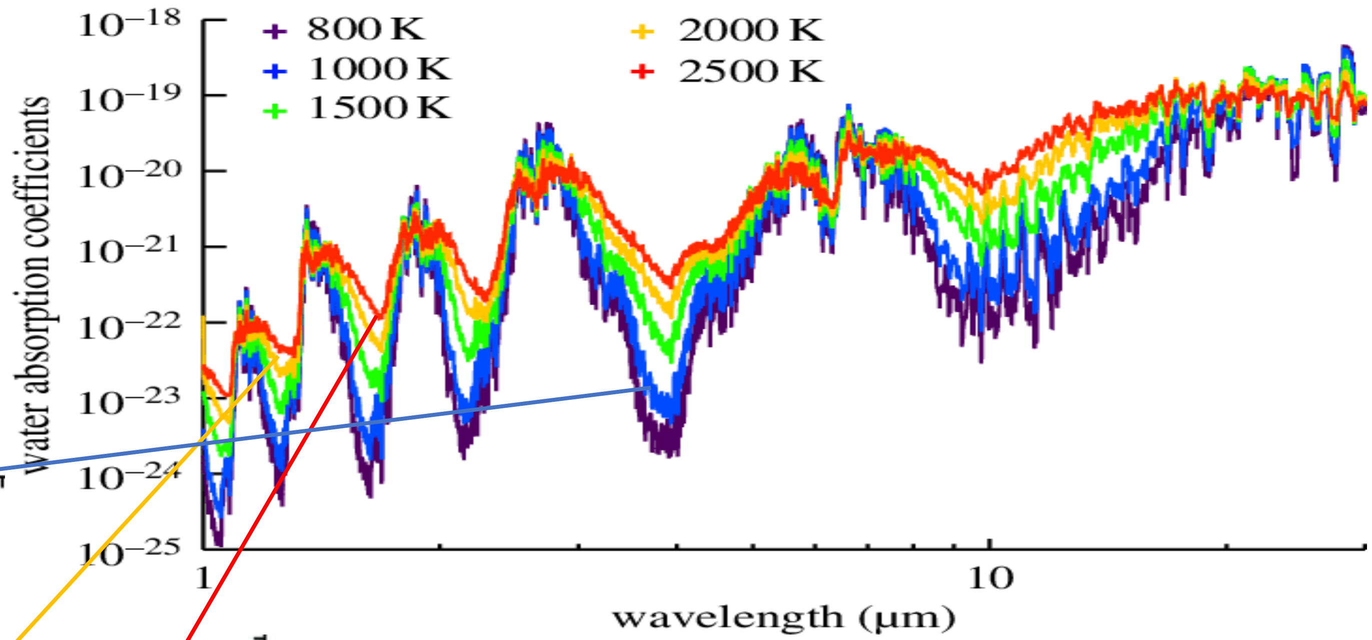

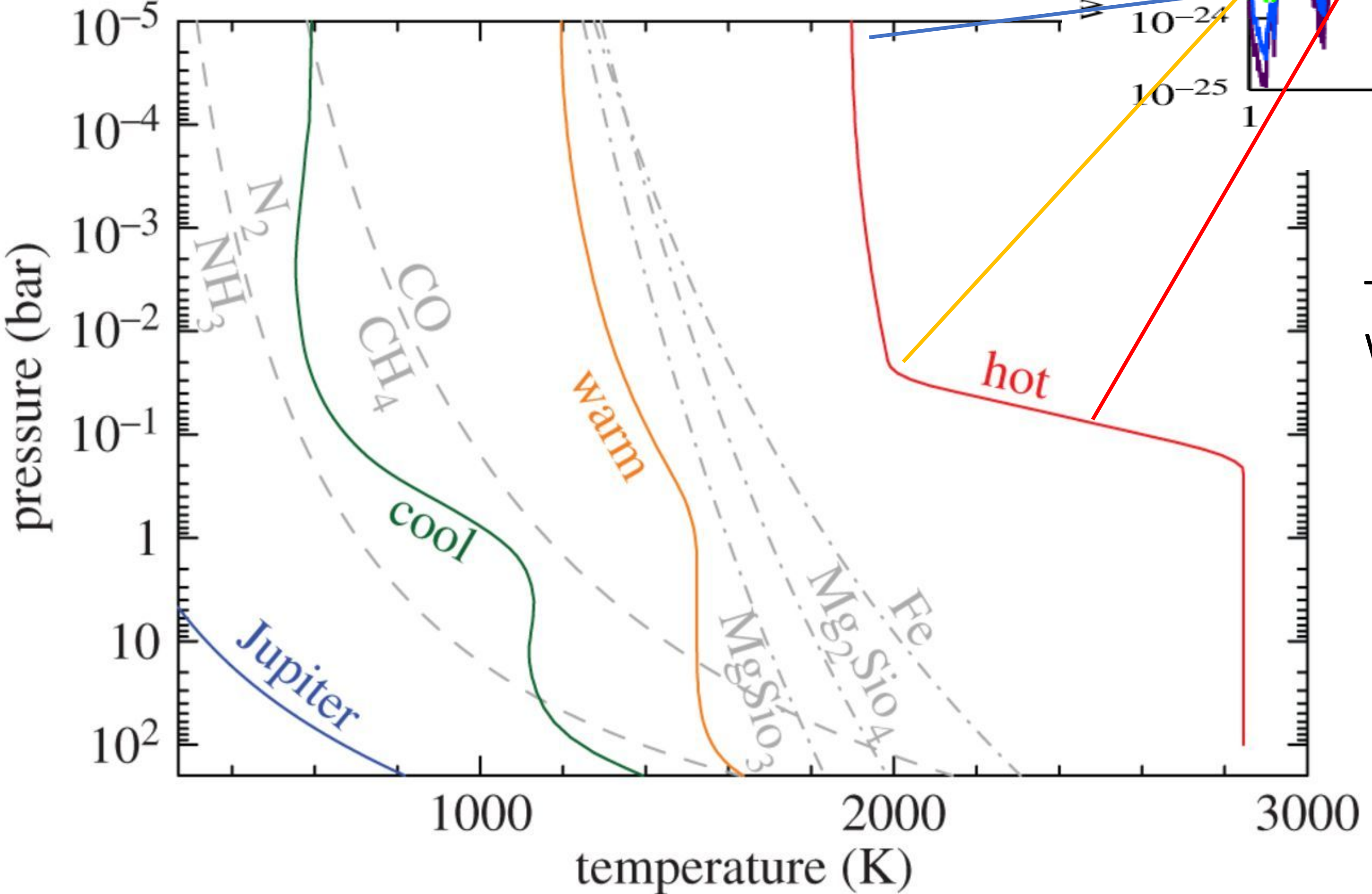

Temperature varies in the atmosphere

Water absorption depends on temperature too !

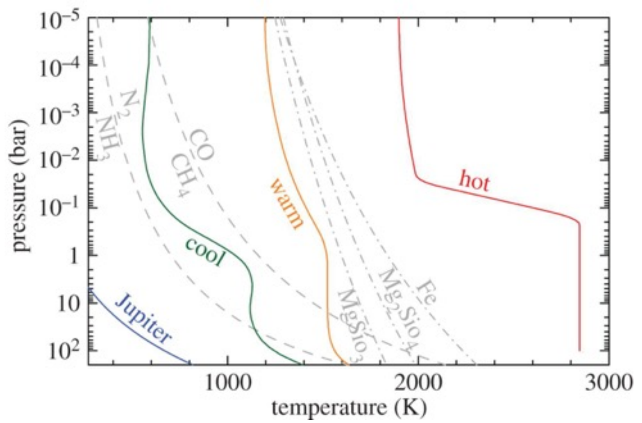

Temperature-pressure Profile

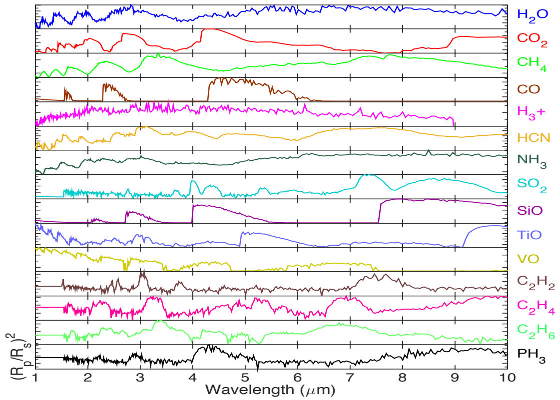

Molecules lines list

Chemistry in equilibrium

Which molecules are expected to be abundant ?

(a) (i)

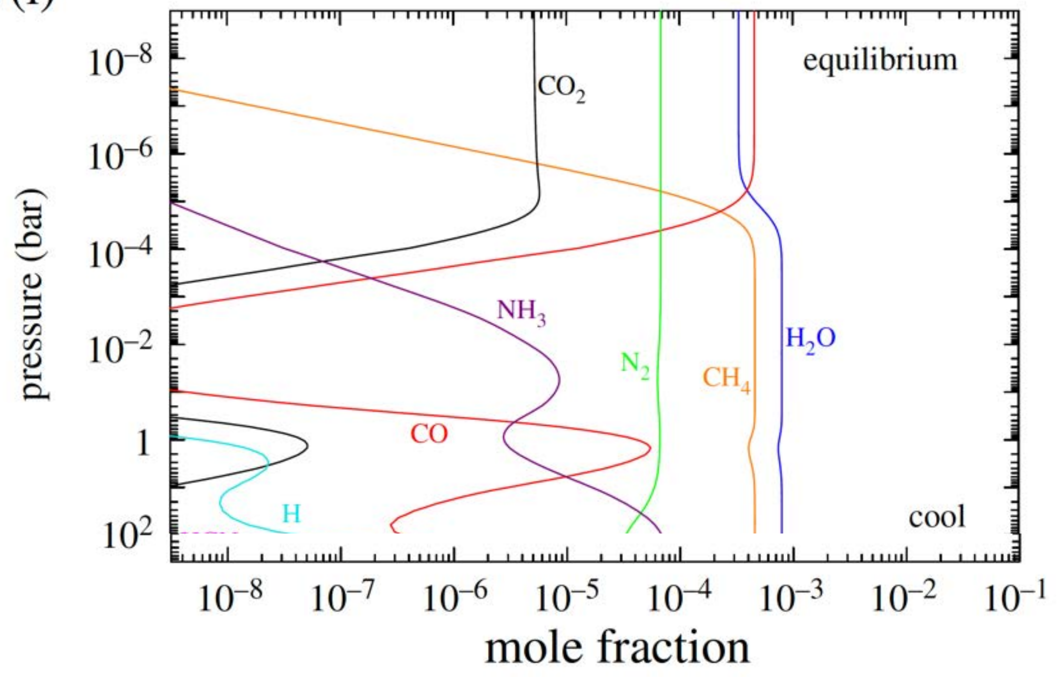

(iii)

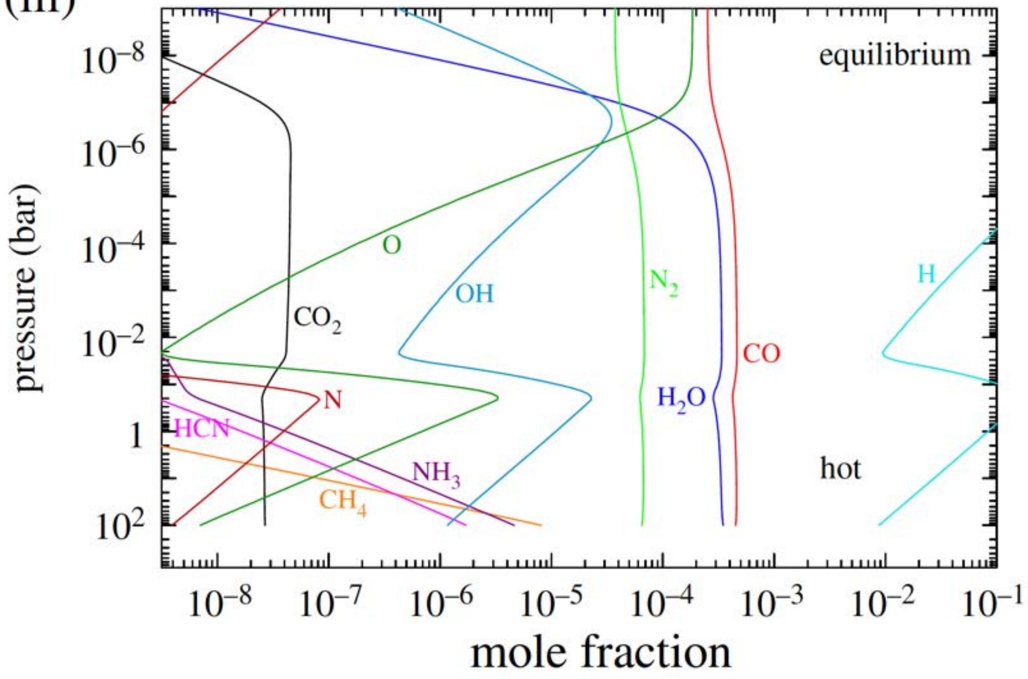

Spectral signature of a transiting planet

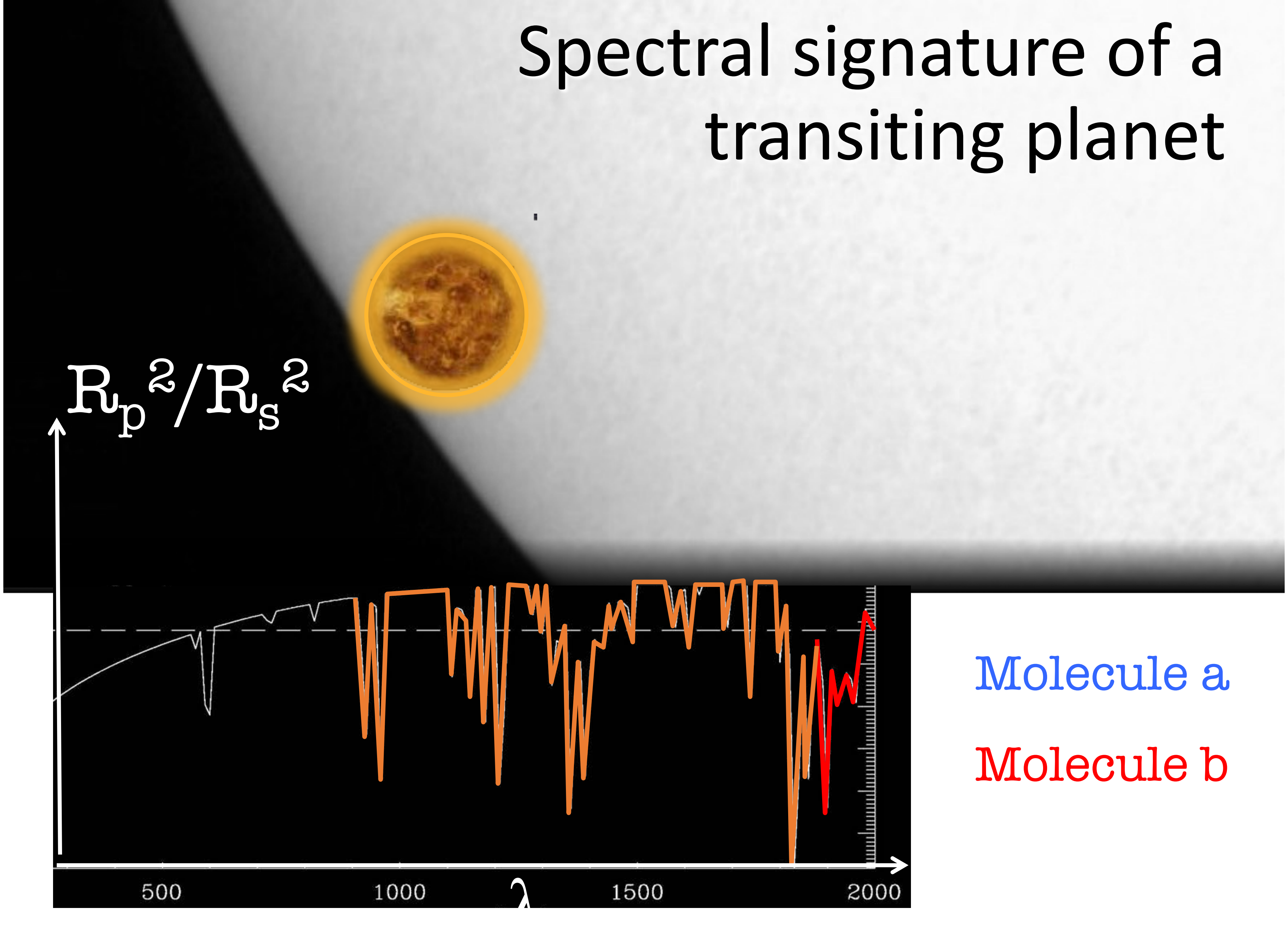

Molecule a

Molecule b

First detection of Na !

Confirmed also from the ground
Sing et al., 2008, Snellen et al. 2009, etc

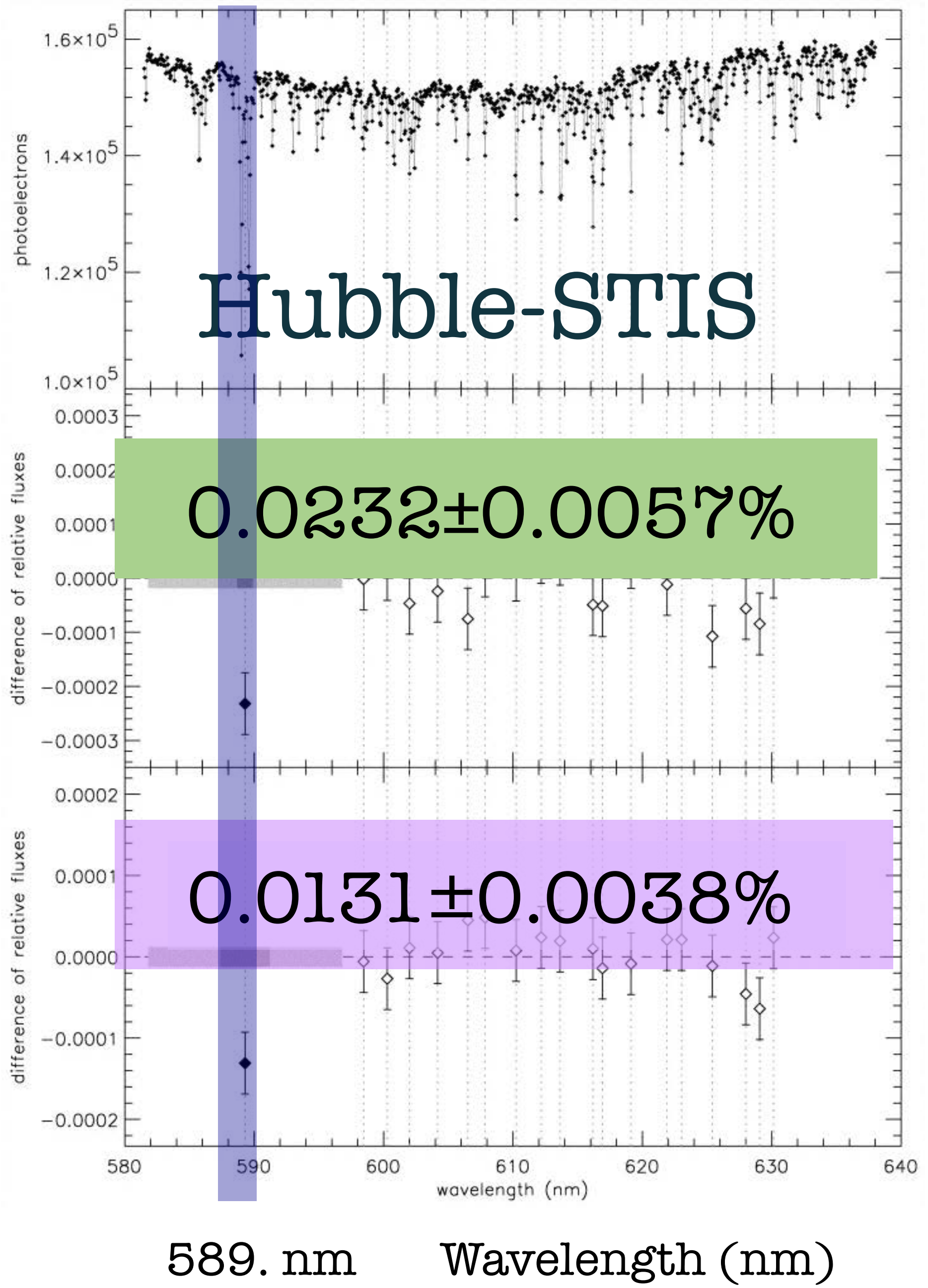

Charbonneau *et al.*, 2002

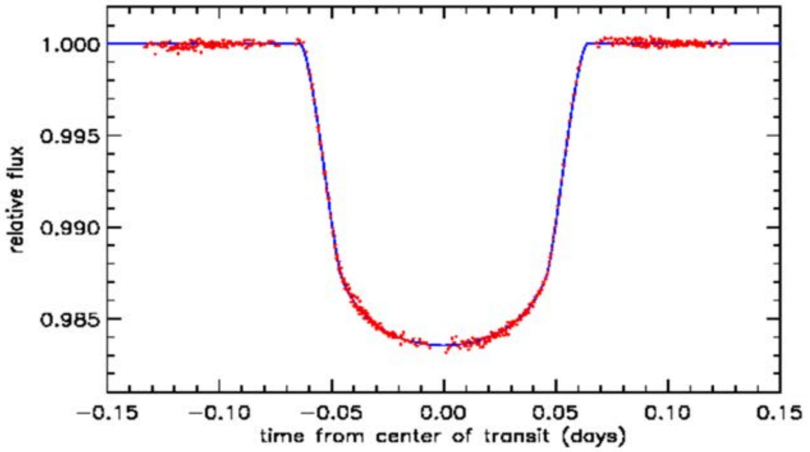

Charbonneau et al. (2000)

First detection of Na !

Confirmed also from the ground
Sing et al., 2008, Snellen et al. 200

the transmission spectra can be explained by the combination of the centre-to-limb variation and the Rossiter-McLaughlin effect.

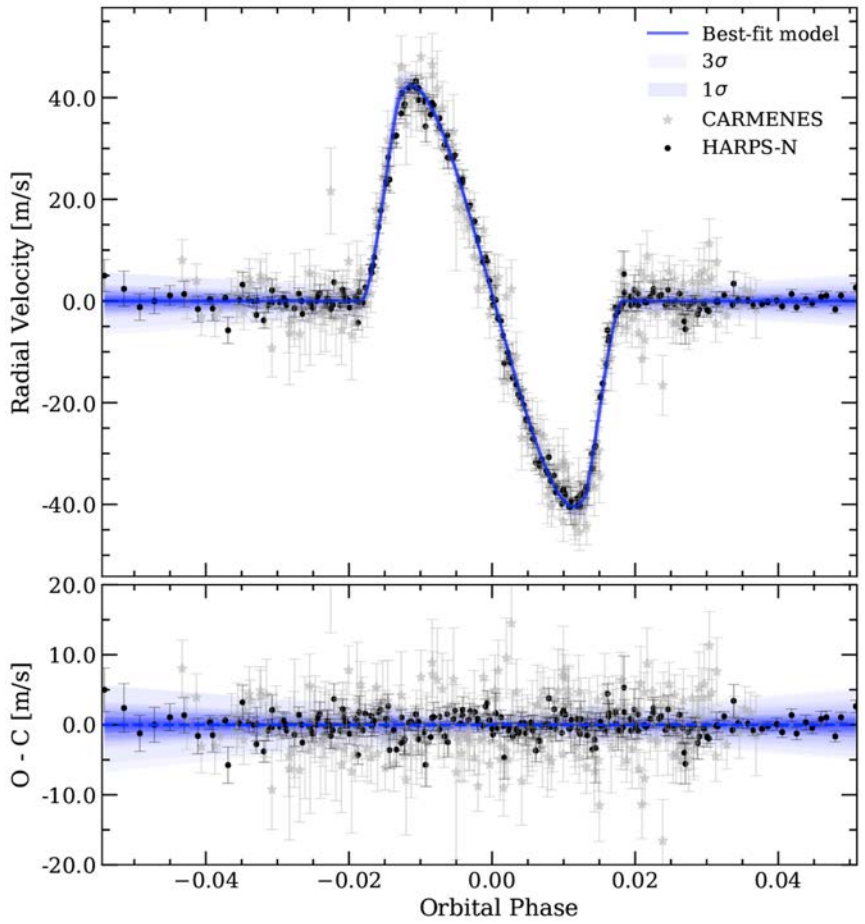

Rule of thumb, if atomic species or molecules are both present in the star and the planet, we'd better be cautious….

N. Casasayas-Barris et al., 2021

STIS: Lyα HD 209458b

~9% absorption in the Lyα line,
No red/blue shift

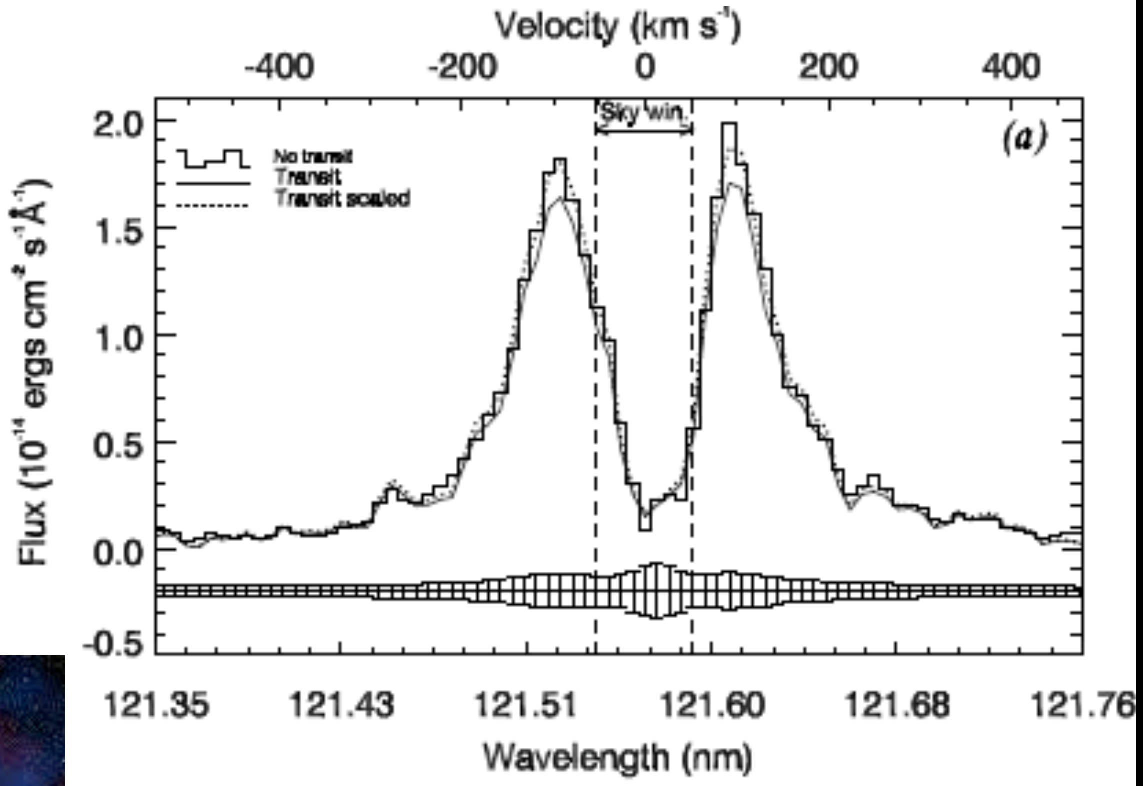

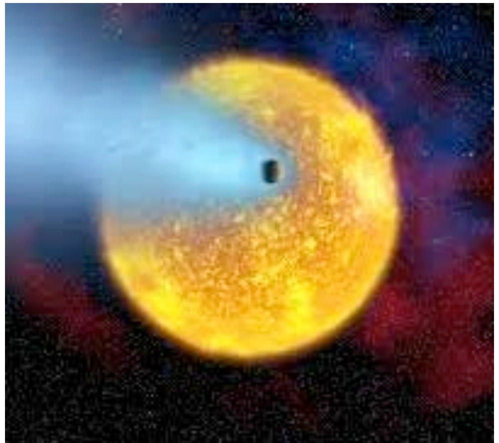

Ben-Jaffel, ApJL, 2008

15% absorption in the Lyα line

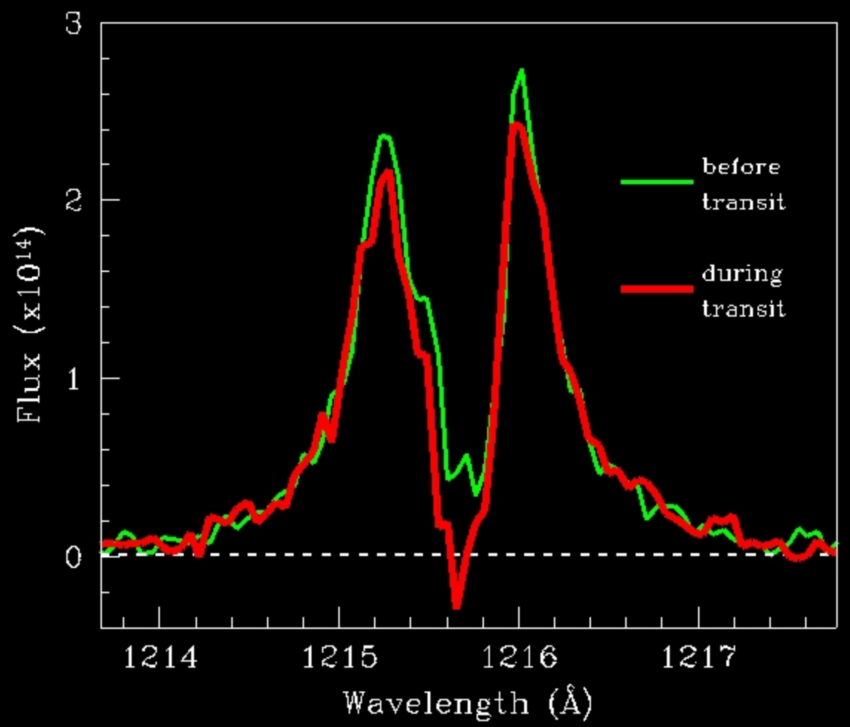

Vidal-Madjar et al., *Nature*, 2003
Ballester, Sing, Herbert, *Nature*, 2007

STIS: Lyα HD 209458b

Planetary properties of the upper atmosphere

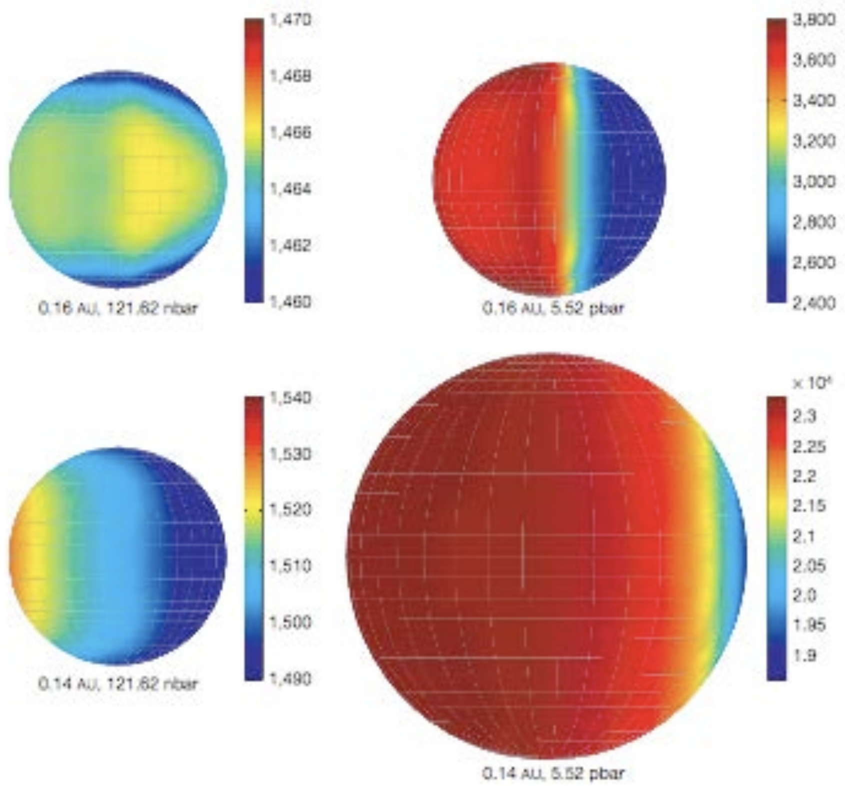

Koskinen et al., Nature, 2008

Stellar wind

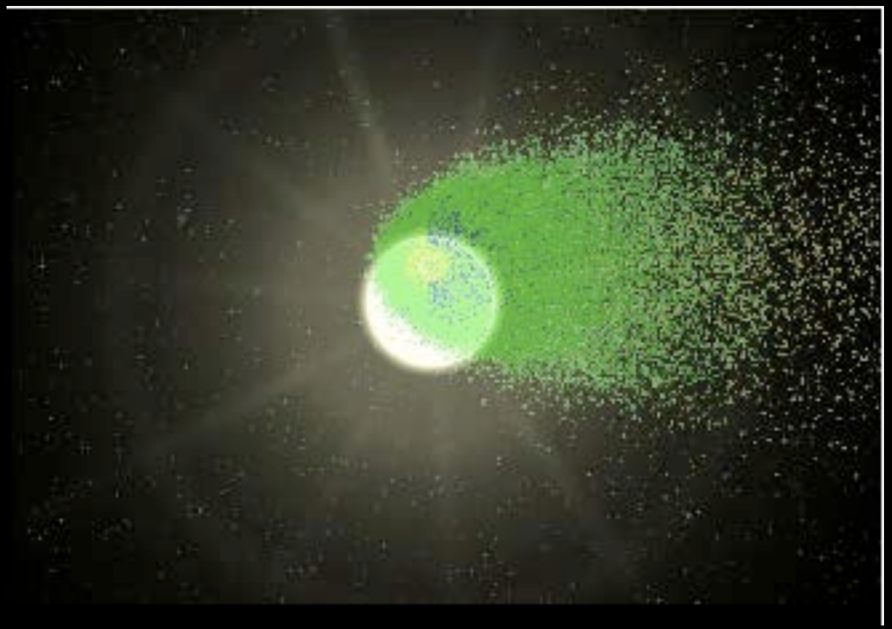

Holmstrom et al., Nature, 2008

Energetic Neutral Atoms around HD 209458b ?
Evaporation ?

Koskinen et al., 2010; Yelle, 2003;
Lecavelier et al., 2003; Lammer..2004, Tian et al. 2005,

CII Transit Measurements

(Linsky et al. 2010)

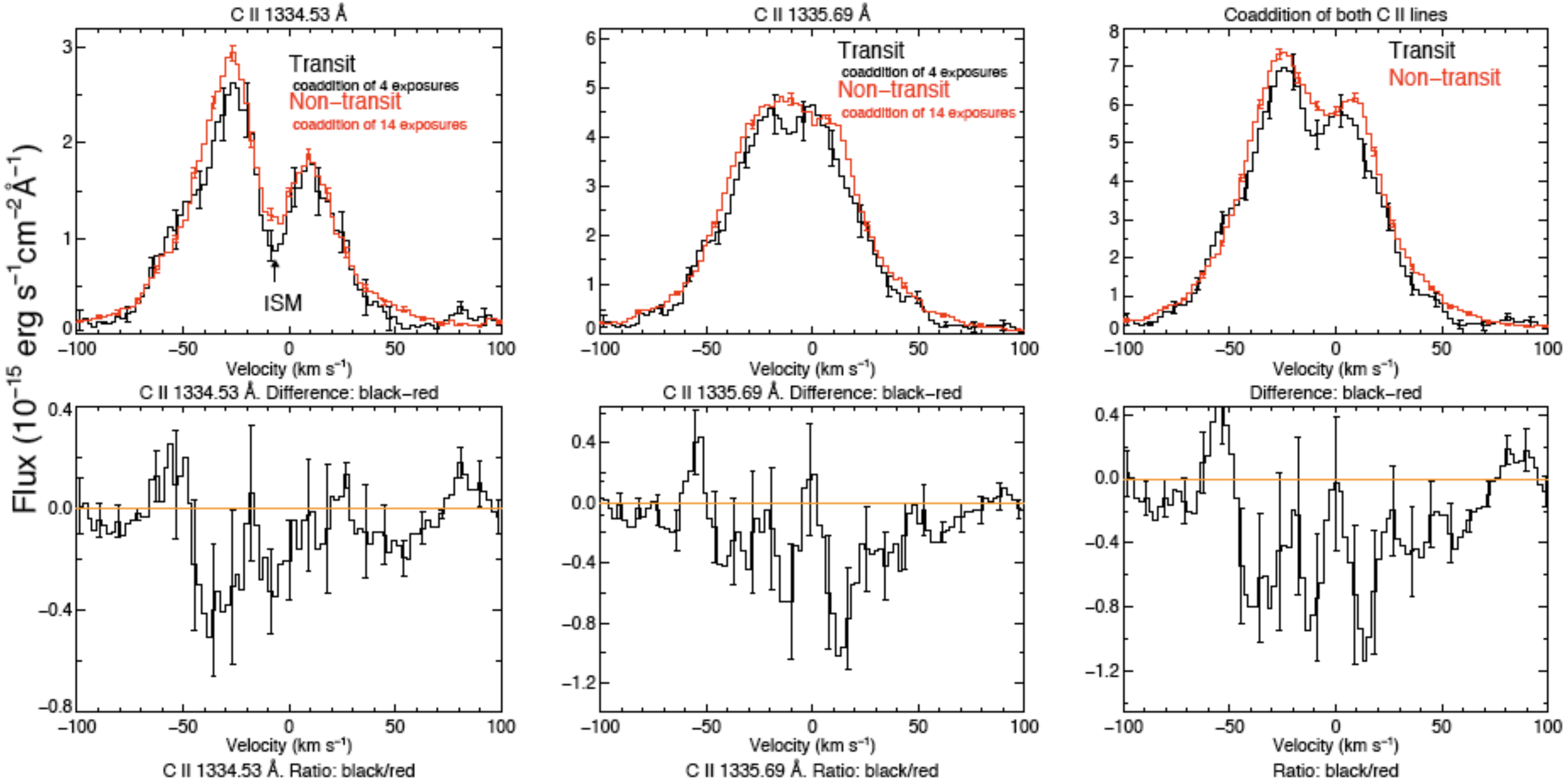

SiIII Transit Measurements

(Linsky et al. 2010)

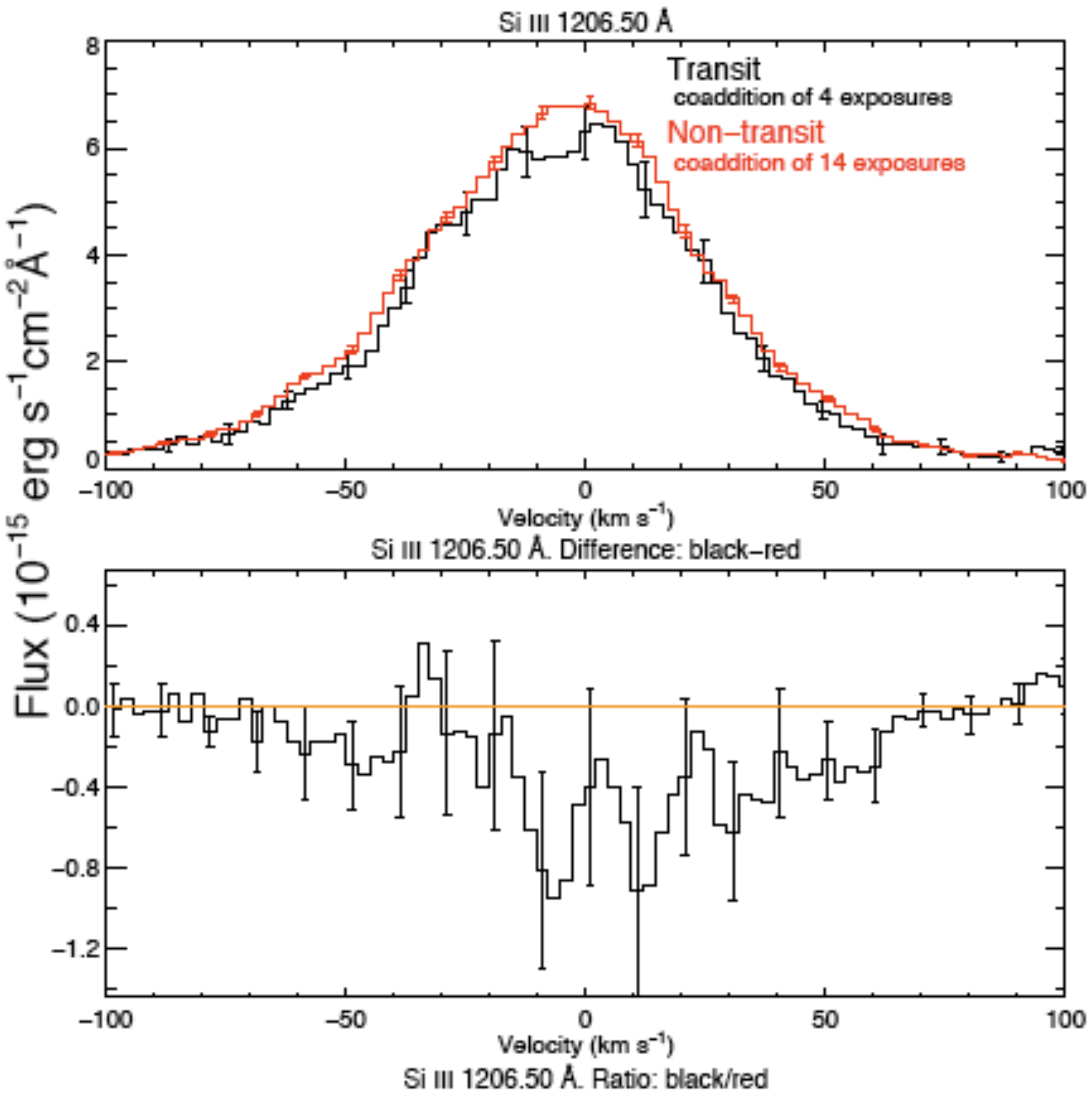

Phase curves
u Andromeda

Harrington et al. 2006

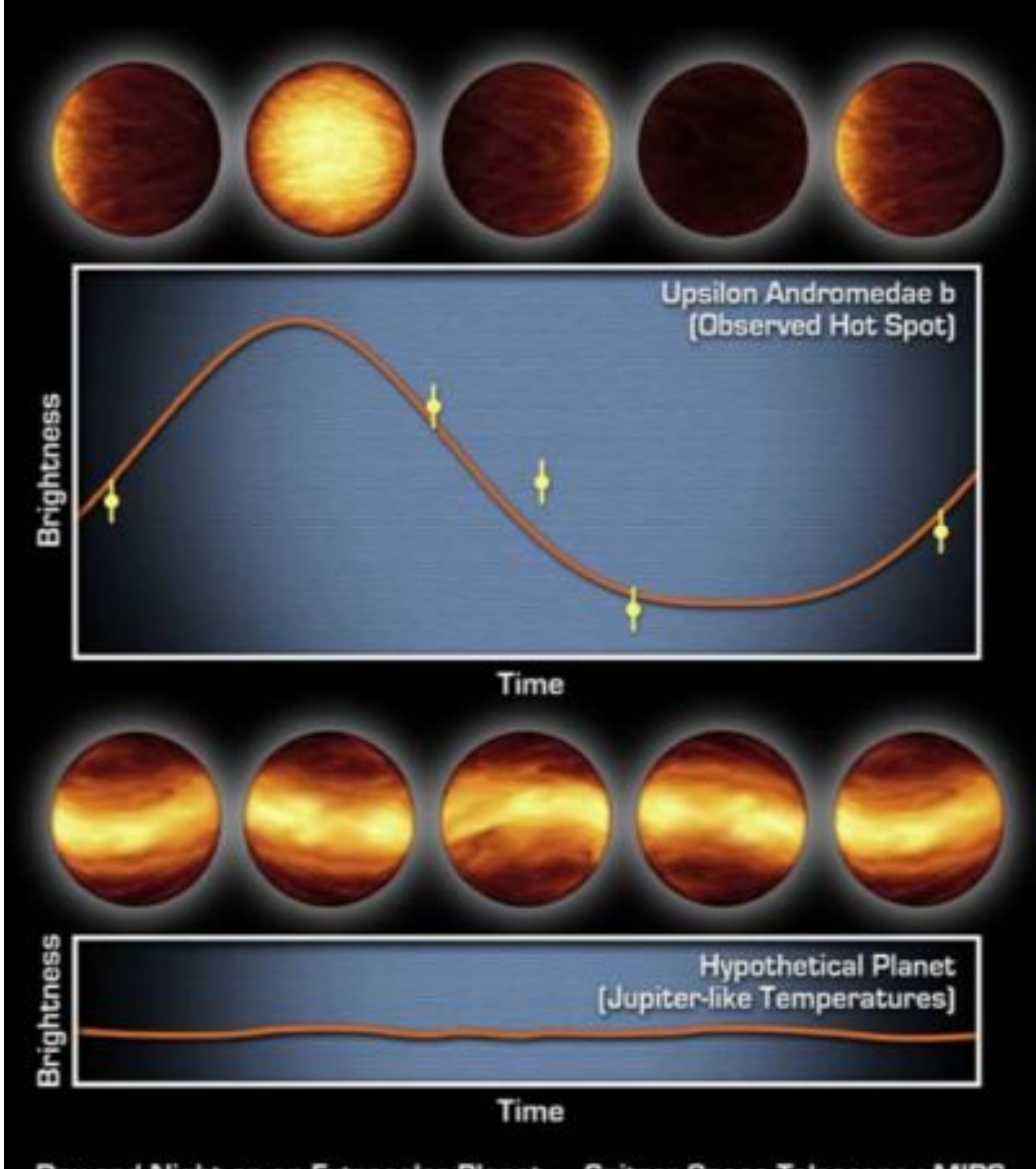

Day/Night phase curves, COROT-2b, HD190733b

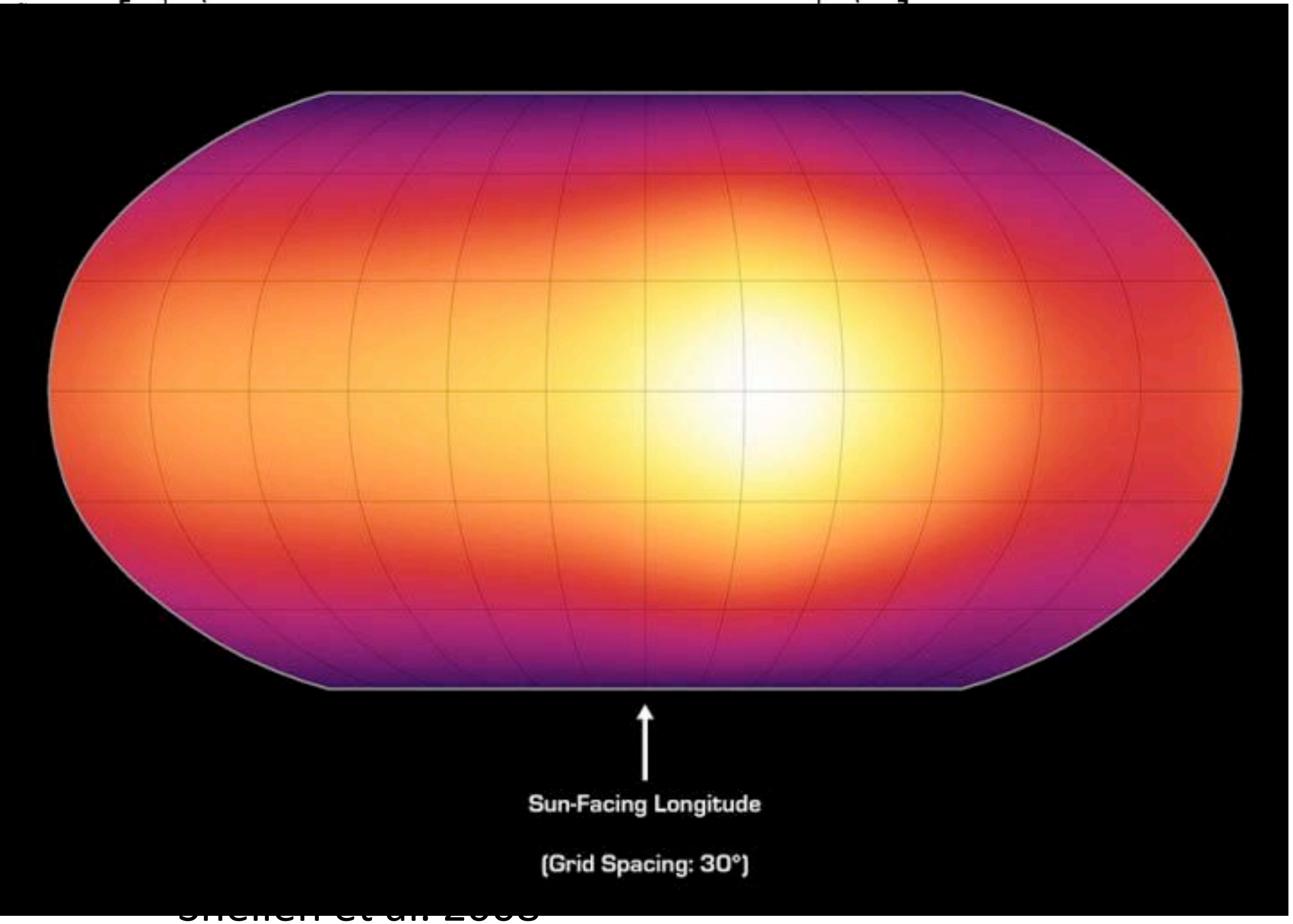

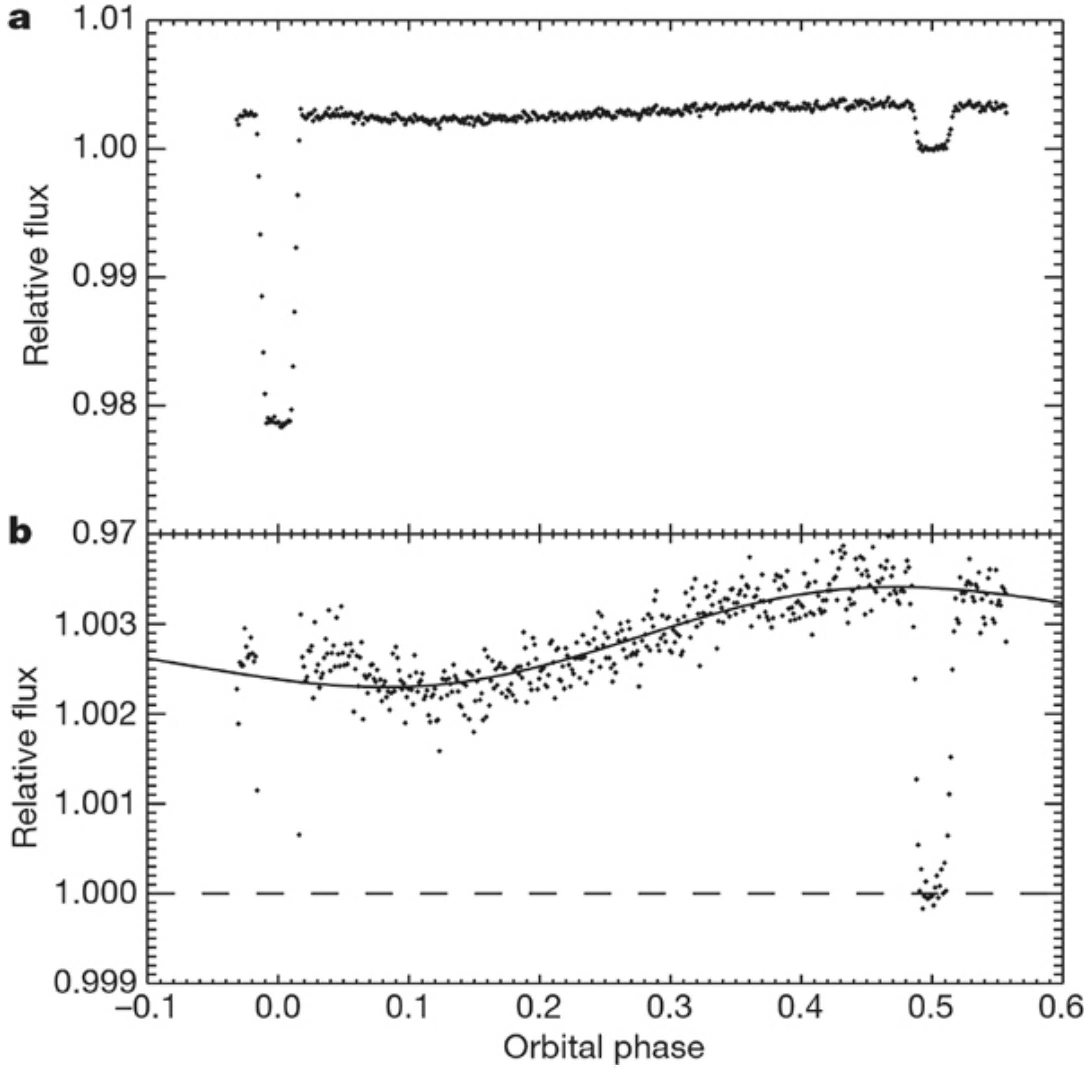

Knutson et al. 2007

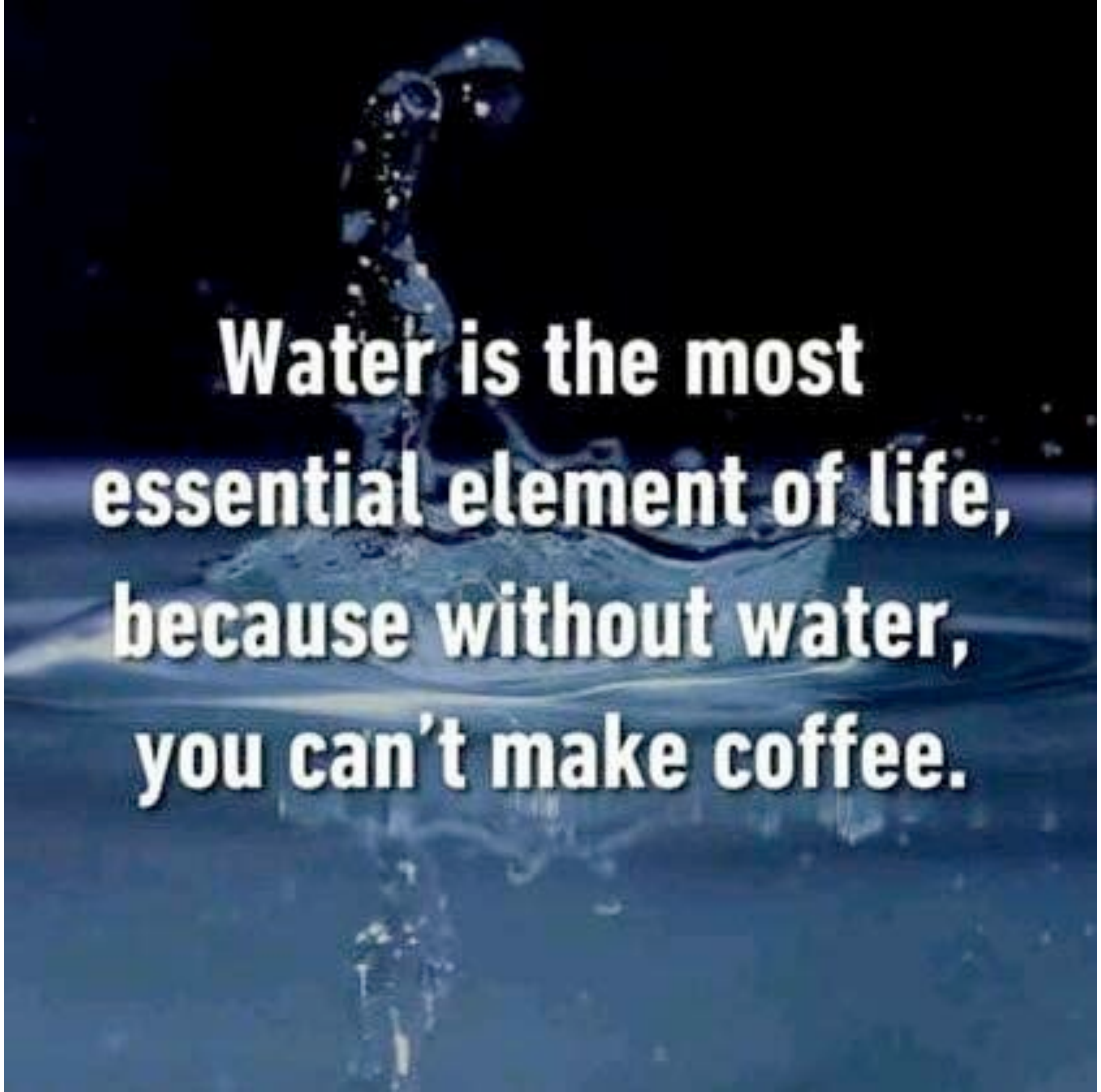
Water is the most
essential element of life,
because without water,
you can’t make coffee.

Water vapor in the hot Jupiter HD189733b

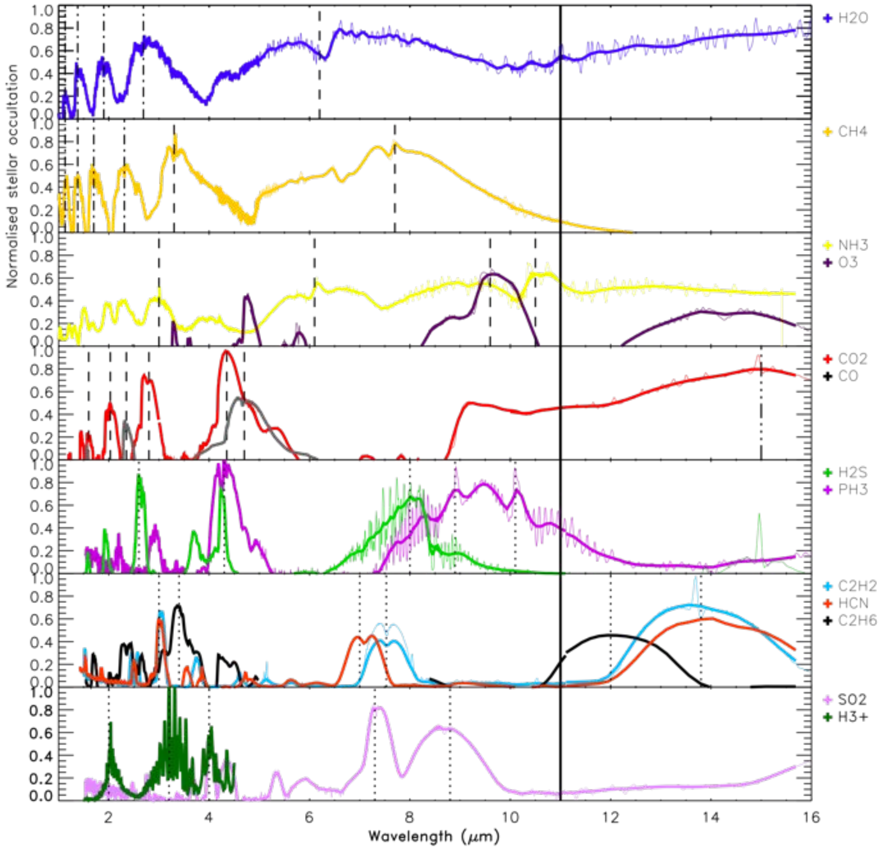

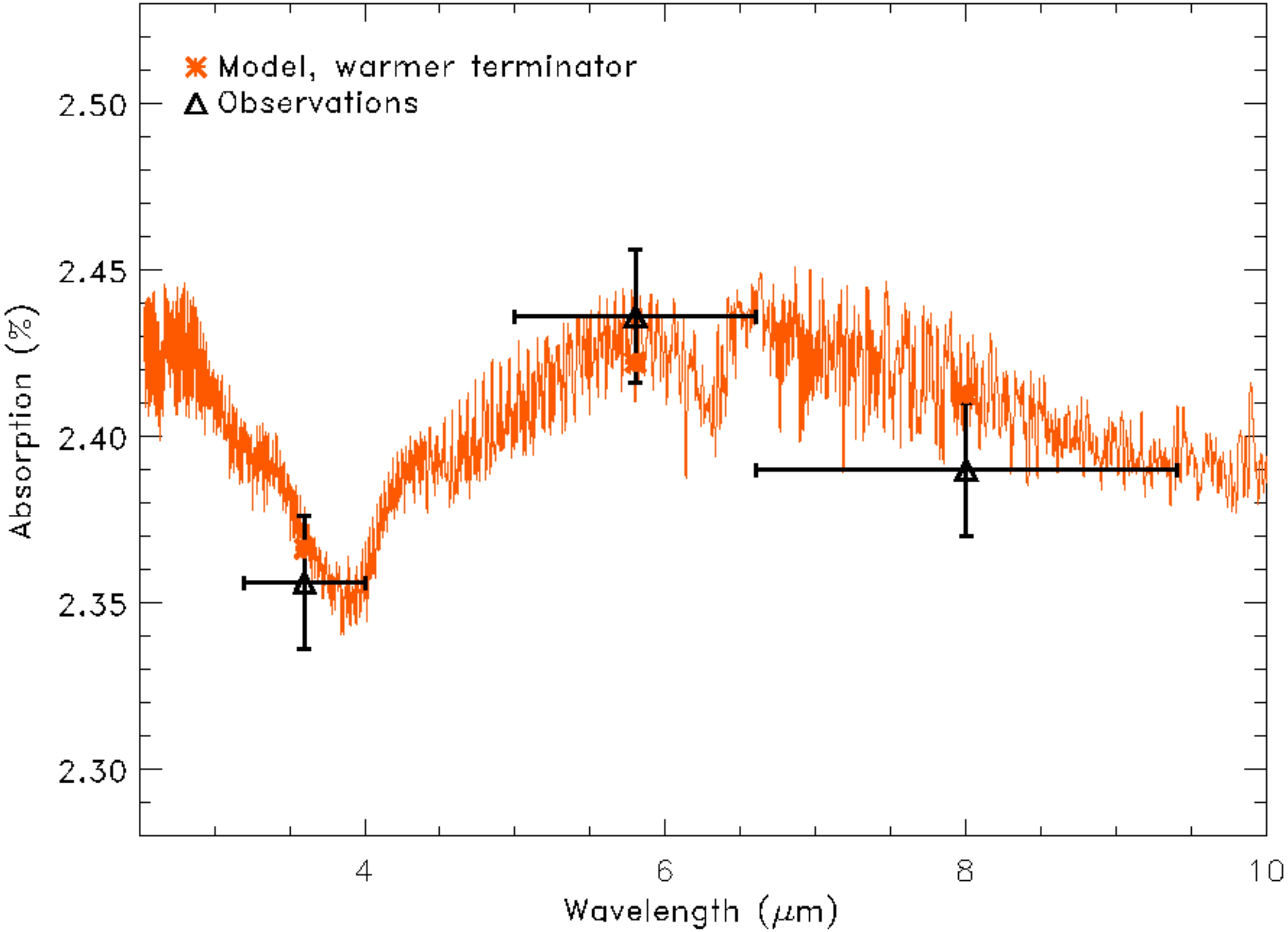

Tinetti *et al.*, Nature, 2007; Beaulieu et al. 2008

SPITZER 3.6 μm, (channel 1)

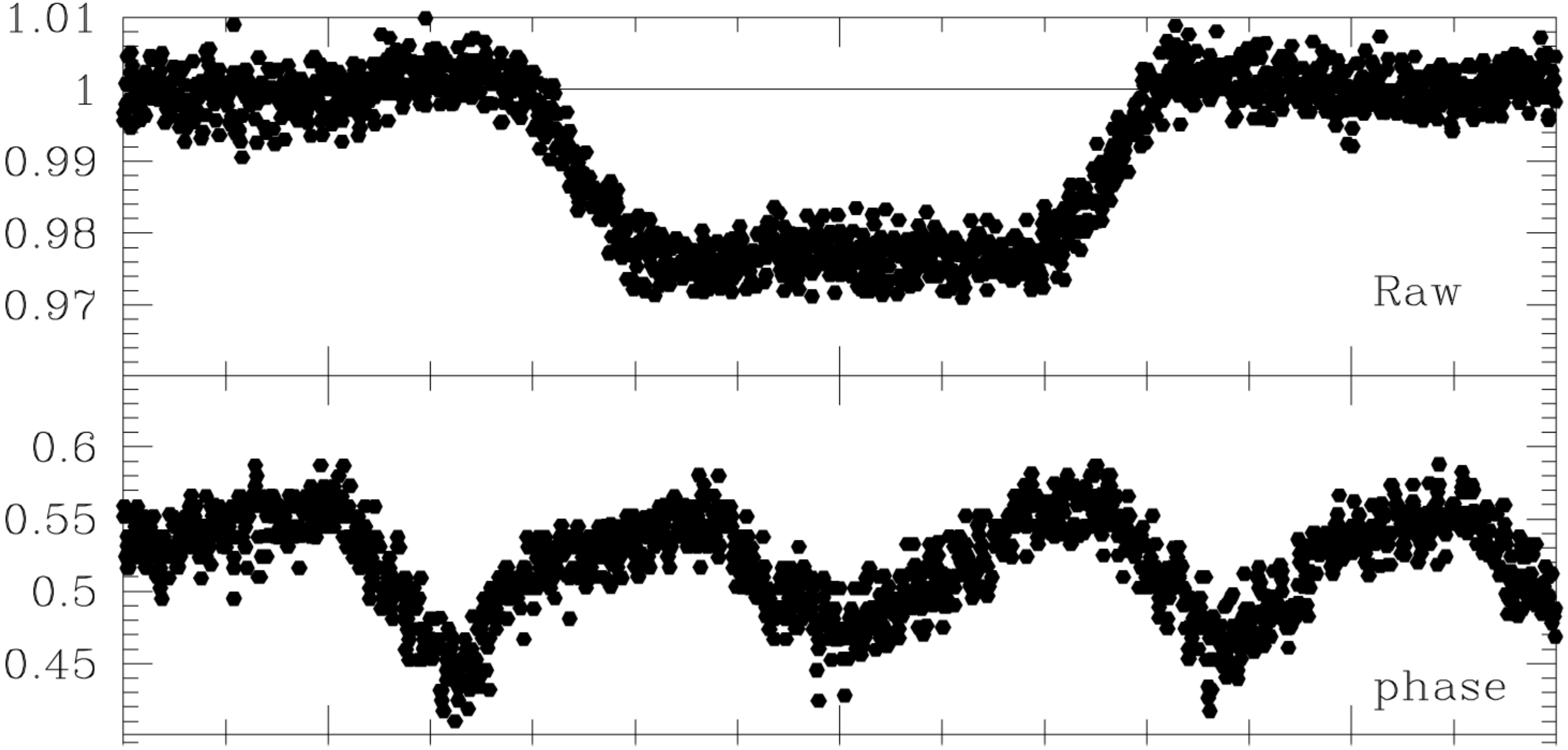

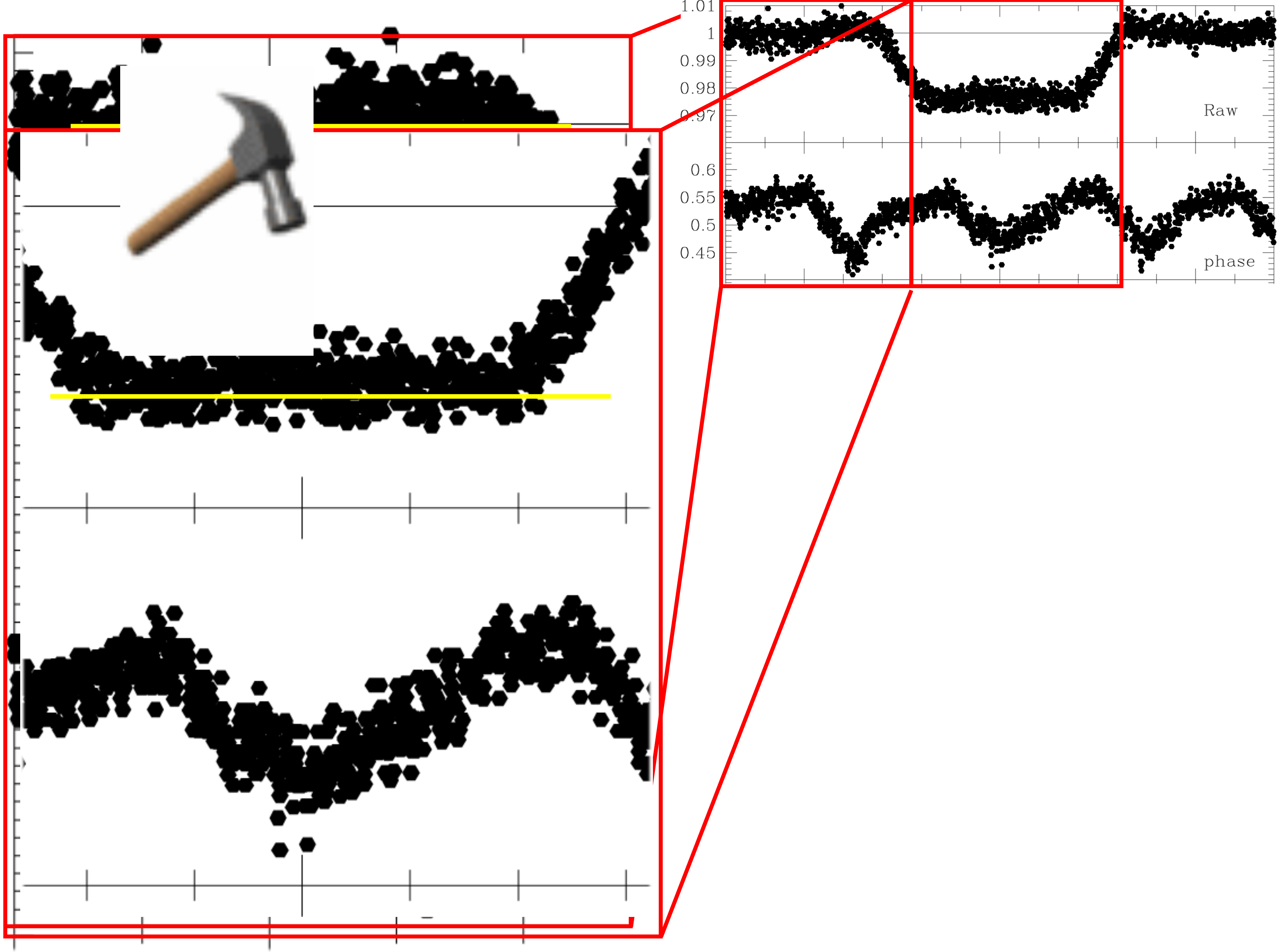

1.01
1
0.99
0.98
0.97
Raw
0.6
0.55
0.5
0.45
phase

Correcting for pixel phase effects

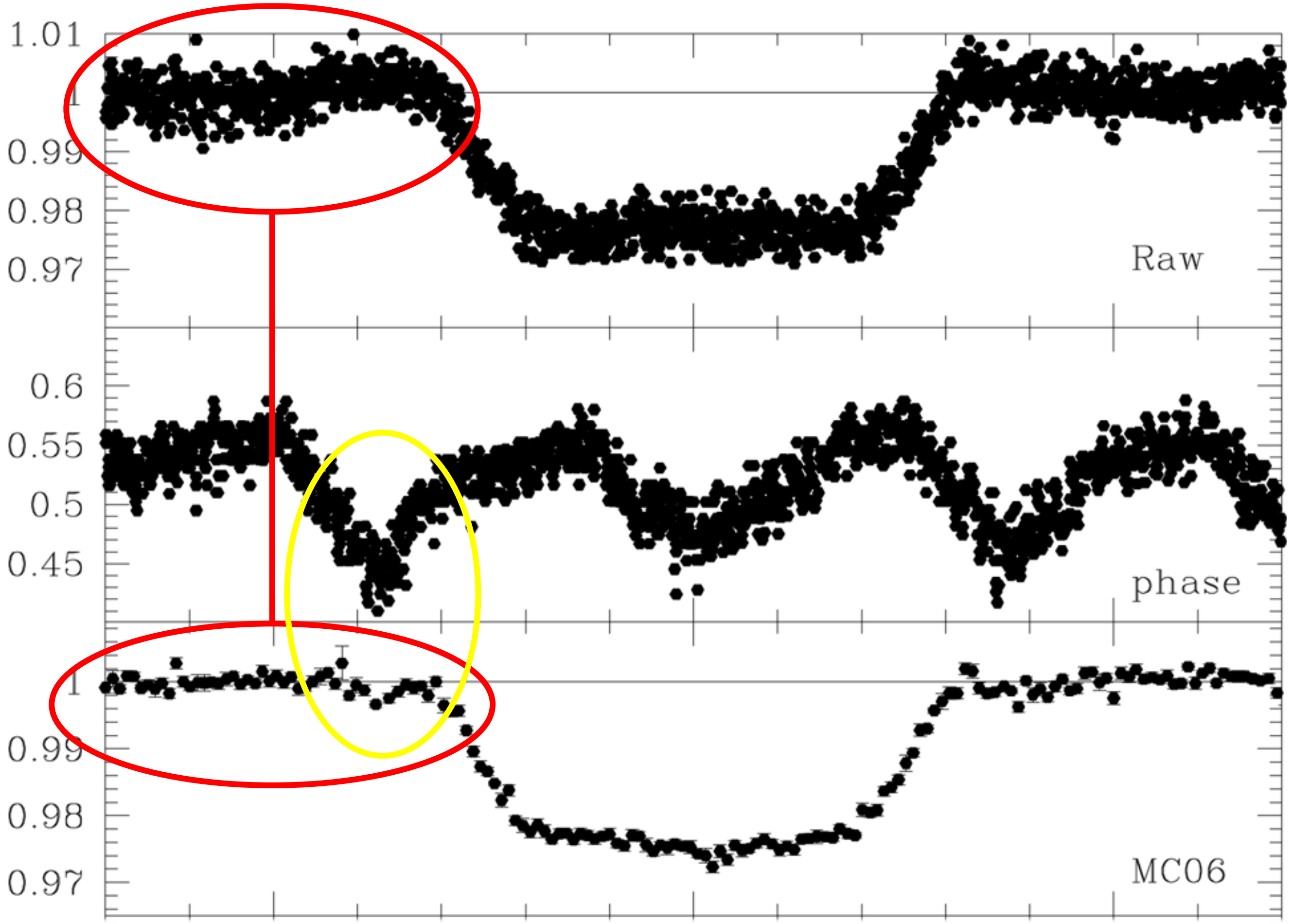

Estimating systematic trends from the data

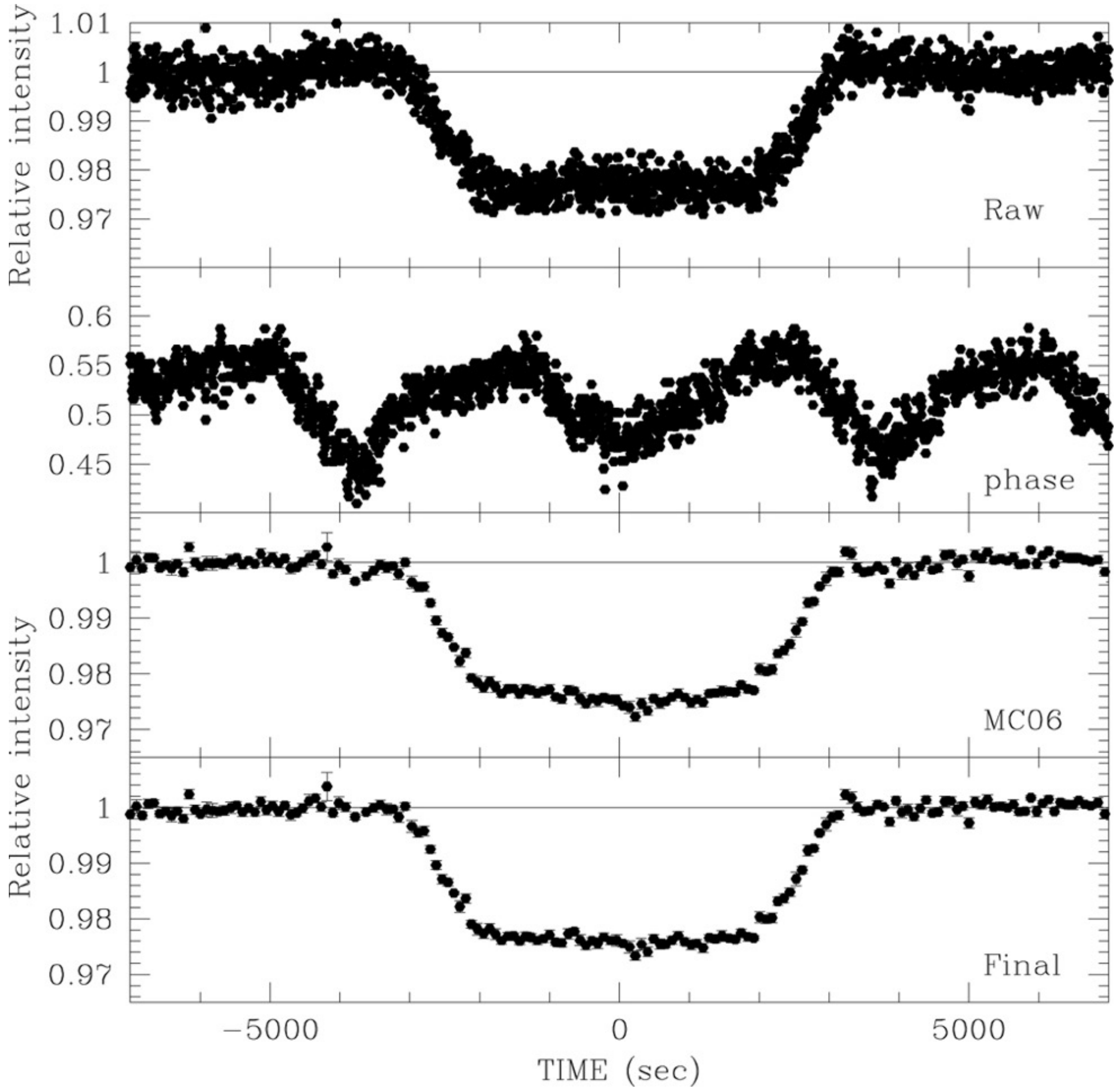

HD189733b, Water + Methane

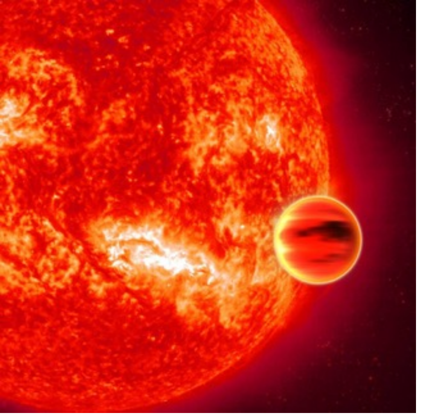

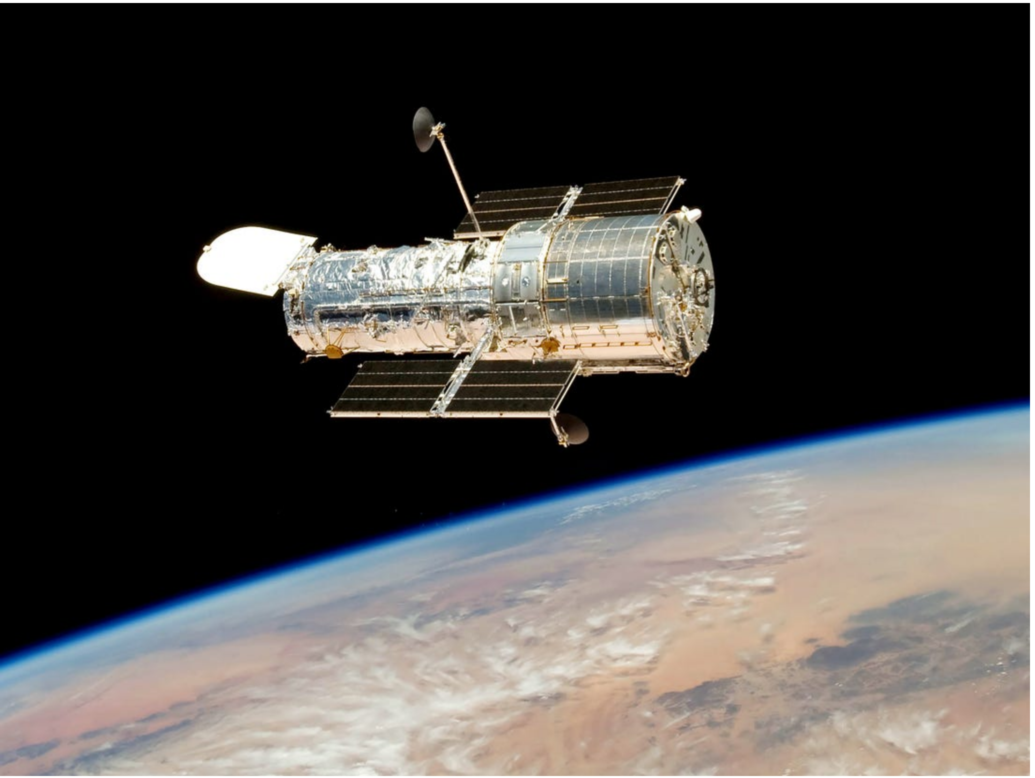

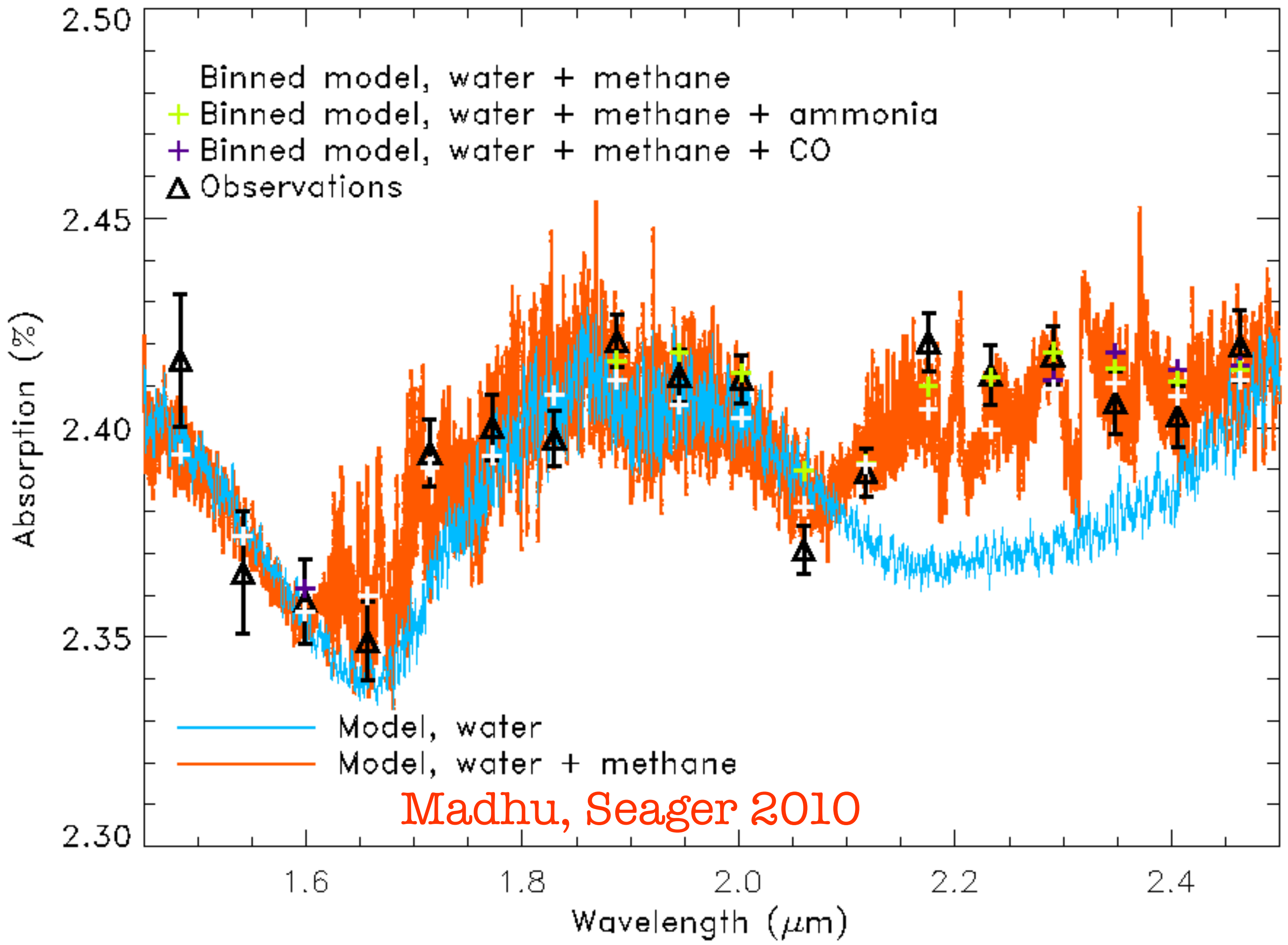

Madhu, Seager 2010

Swain, Vasisht, Tinetti, *Nature*, 2008

HD189733b, Water + Methane

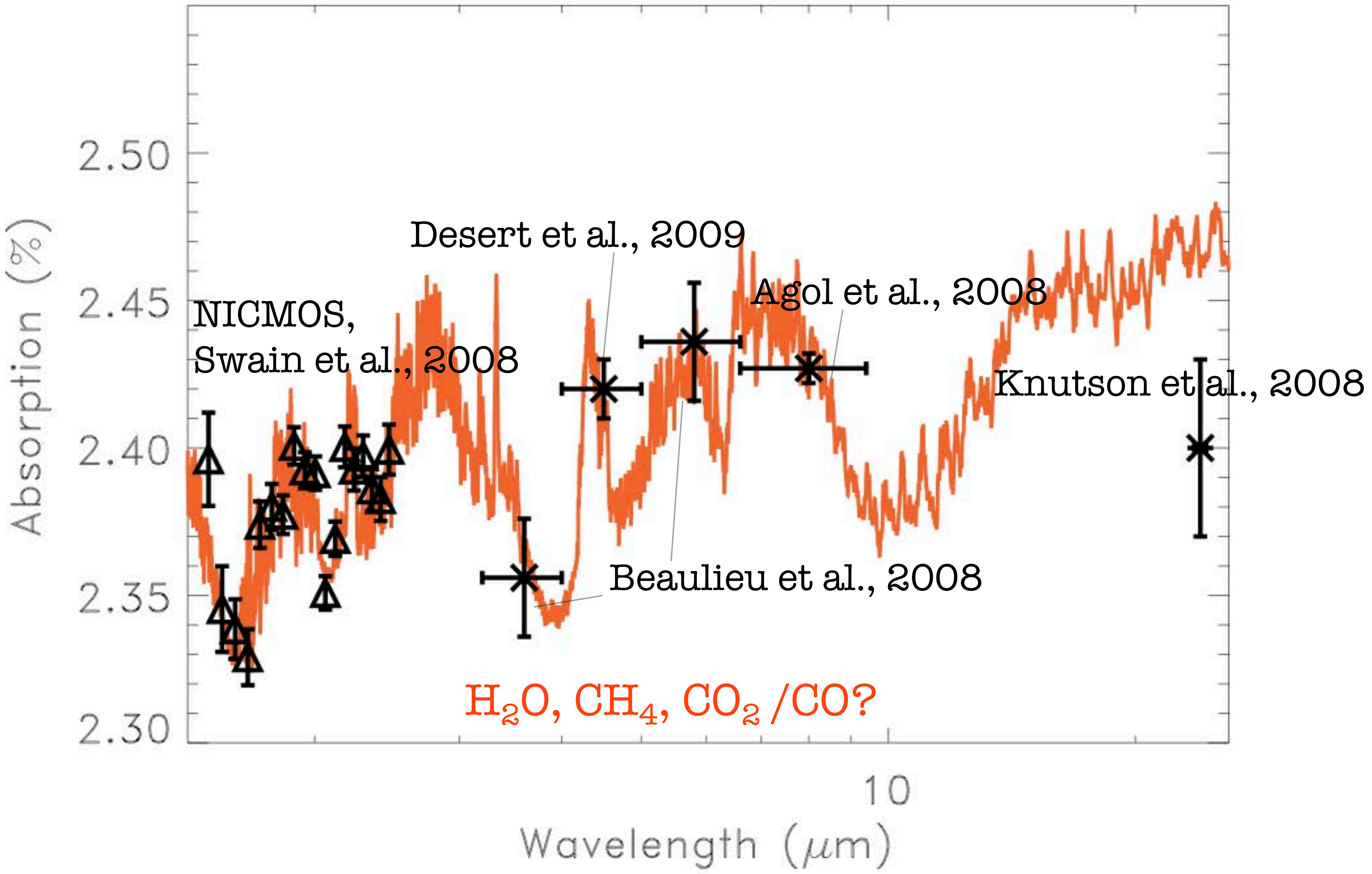

Water, CO on HD 189733b occultation obs: Spitzer

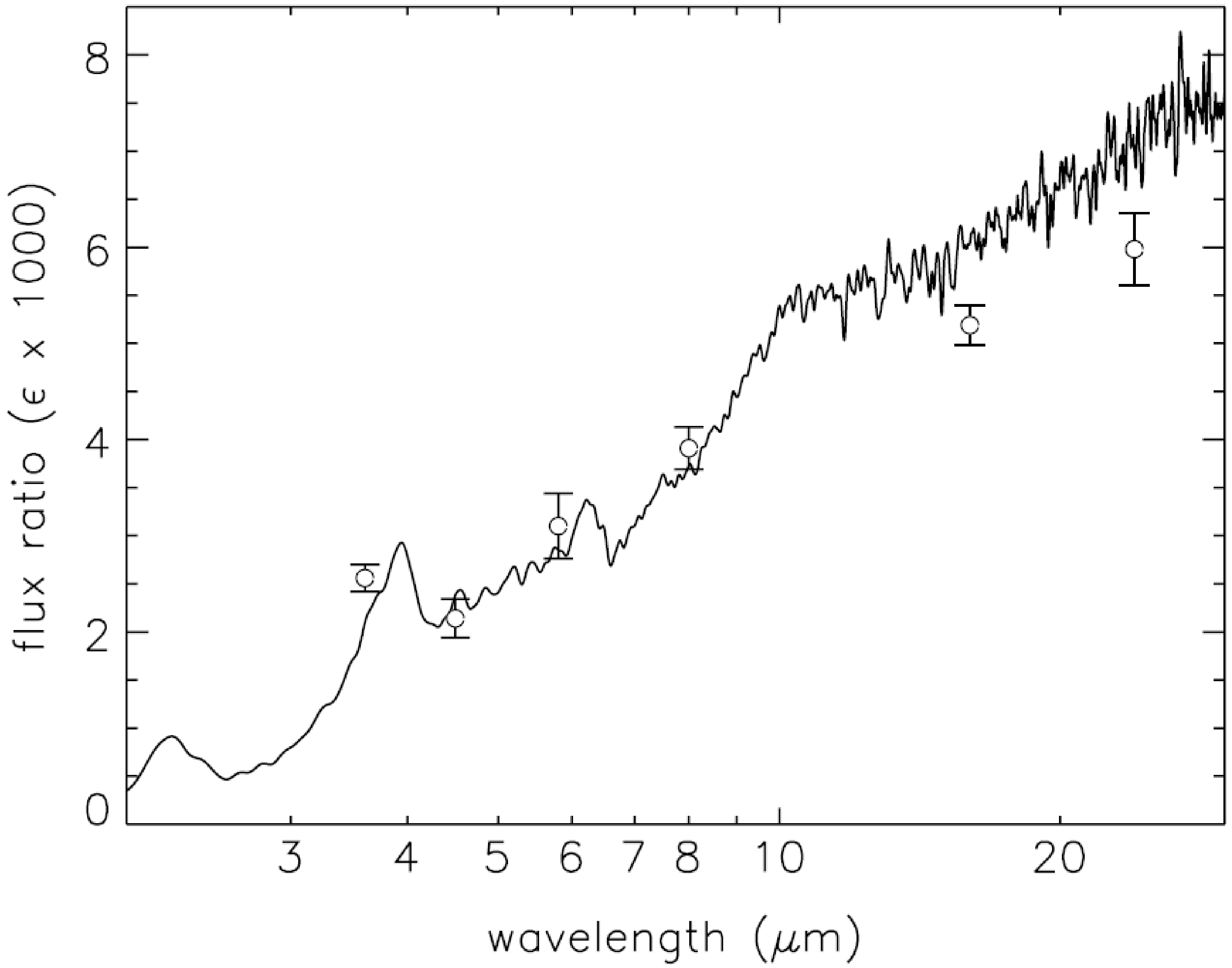

Charbonneau et al., *ApJ*, 2008; Barman, *ApJL*, 2008

HD209458b

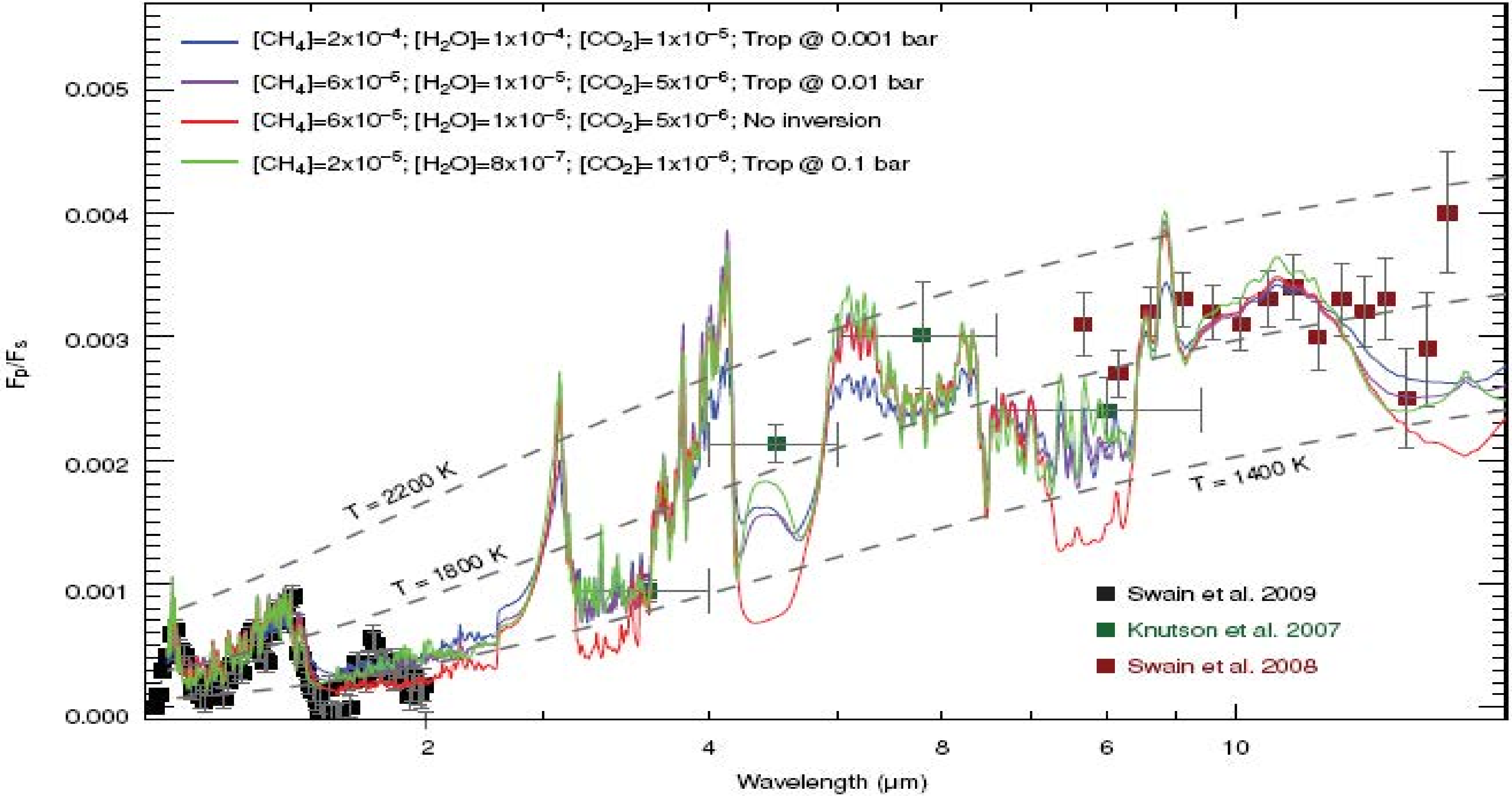

[CH4]=2x10^-4; [H2O]=1x10^-4; [CO2]=1x10^-5; Trop @ 0.001 bar
[CH4]=6x10^-5; [H2O]=1x10^-5; [CO2]=5x10^-6; Trop @ 0.01 bar
[CH4]=6x10^-5; [H2O]=1x10^-5; [CO2]=5x10^-6; No inversion
[CH4]=2x10^-5; [H2O]=8x10^-7; [CO2]=1x10^-6; Trop @ 0.1 bar
0.005
0.004
0.003
0.002
0.001
0.000
Fp/Fs
T = 2200 K
T = 1800 K
T = 1400 K
Swain et al. 2009
Knutson et al. 2007
Swain et al. 2008
2
4
8
6
10
Wavelength (μm)

GJ1214, super Earth ? Mini Neptunes ? With HST clouds are currently hidding molecules
Need to go further to the IR

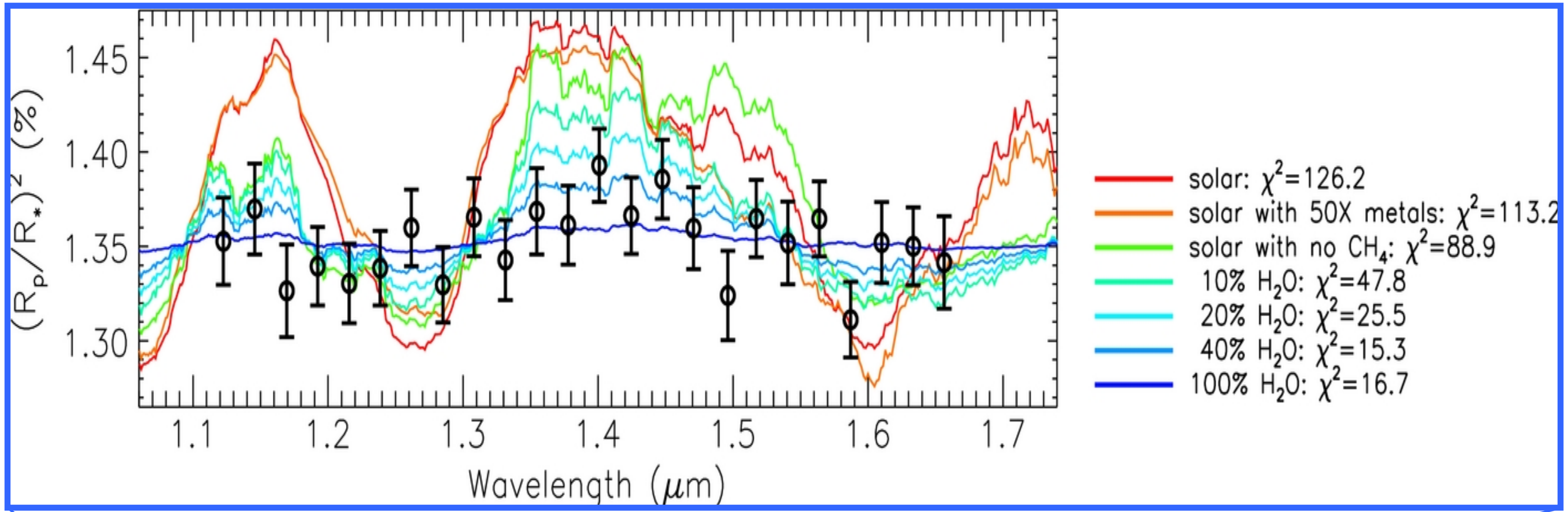

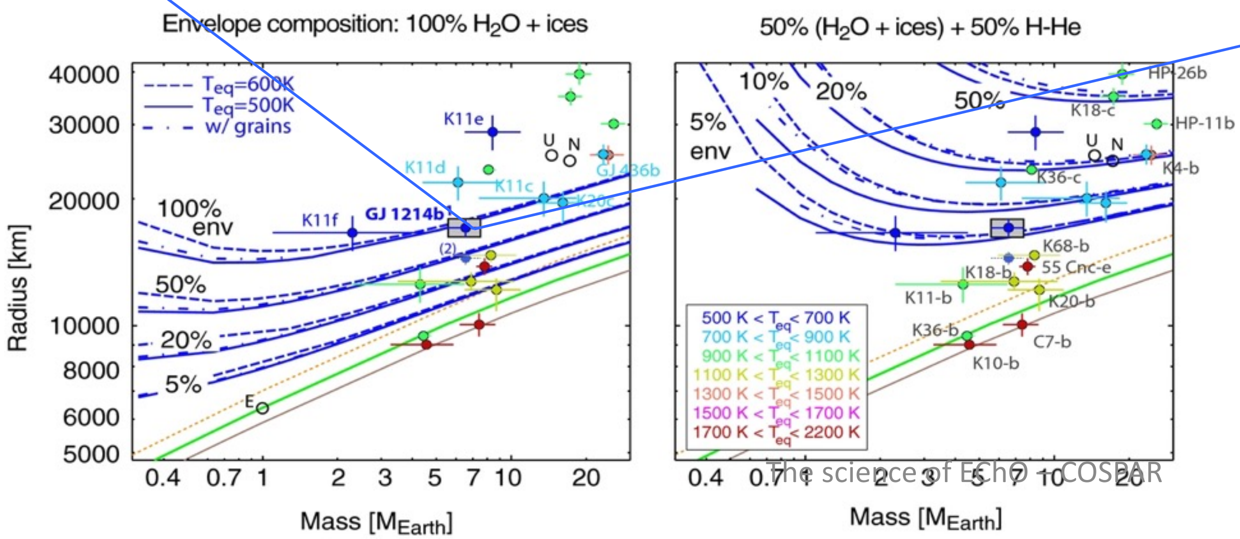

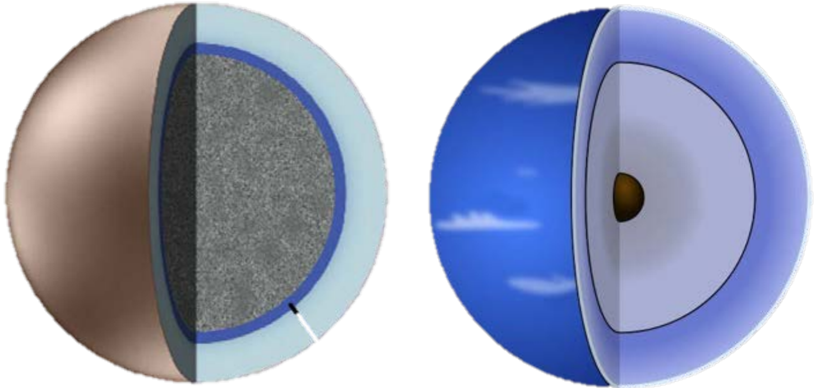

Snellen et al., 2010, VLT spectra of HD209458b

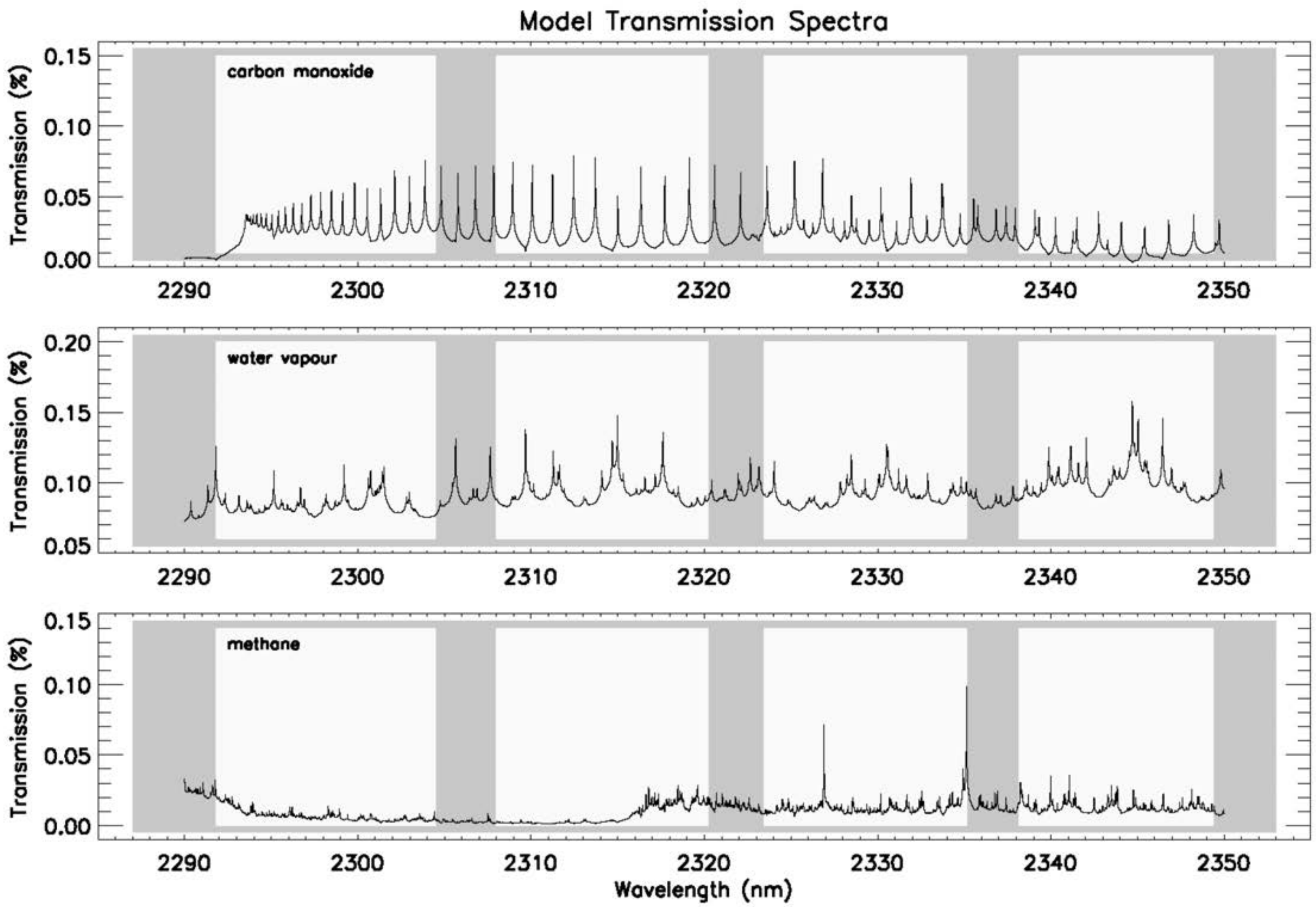

Figure S2: Models used for the transmission of carbon monoxide (top panel), water vapour (middle panel), and methane (lower panel) in the atmosphere of HD209458b.

- strong wind flowing from the irradiated dayside to the non-irradiated nightside of the plan within the 0.01-0.1 mbar atmospheric pressure range probed by these observations.

- CO mixing ratio of 1-3x10^{-3} in the upper atmosphere.

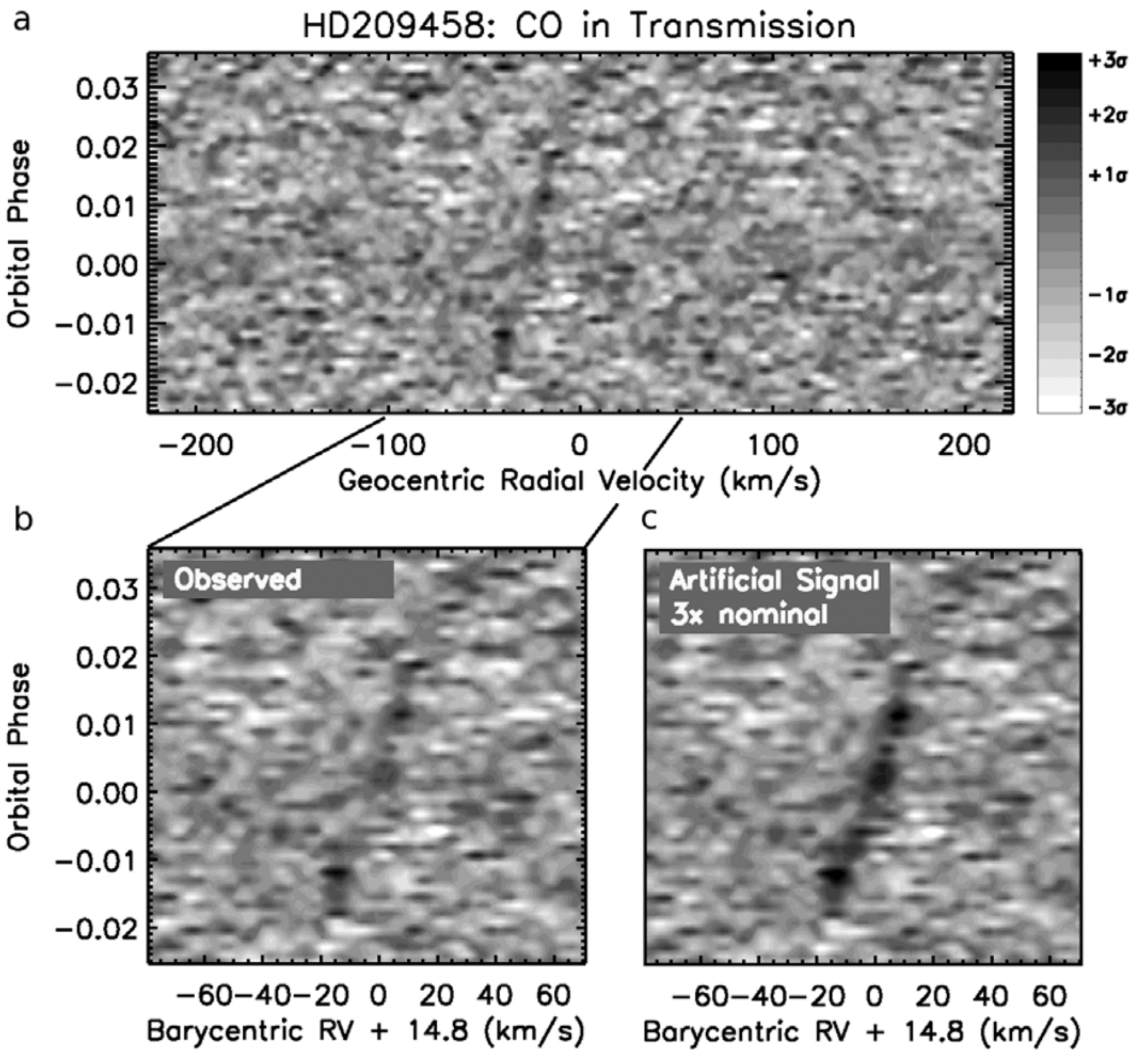

Gravity spectra of betapicb, R=500 and R=70

1) mass ~ brown dwarf
2) low C/O ratio for the planet suggests a formation through core-accretion, with strong planetesimal enrichment.

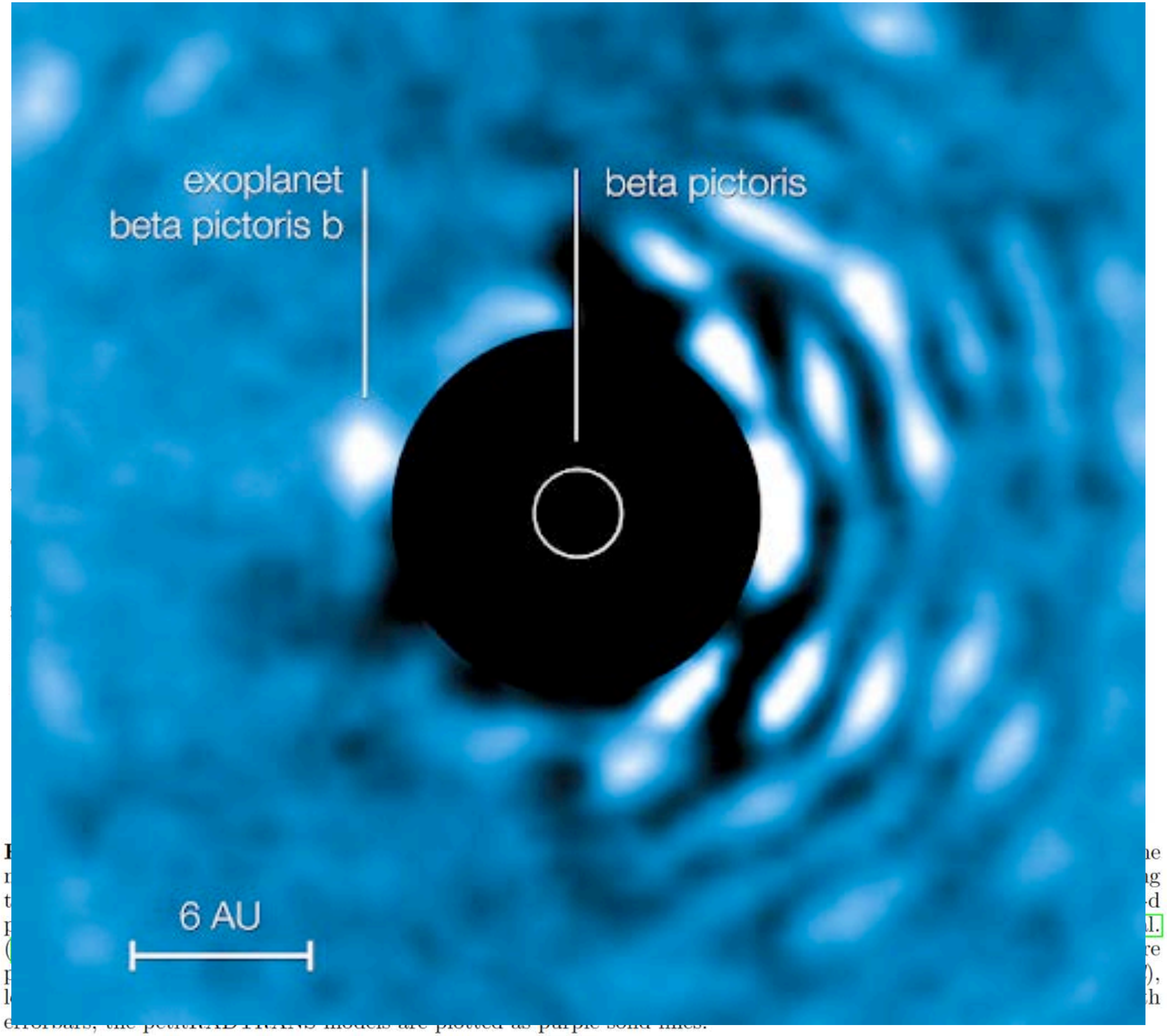

Analysing exoplanet data, Chef’s cooking recipie

HST Archives

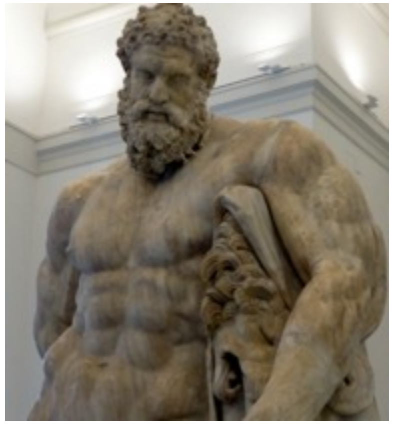

IRACLIS code

Tsiaras et al.

TauREX code

Waldmann, Al Refaie
Changeat, Edwards,
et al

Computing power

Ariel school 2019

In White light

We fit a transit model x systematics model

Models for systematics

$$n_w^{scan} = (1 - ra_1(t - T0))\ (1 - rb_1 e^{-rb2(t-to)})$$

Linear ramp

Exponential ramp

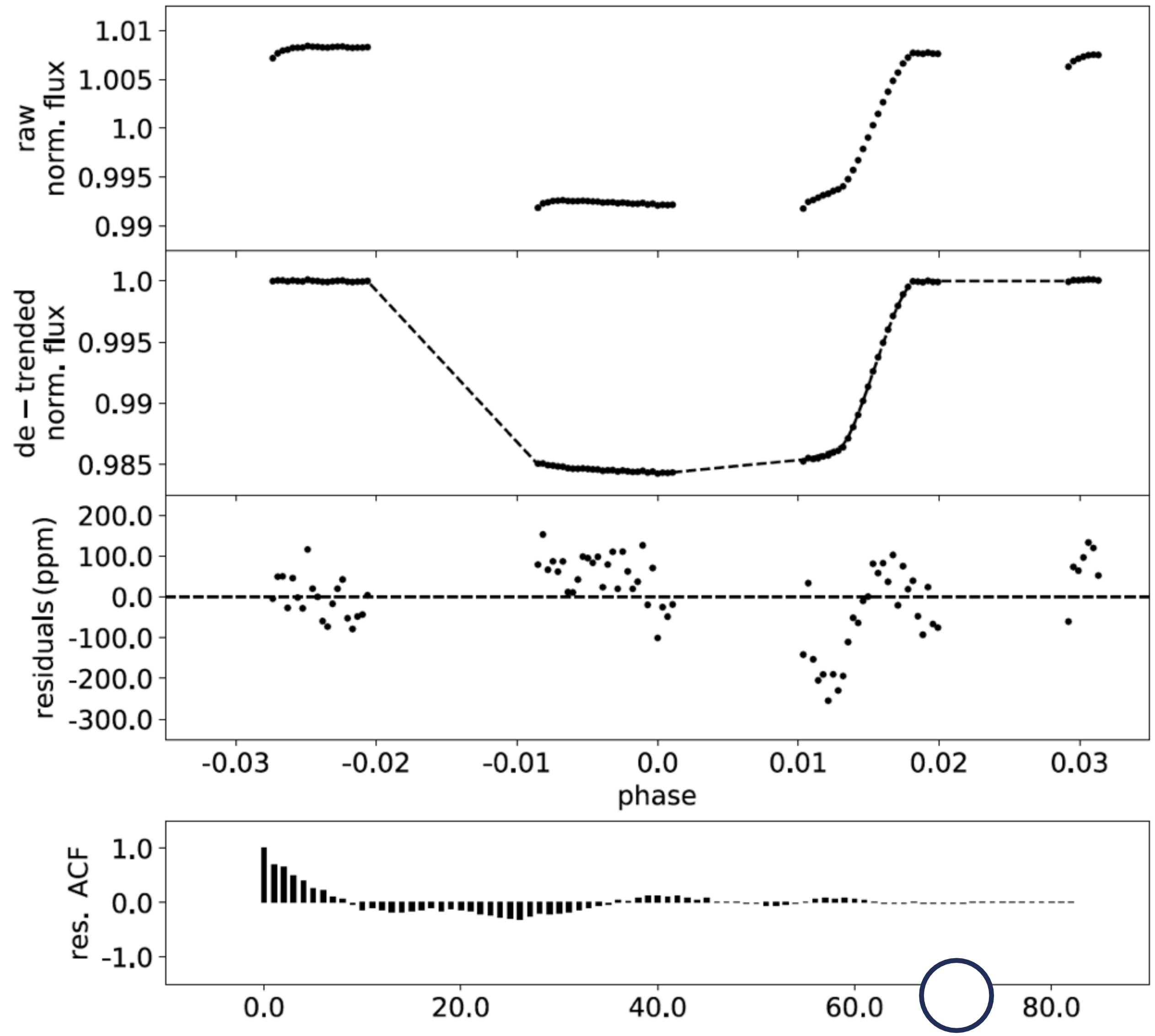

Figure 4.7: Results from the analysis of the white light-curve for the test case of HD 209458 b. Top panel: Normalised raw light-curve. Second panel: Light-curve divided by the best-fit model for the systematics. Third panel: Fitting residuals. Bottom panel: Autocorrelation function of the residuals.

In white light

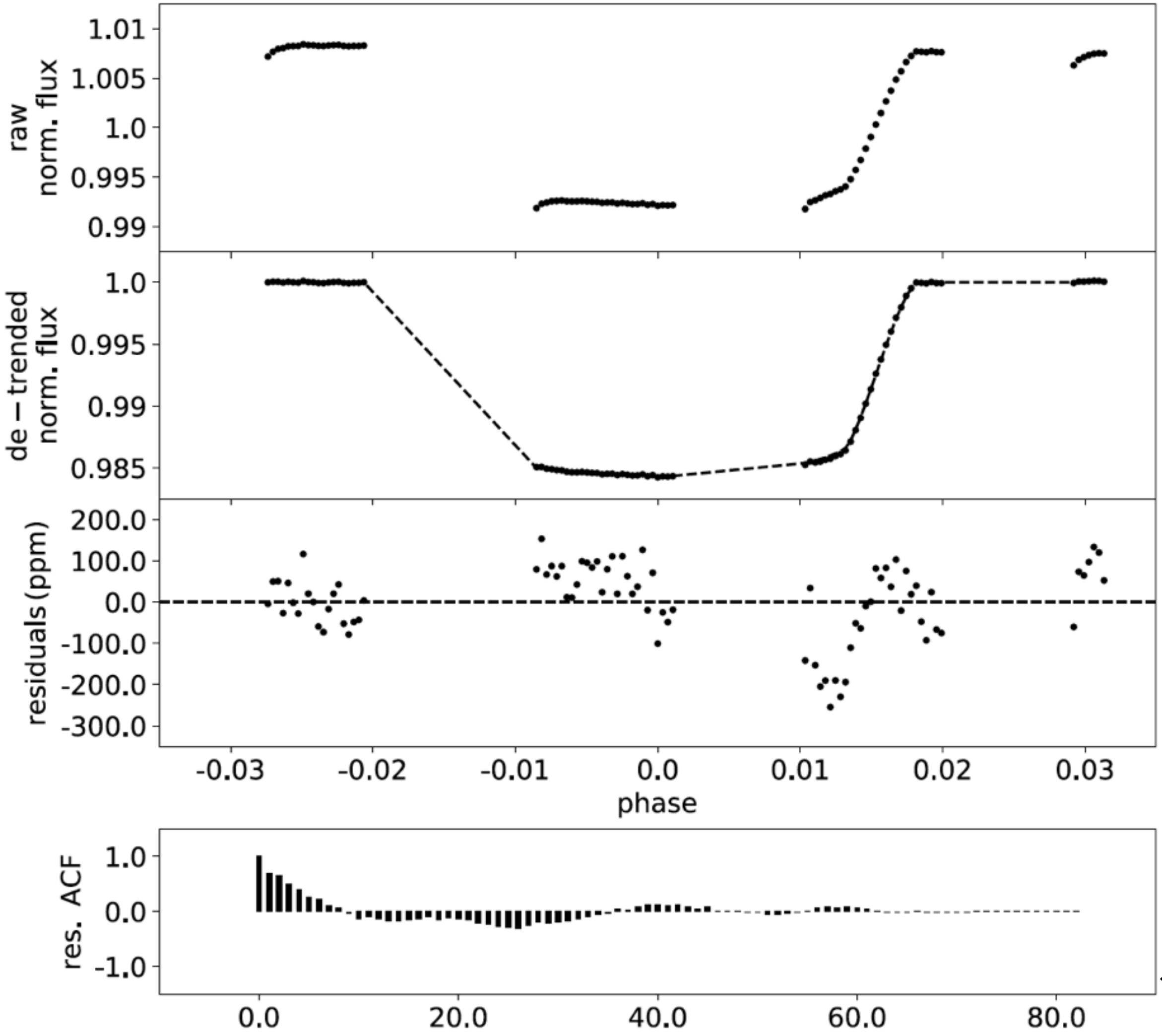

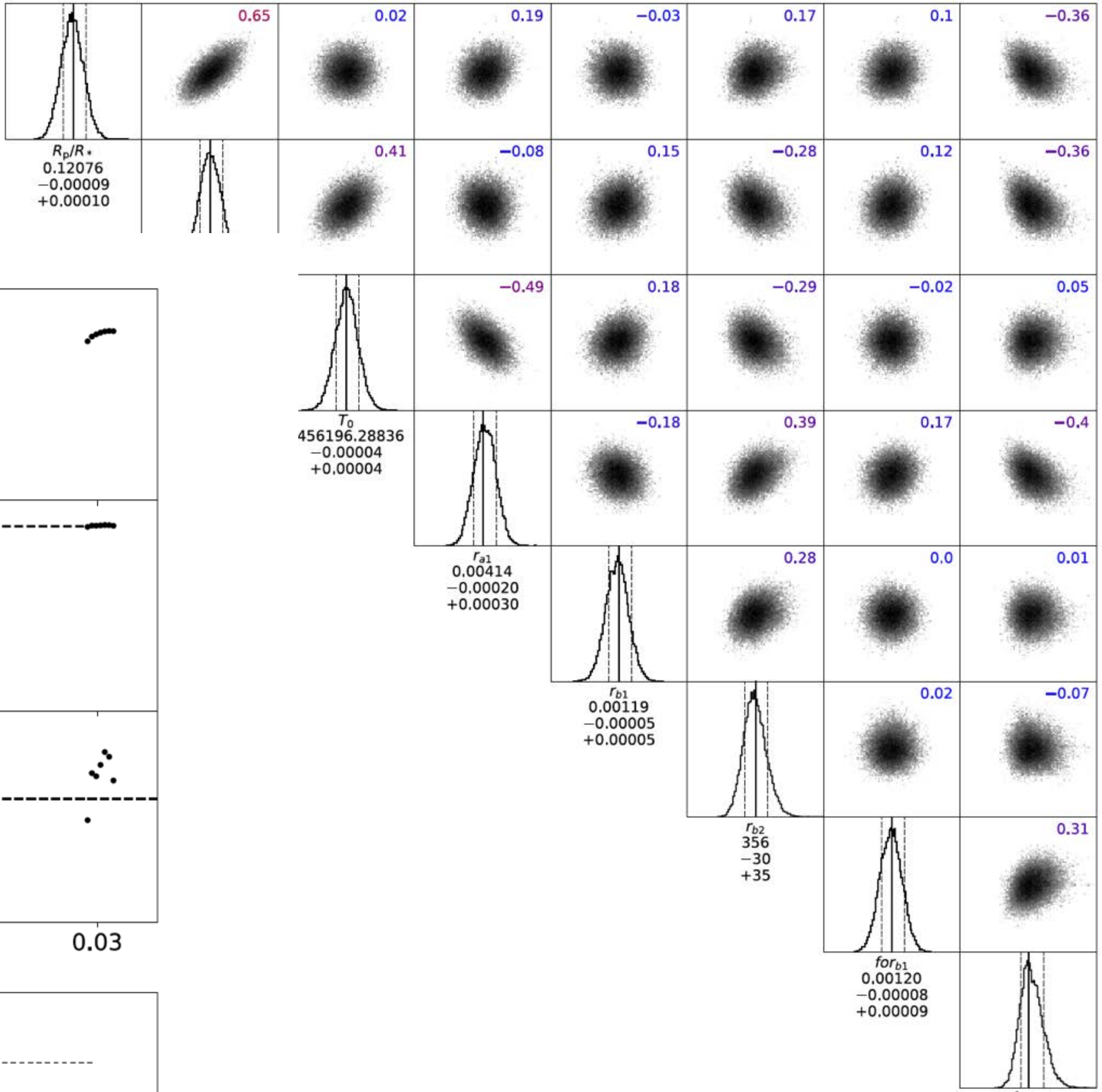

$$n_w^{scan} = (1 - ra_1(t - T0))\ (1 - rb_1 e^{-rb2(t-to)})$$

White light versus 1.3 microns

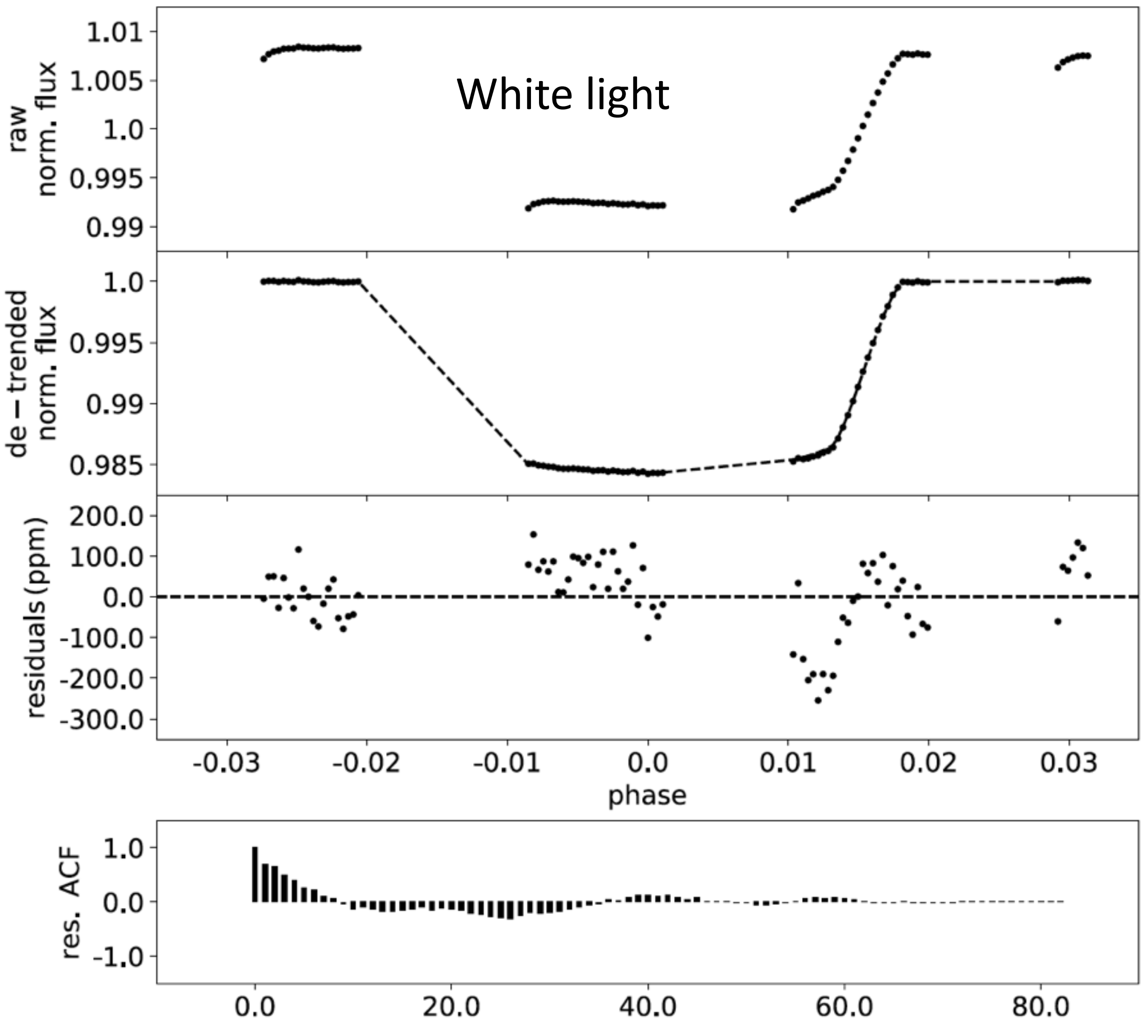

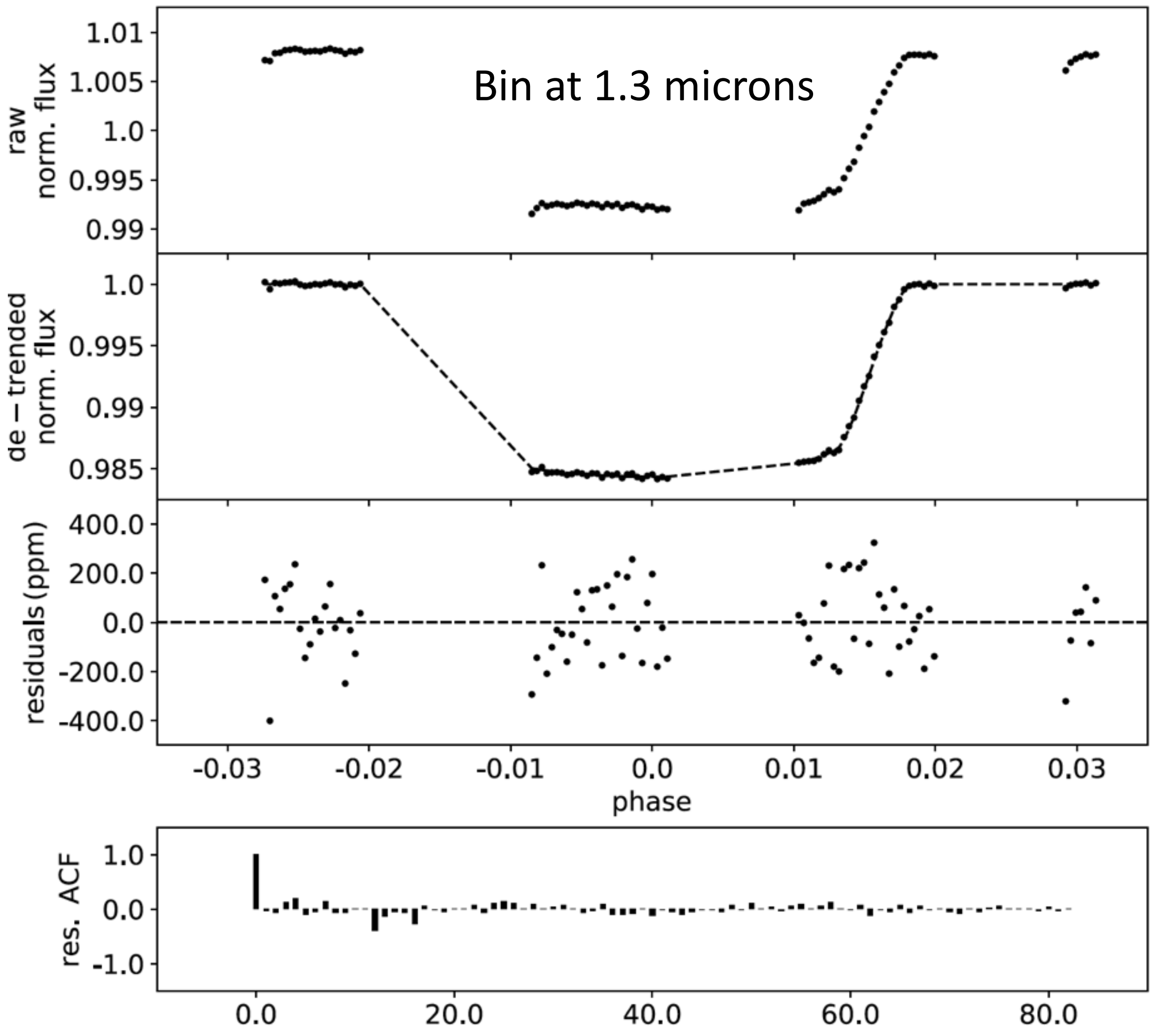

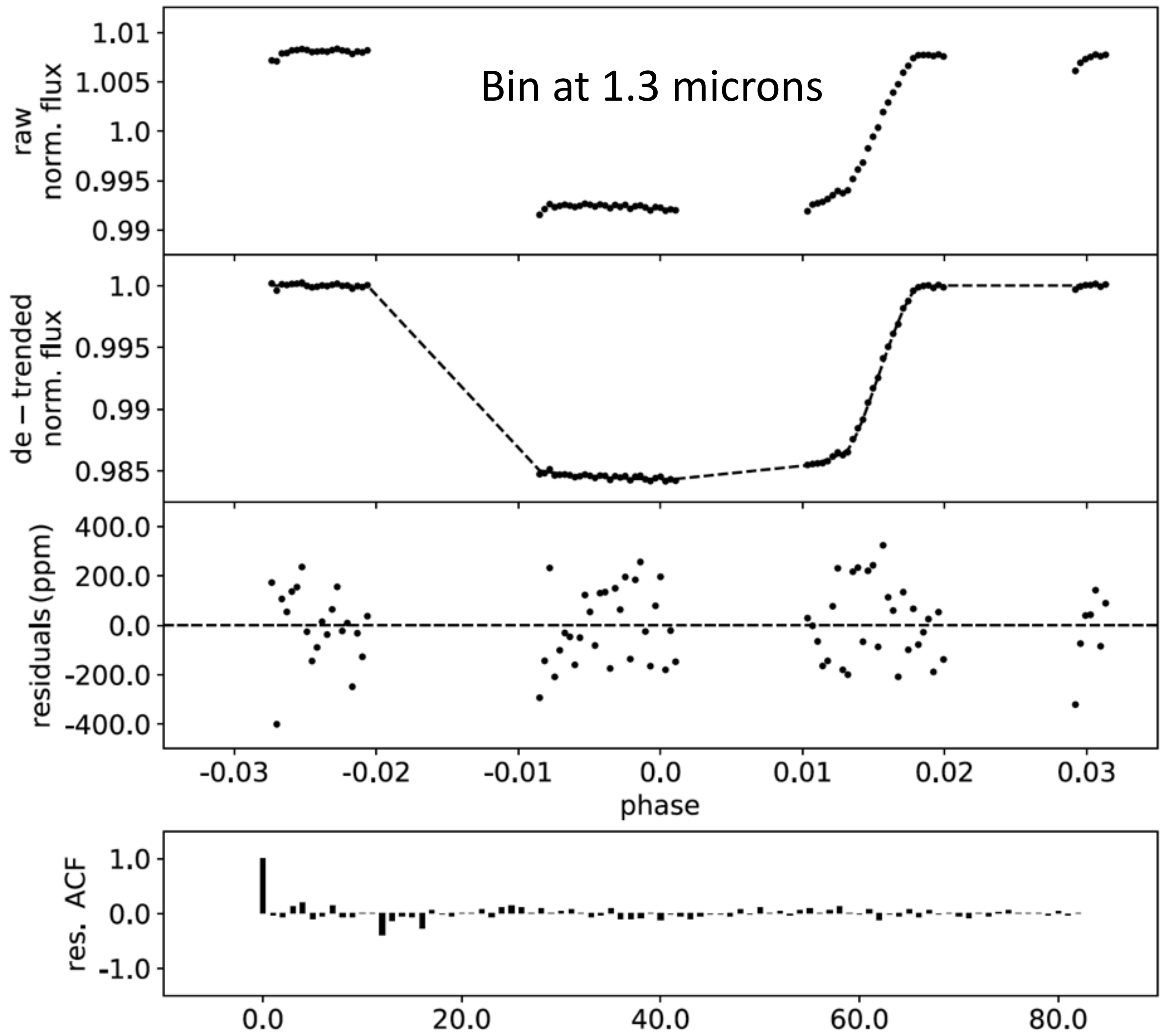

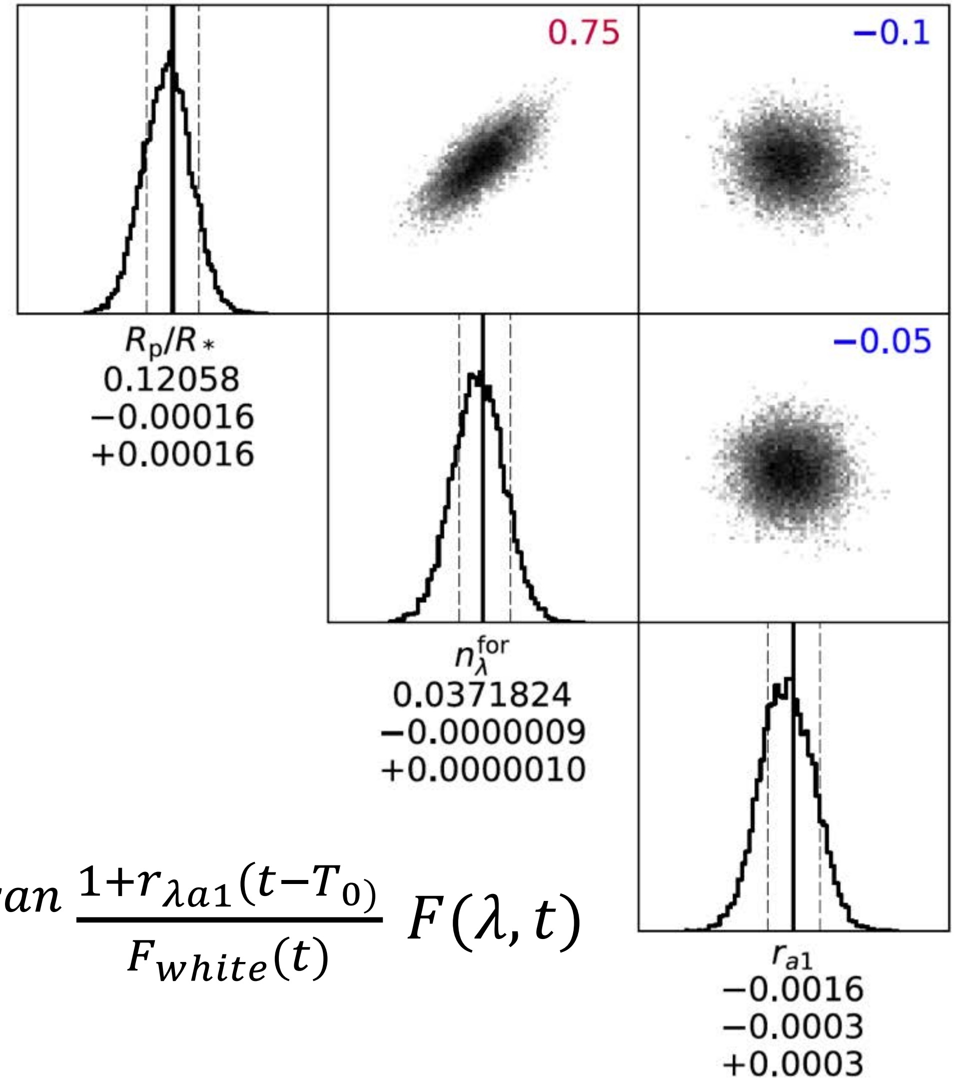

$$n_\lambda^{scan} \frac{1+r_{\lambda a1}(t-T_0)}{F_{white}(t)} \, F(\lambda, t)$$

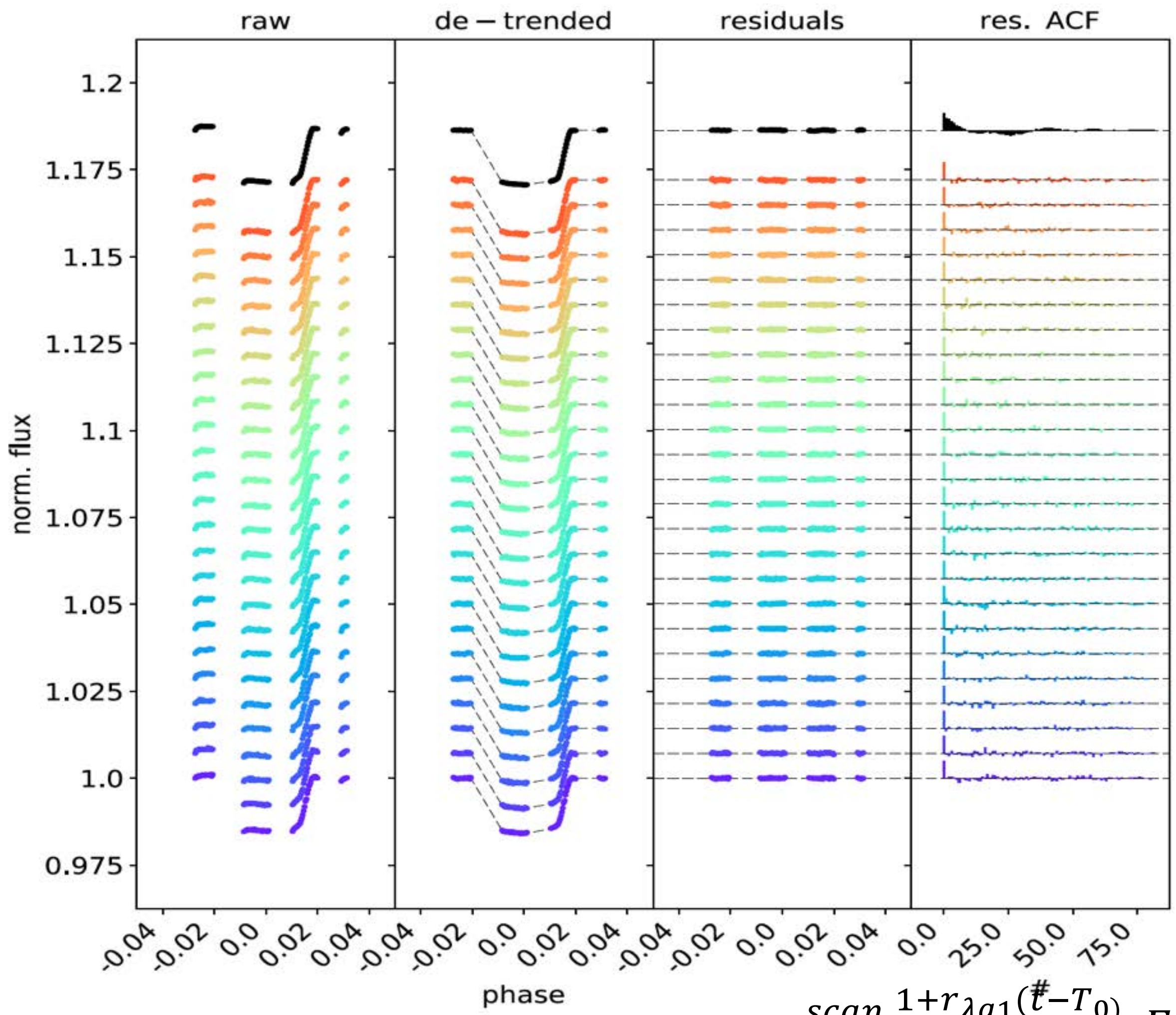

$$n_{\lambda}^{scan} \frac{1+r_{\lambda a1}(t-T_{0})}{F_{white}(t)} \; F(\lambda,t)$$

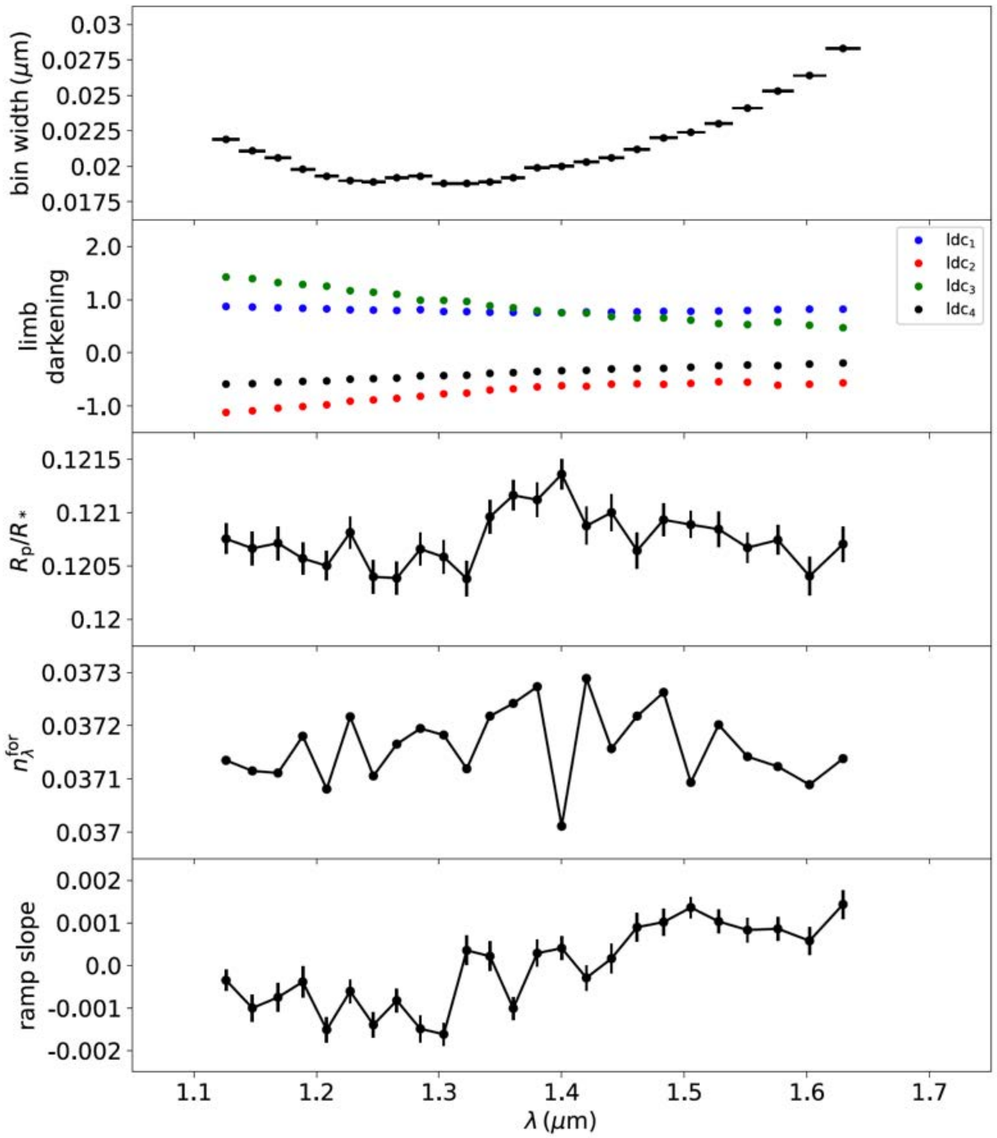

planet WASP-127b, Skaf et al. 2021
Ariel School)

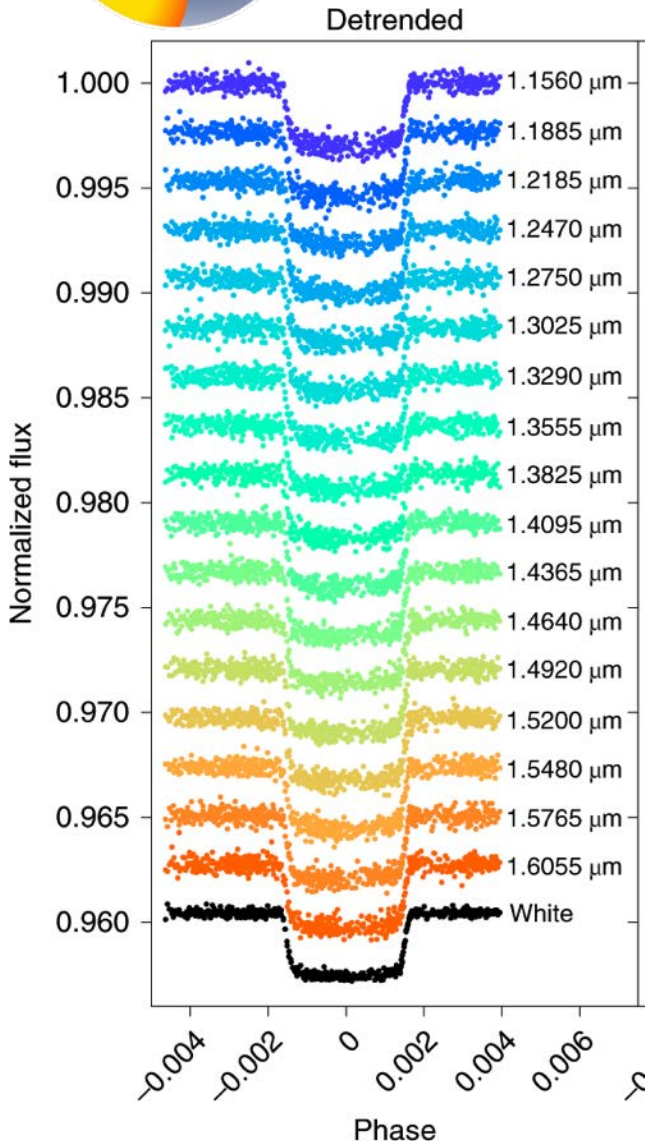

1.1-1.7 microns
H20 dominated spectra

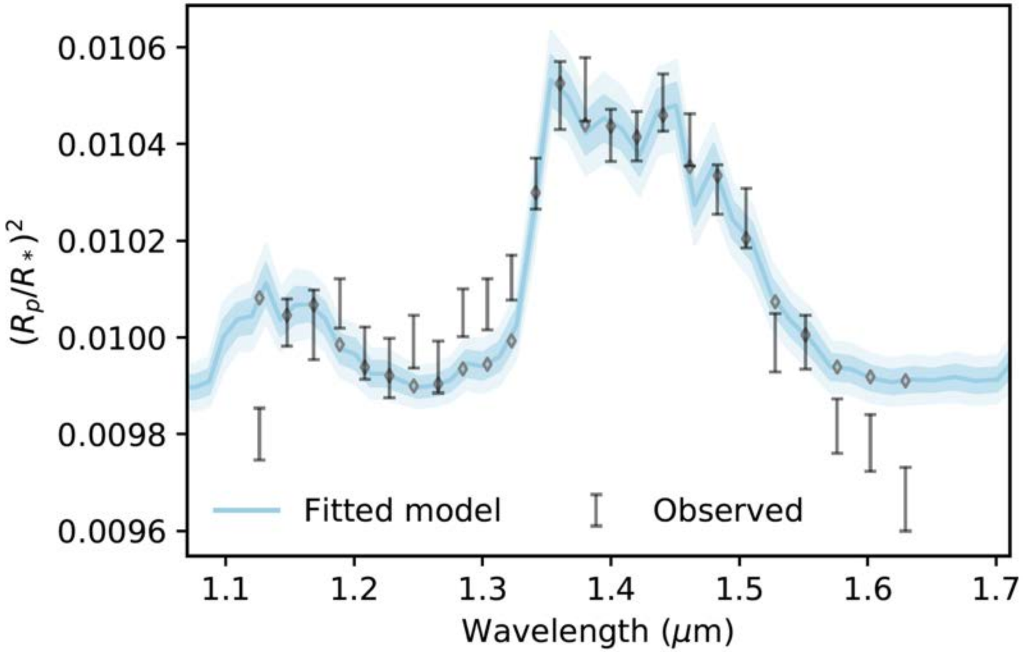

ARES I: CHARACTERISING HOT JUPITERS WASP-127 B, WASP-79 B AND WASP-62 B WITH HUBBLE WFC3 TRANSMISSION SPECTRA*

Nour Skaf,[1,2] Michelle Fabienne Bieger,[3] Billy Edwards,[2] Quentin Changeat,[2] Mario Morvan,[2] Flavien Kiefer,[4] Doriann Blain,[1] Tiziano Zingales,[5] Mathilde Poveda,[6,7] Ahmed Al-Refaie,[2] Robin Baeyens,[8] Amélie Gressier,[4,1,9] Gloria Giulluy,[10,11] Adam Yassin Jaziri,[5] Darius Modirrousta-Galian,[11] Lorenzo Mugnai,[12] William Pluriel,[5] Niall Whiteford,[13] Sam Wright,[2] Benjamin Charnay,[1] Angelos Tsiaras,[2] Ingo Waldmann,[2] and Jean-Philippe Beaulieu[14,4]

Table 1. Target Parameters

Parameter	WASP-127b	WASP-79b	WASP-62b
Stellar parameters			
Spectral type	G5	F5	F7
$T_{\rm eff}$ (K)	5750	6600	6230
$\log g$ (cgs)	3.9	4.06	4.45
[Fe/H]	-0.18	0.03	0.04
Planetary parameters			
P (d)	4.17807015	3.662387	4.411953
$T_{\rm mid}$ (BJD−2450000)	8138.670144	7815.89868	5855.39195
I_c (°)	87.88	83.3	88.3
$M_{\rm P}(M_J)$	0.18	0.9	0.57
$R_{\rm P}(R_J)$	1.37	2.09	1.39
$T_{{\rm eq},A=0}$	1400	1900	1440
Derived parameters used for the Iraclis runs			
$R_{\rm P}/R_\star$	0.09992	0.112606	0.1091
$a_{\rm pl}/R_\star$	7.846	6.069	9.5253

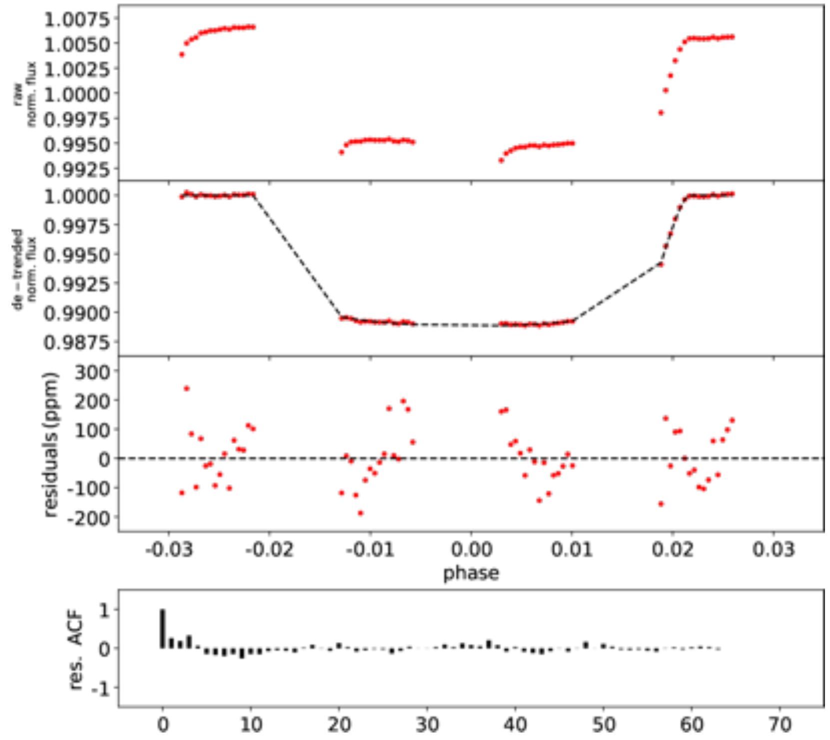

Skaf et al.

Table 4. Comparison of the Bayesian log evidence for different models. For WASP-79b and WASP-62b, the retrieved temperature is always significantly below the equilibrium temperature for the planet, particularly if FeH is not included as an opacity source.

WASP-127b (No Molecules Log Evidence: 1.73)			
Setup	Log Evidence	Retrieved Temperature [K]	Equilibrium Temperature [K]
H_2O	161.87	1027	~1400
H_2O, CH_4, CO, CO_2, NH3	161.27	1005	
H_2O, FeH	170.20	1305	
H_2O, CH_4, CO, CO_2, NH3, FeH	169.64	1304	
WASP-79 (No Molecules Log Evidence: 173.53)			
Setup	Log Evidence	Retrieved Temperature [K]	Equilibrium Temperature [K]
H_2O	188.34	621	~1800
H_2O, CH_4, CO, CO_2, NH3	187.98	603	
H_2O, FeH	190.87	888	
H_2O, CH_4, CO, CO_2, NH3, FeH	190.60	924	
WASP-62 (No Molecules Log Evidence: 184.49)			
Setup	Log Evidence	Retrieved Temperature [K]	Equilibrium Temperature [K]
H_2O	191.65	607	~1450
H_2O, CH_4, CO, CO_2, NH3	190.92	597	
H_2O, FeH	193.40	842	
H_2O, CH_4, CO, CO_2, NH3, FeH	193.11	894	

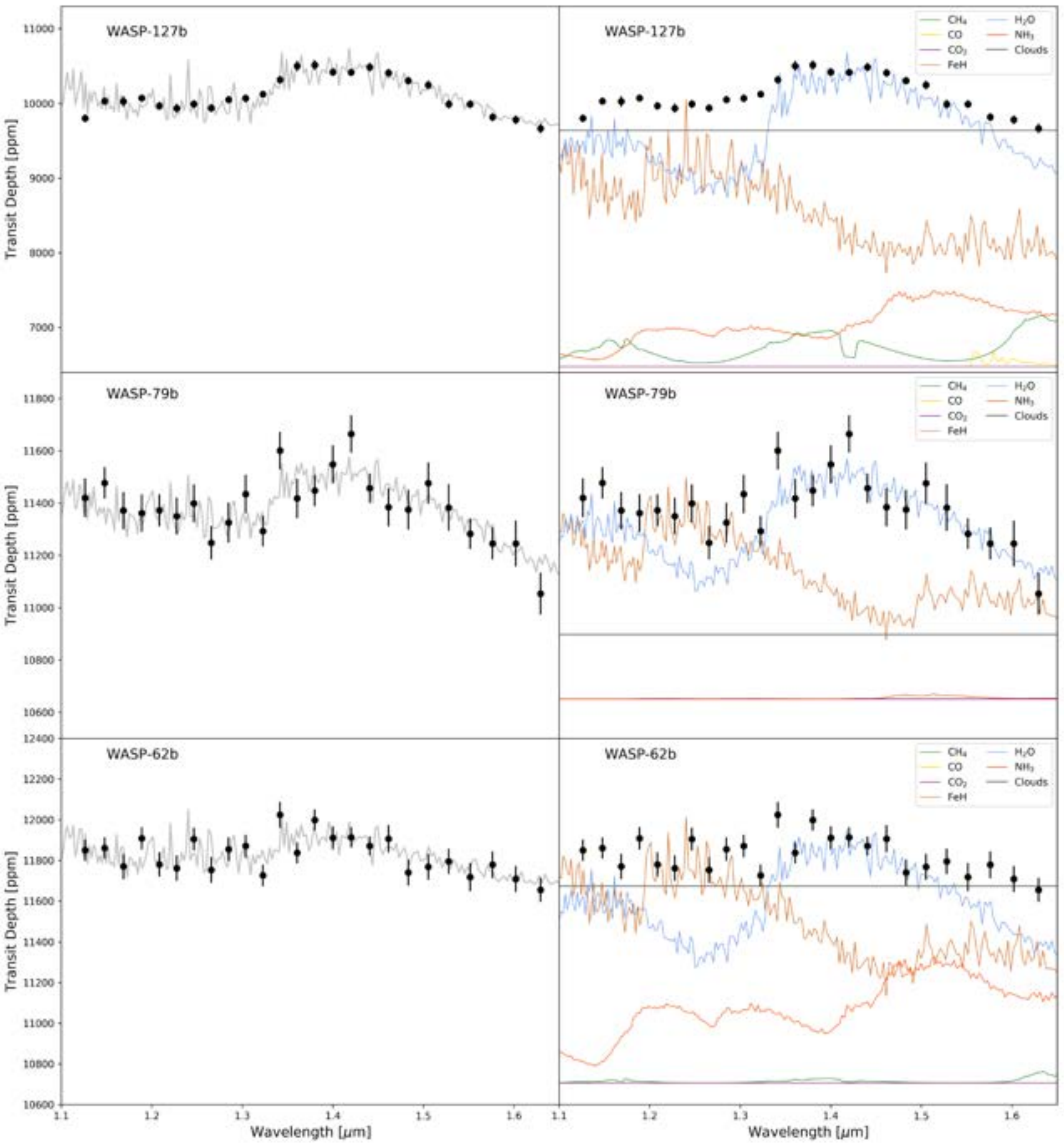

Table 3. Table of fitted parameters for the retrievals performed on our targets

Retrieved Parameters	bounds	**WASP-127b**	**WASP-79b**	**WASP-62b**
$\log[H_2O]$	1e-12 - 1e-1	$-2.71^{+0.78}_{-1.05}$	$-2.34^{+0.51}_{-0.72}$	$-2.56^{+0.76}_{-1.17}$
$\log[FeH]$	1e-12 - 1e-1	$-5.25^{+0.88}_{-1.10}$	$-4.39^{+0.88}_{-1.12}$	$-4.10^{+1.26}_{-1.82}$
$\log[CH_4]$	1e-12 - 1e-1	< -5	< -5	< -5
$\log[CO]$	1e-12 - 1e-1	< -3	< -3	< -3
$\log[CO_2]$	1e-12 - 1e-1	< -3	< -3	< -3
$\log[NH3]$	1e-12 - 1e-1	< -5	< -5	< -5
T_p (K)	400-2500	1304^{+185}_{-175}	924^{+242}_{-204}	894^{+248}_{-239}
R_p (R_{jup})	± 50%	$1.15^{+0.04}_{-0.04}$	$1.69^{+0.02}_{-0.02}$	$1.34^{+0.02}_{-0.02}$
$\log P_{clouds}$	1e-2 - 1e6	$1.7^{+0.93}_{-0.66}$	> 3	$2.5^{+1.1}_{-0.88}$
μ (derived)		$2.34^{+0.20}_{-0.03}$	$2.38^{+0.33}_{-0.07}$	$2.46^{+0.32}_{-0.04}$
ADI	-	167.9	17.1	8.6
σ-level	-	$> 5\sigma$	$> 5\sigma$	$3 - 5\sigma$

Changeat Q., et al. 2022 «Five Key Exoplanet Questions Answered via the Analysis of 25 Hot-Jupiter Atmospheres in Eclipse ». ApJS

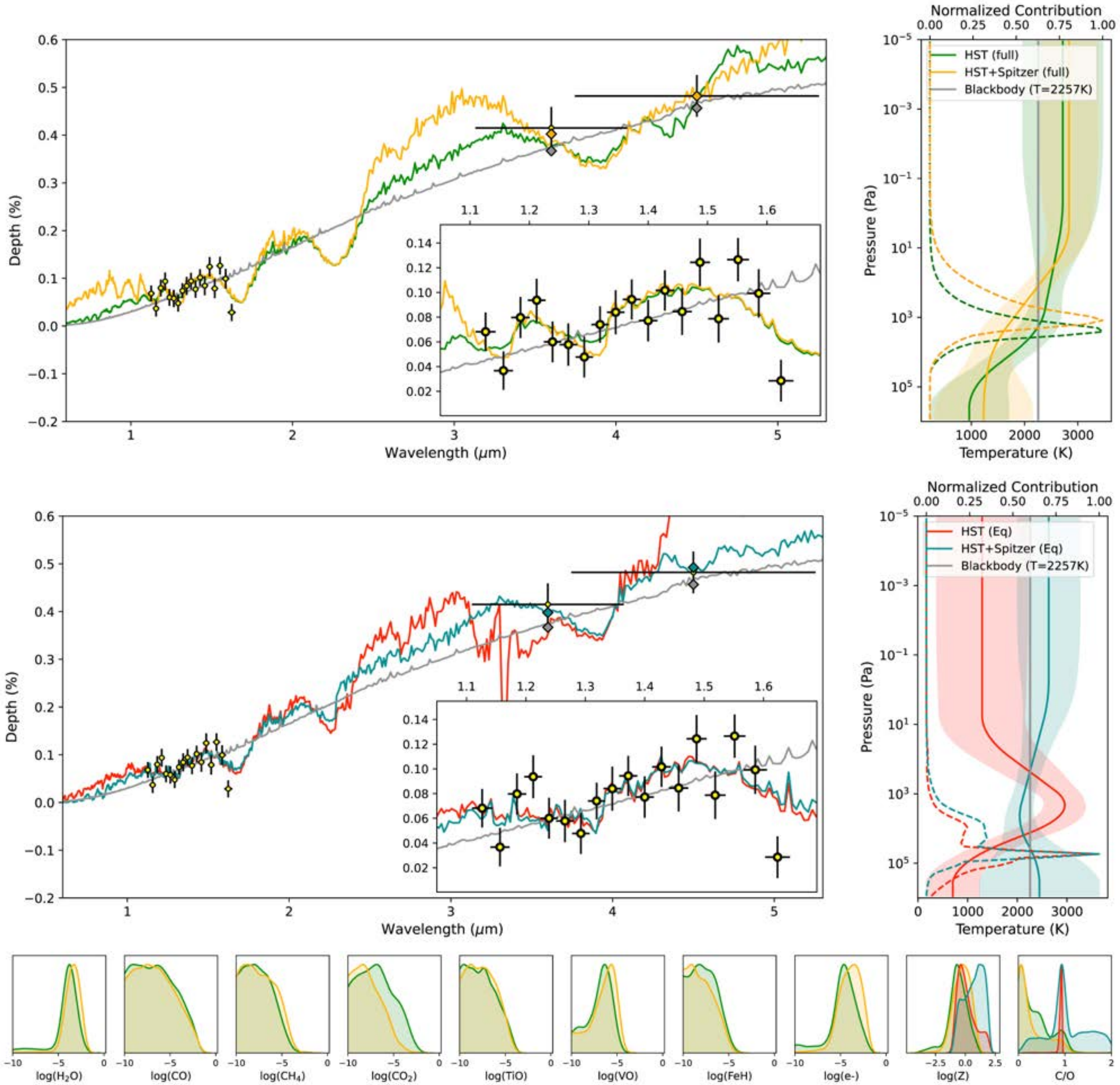

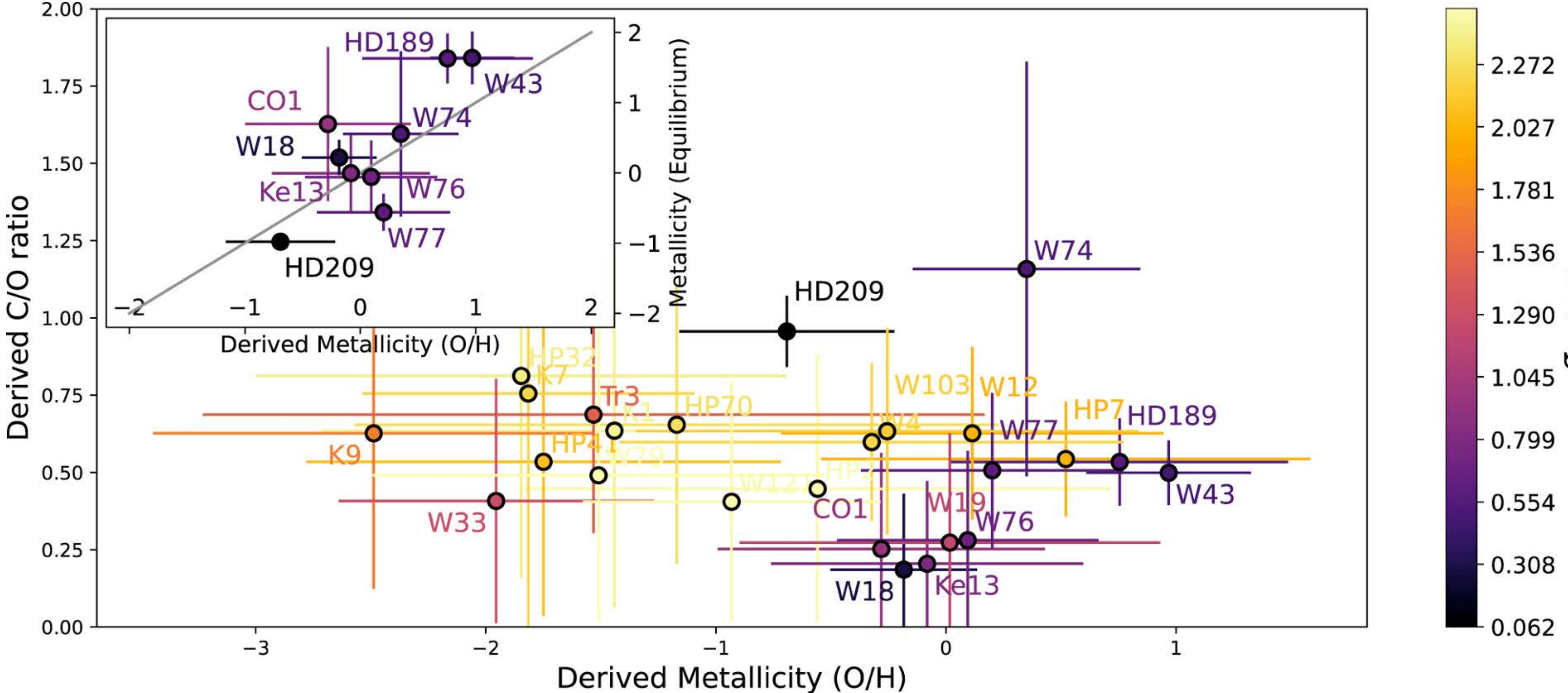

Derived C/O ratio
Derived Metallicity (O/H)
Metallicity (Equilibrium)
$\sigma_{log(H_2O)}$
HD189
W43
CO1
W74
W18
Ke13
W76
W77
HD209
HP32
K7
Tr3
K1
HP70
W103
W12
W4
HP7
W77
HD189
K9
HP41
W79
W12
HP
W33
CO1
W19
W76
W18
Ke13
W74
W43

Population study, 26 planets < 6 Rearth

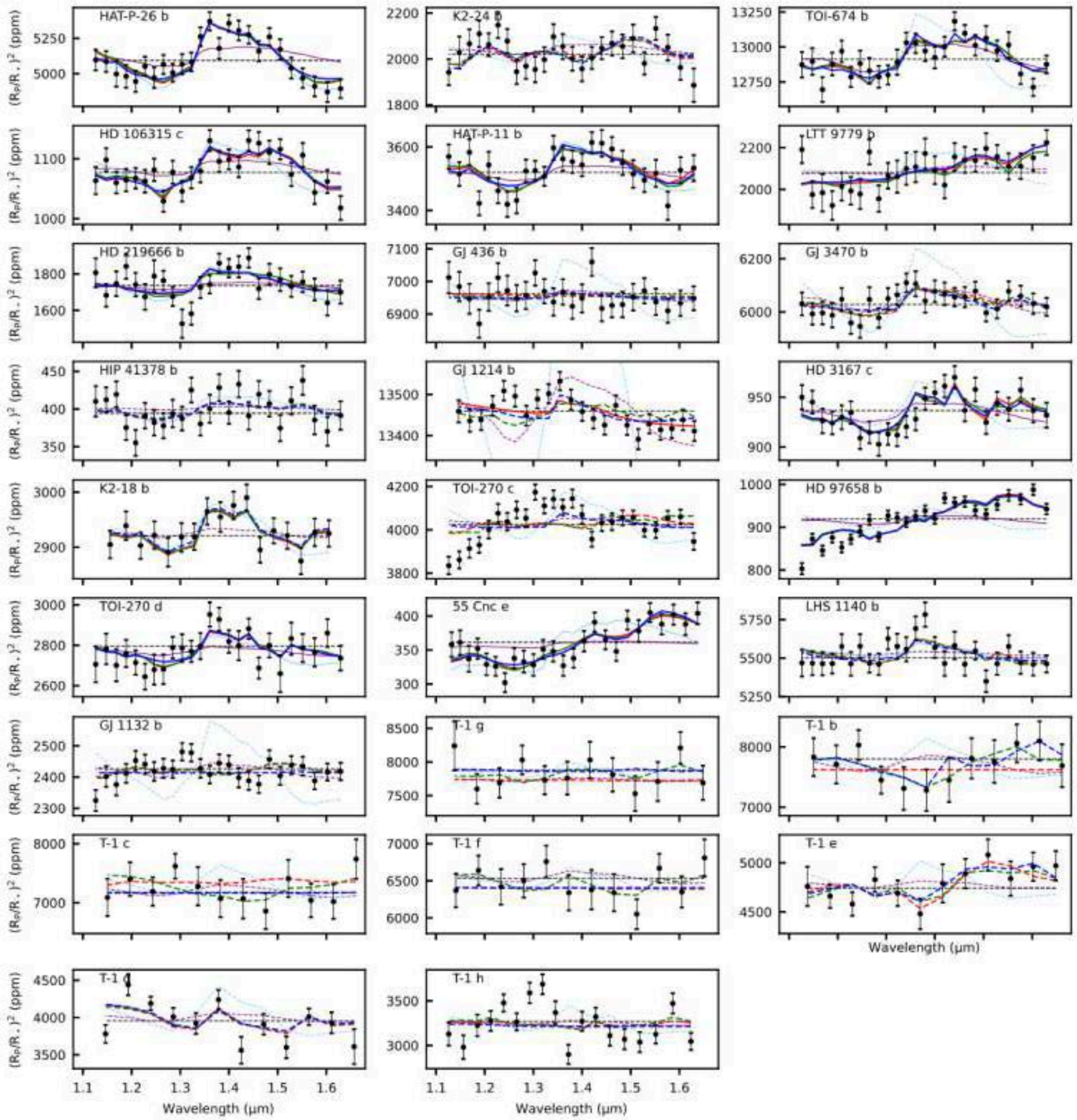

Gressier, Changeat, Edwards et al. 2022 submitted

Planet	H_2O	CH_4	CO	CO_2	NH_3	HCN	N_2	references
55 Cancri e								T16a
GJ 436 b								
GJ 1132 b								
GJ 1214 b								
GJ 3470 b								B19a, E22
HAT-P-11 b								F14,E22
HAT-P-26 b								W17, MD19, E22
HD 3167 c								G20, ME20, E22
HD 97658 b								E22
HD 106315 c								G20, K20, E22
HD 219666 b								
HIP 41378 b								
K2-18 b								T19, B19b, E22
K2-24 b								
LHS 1140 b								E22
LTT 9779 b								
TOI-270 c								
TOI-270 d								E22
TOI-674 b								B22, E22
TRAPPIST-1 b								
TRAPPIST-1 c								
TRAPPIST-1 d								
TRAPPIST-1 e								
TRAPPIST-1 f								
TRAPPIST-1 g								
TRAPPIST-1 h								

First JWST direct imaging of HIP 65426b, NIRCAM+MIRI

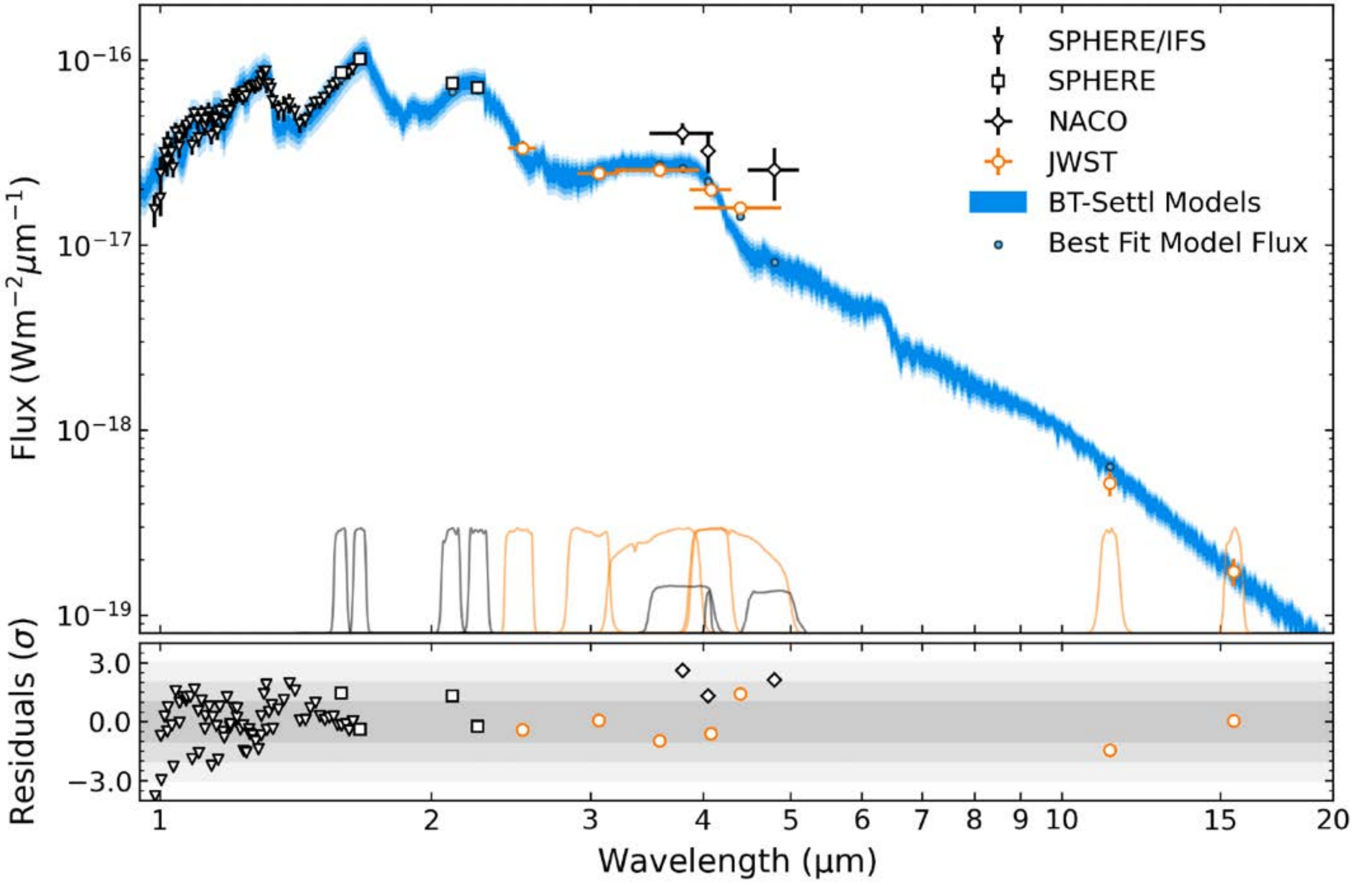

Figure 9. All existing spectroscopic and photometric observations of HIP 65426 b as obtained from SPHERE/IFS (triangles), SPHERE/IRDIS (squares), NaCo (diamonds), and *JWST* (circles). ***Top:*** Data are plotted alongside the 1, 2, and 3σ confidence intervals obtained from fitting to a collection of BT-SETTL atmospheric forward models (blue shaded regions), and the model values in the photometric bandpasses (small blue circles). At 3σ, the best fit models occupy parameter ranges of $T_{\rm eff} = 1673^{+27}_{-25}$ K, $\log(g) = 4.10^{+0.20}_{-0.17}$ dex, and $R = 0.90^{+0.04}_{-0.04}$ $R_{\rm Jup}$. The NaCo data have not been included in the model fitting process. Also plotted are the normalised filter throughput profiles for all photometric observations, with the NaCo throughputs scaled by a factor of 2 to improve clarity. ***Bottom:*** Residuals of each data point relative to the best fit model in addition to 1, 2, and 3σ regions (grey shading).

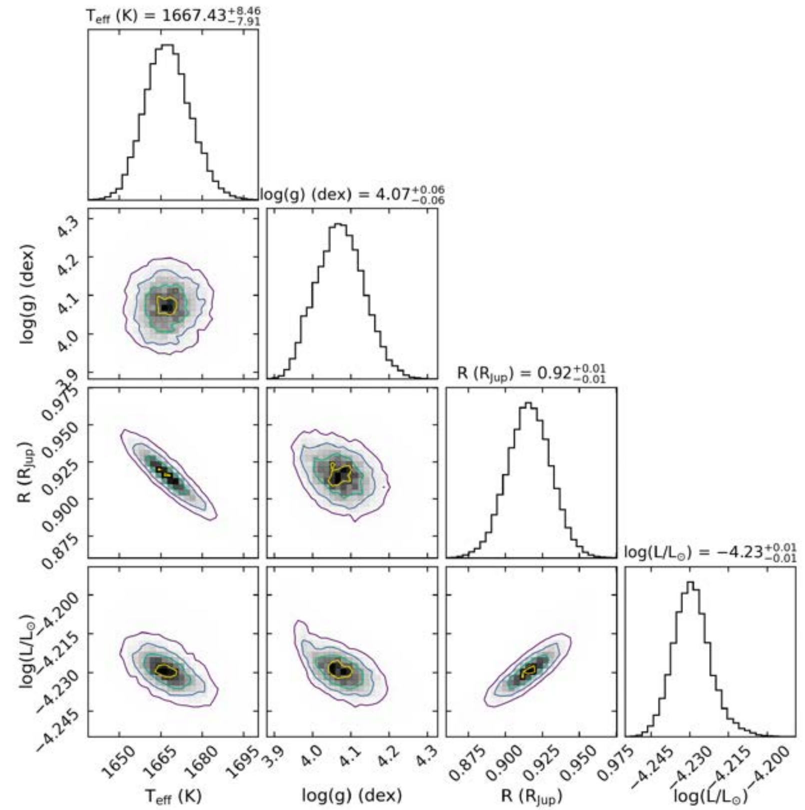

Figure 11. Posterior distributions for the BT−Settl atmospheric model fitting to both *JWST* and *VLT*/SPHERE observations of HIP 65426 b. Best fit values and 1σ uncertainties are indicated, however, these should be interpreted as the model phase space that fits these data, and not the precision to which these properties can be empirically measured.

Hot saturn WASP-39b

- Orbit a G7 star in 4.05 days
- 0.28 Mjup and 1.28 Rjup
- Temperature 1170 K

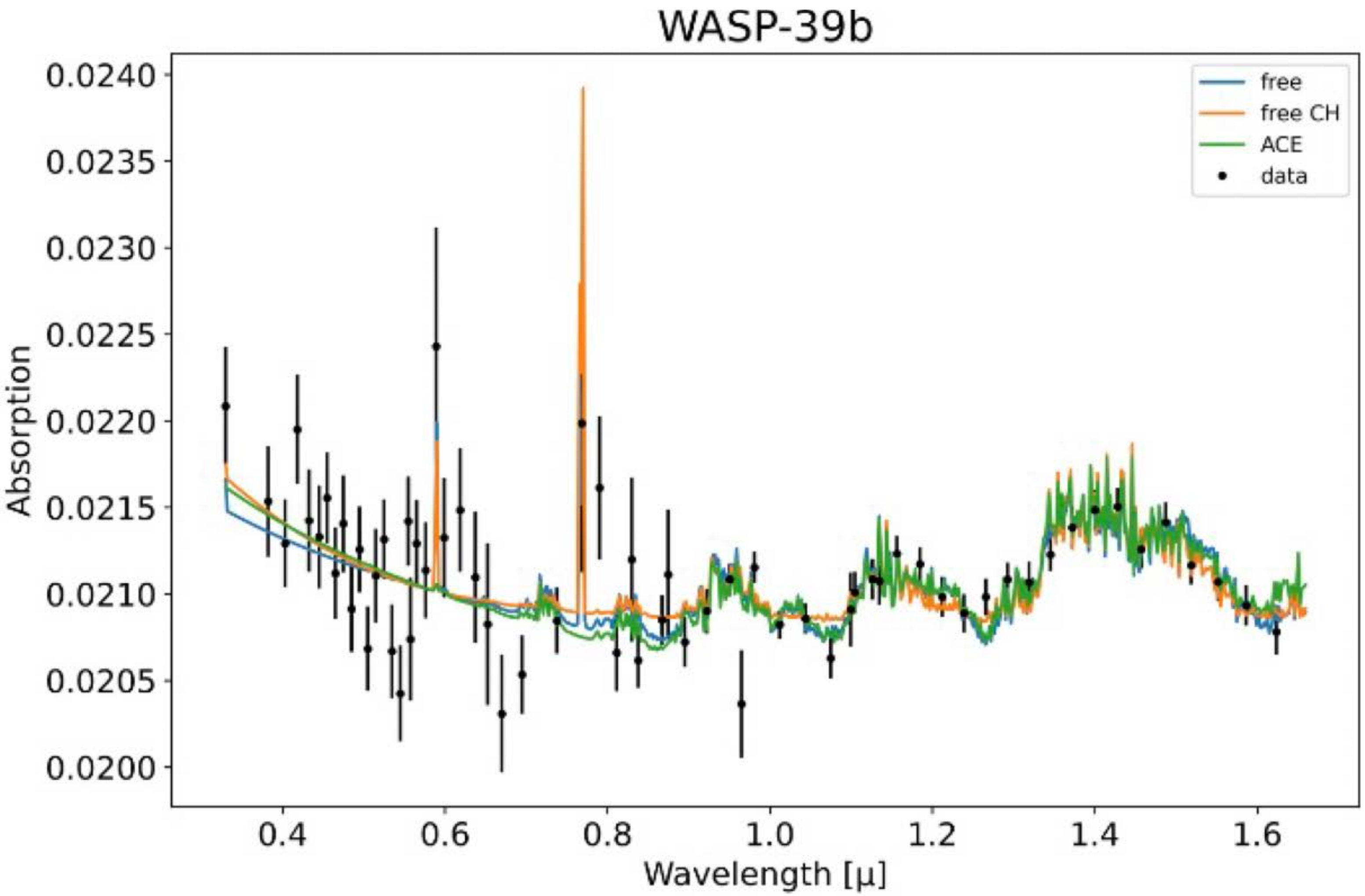

Panek et al., 2022 in prep

Hot saturn WASP-39b

Notice the two Spitzer points 3.6 and 4.5 microns

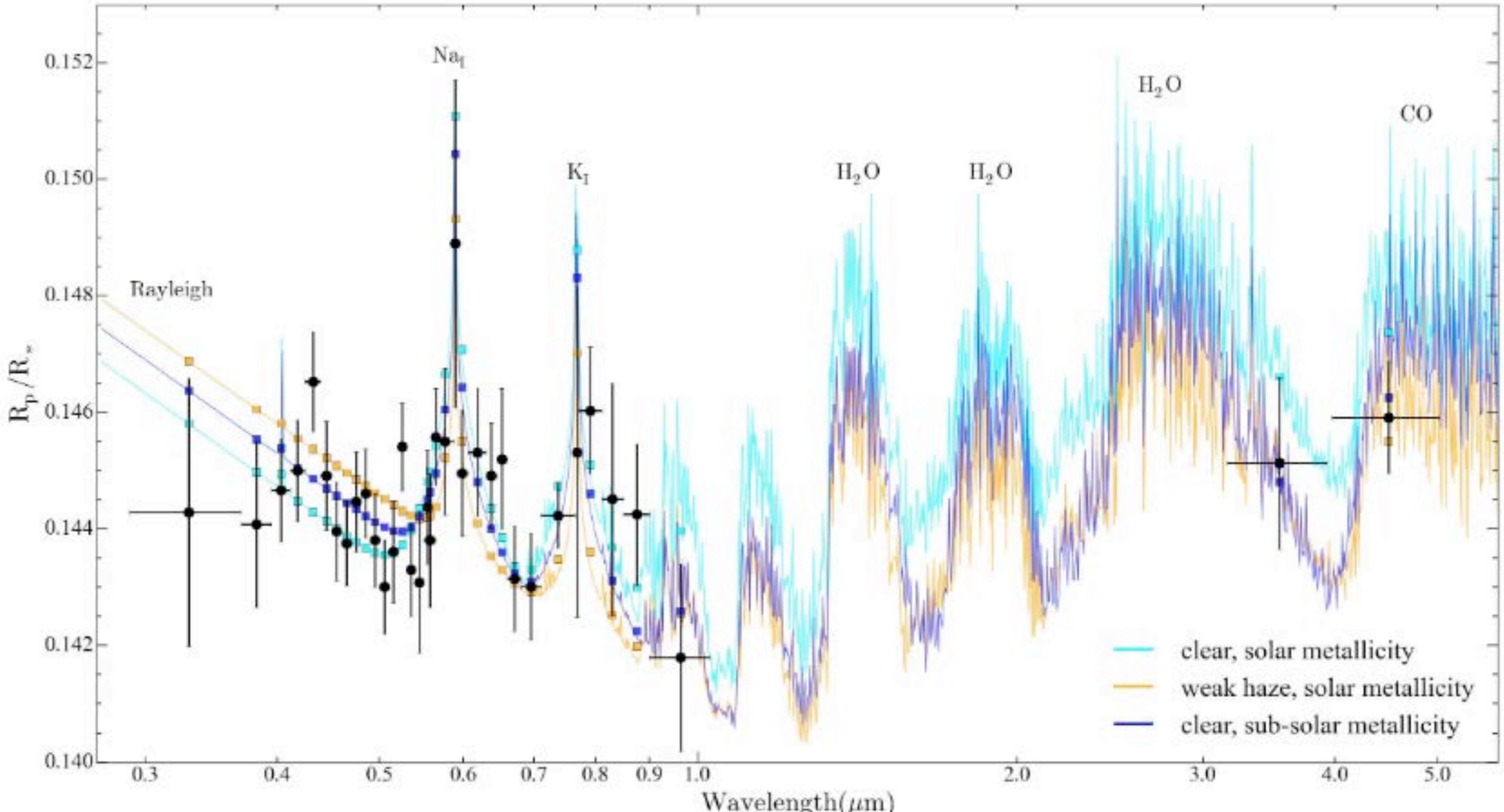

WASP-39b

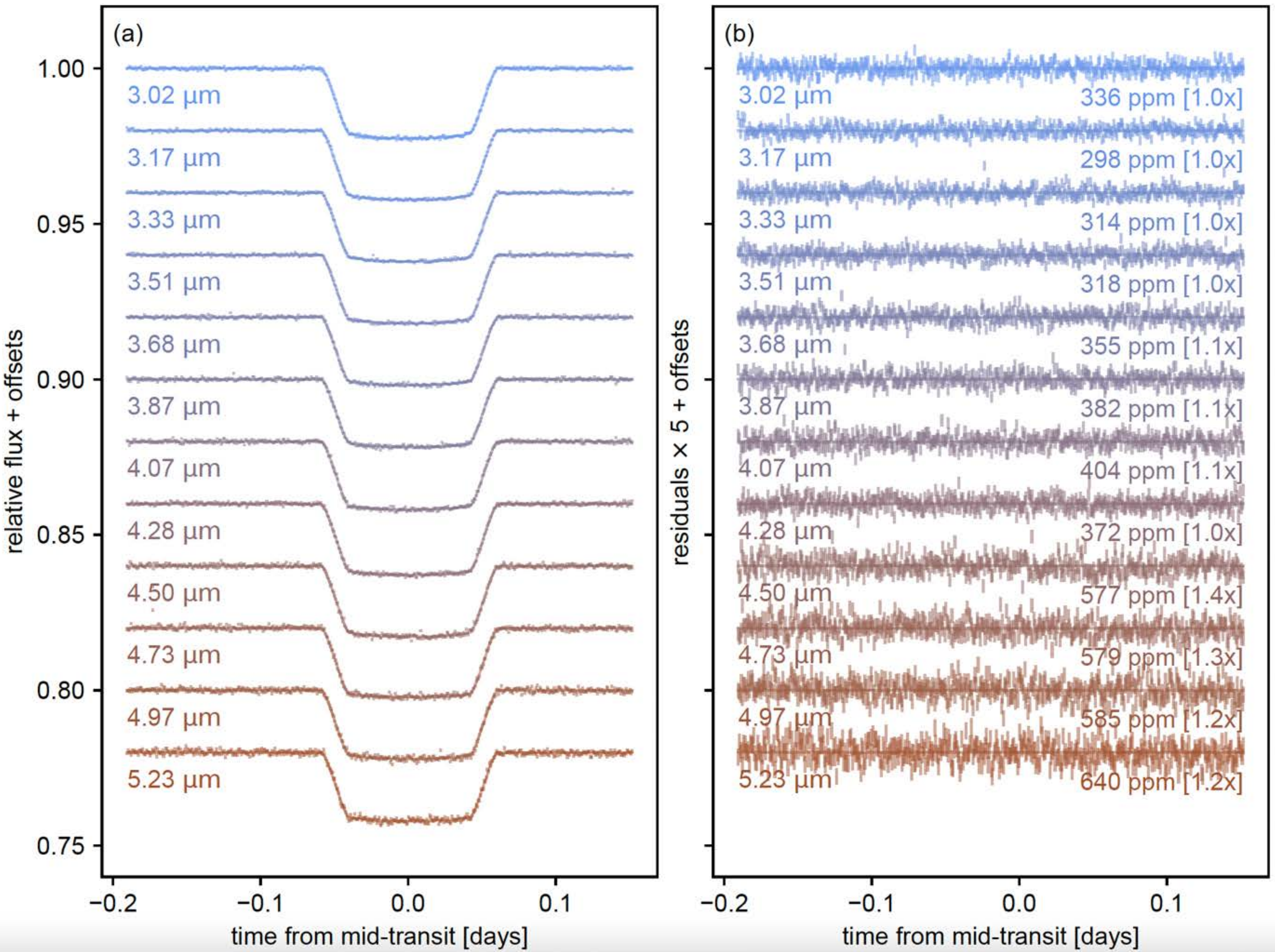
(a)
relative flux + offsets
1.00
0.95
0.90
0.85
0.80
0.75
3.02 µm
3.17 µm
3.33 µm
3.51 µm
3.68 µm
3.87 µm
4.07 µm
4.28 µm
4.50 µm
4.73 µm
4.97 µm
5.23 µm
−0.2
−0.1
0.0
0.1
time from mid-transit [days]
(b)
residuals × 5 + offsets
3.02 µm
336 ppm [1.0x]
3.17 µm
298 ppm [1.0x]
3.33 µm
314 ppm [1.0x]
3.51 µm
318 ppm [1.0x]
3.68 µm
355 ppm [1.1x]
3.87 µm
382 ppm [1.1x]
4.07 µm
404 ppm [1.1x]
4.28 µm
372 ppm [1.0x]
4.50 µm
577 ppm [1.4x]
4.73 µm
579 ppm [1.3x]
4.97 µm
585 ppm [1.2x]
5.23 µm
640 ppm [1.2x]
−0.2
−0.1
0.0
0.1
time from mid-transit [days]

Hot saturn WASP-39b

- Orbit a G7 star in 4.05 days
- 0.28 Mjup and 1.28 Rjup
- Temperature 1170 K